

Site U1314¹

Expedition 306 Scientists²

Chapter contents

Background and objectives	1
Operations	2
Lithostratigraphy	3
Biostratigraphy	5
Paleomagnetism	11
Stratigraphic correlation	11
Geochemistry	12
Physical properties	14
References	15
Figures	17
Tables	61

Background and objectives

Integrated Ocean Drilling Program Site U1314 is located on the southern Gardar Drift in a water depth of 2820 m (Fig. F1). Seismic data for positioning of Site U1314, including multichannel seismic profiling (Fig. F2), 3.5 kHz high-resolution profiling (Fig. F3), and a SeaBeam survey, were collected during the *Knorr* KN166-14 cruise (principal investigator: Greg Mountain) in summer 2002. The high-quality seismic profiles indicate that Site U1314 is optimally positioned in a thick (>700 ms two-way travel-time), well-stratified sediment pile (Fig. F2).

On the crest of the Gardar Drift, a 33 m core (MD99-2253) was collected by the *Marion Dufresne* in 1999 (56°21.78'N, 27°48.95'W; water depth = 2840 m). This is close to the location of Site U1314 (Fig. F1). It lies on oceanic crust close to Anomaly 10 (~30 Ma), and the total sediment thickness is ~600 m. Piston Core MD99-2253 revealed a high sedimentation rate of ~9 cm/k.y. for the last glacial cycle and produced well-defined planktonic $\delta^{18}\text{O}$ and geomagnetic paleointensity records (Channell et al., 2004).

During Ocean Drilling Program (ODP) Leg 162, Site 983 (60°24.2'N, 23°38.4'W) and Site 984 (61°25.5'N, 24°4.9'W) were drilled south of Iceland on the northern part of the Gardar and Bjorn Drifts, respectively (Fig. F1) (Jansen, Raymo, Blum, et al., 1996). These sites have mean Pleistocene sedimentation rates in the 10–15 cm/k.y. range and have produced high-resolution climatic (Fig. F4) and geomagnetic records (e.g., Raymo et al., 1998; Channell et al., 1998; Flower et al., 2000). Sites 983 and 984, however, are located outside the main ice-raftered debris (IRD) belt (*sensu* Ruddiman, 1977) and do not contain a robust detrital carbonate (Heinrich layer) signal. Furthermore, both sites are at shallower water depths (<2000 m) than Site U1314 and therefore monitor intermediate water but not North Atlantic Deep Water (NADW). Thus, the location of Site U1314 in the southern part of the Gardar Drift has been selected for the following objectives:

1. The location of Site U1314 is close enough to the IRD belt to record the Heinrich-type detrital layers that monitor ice sheet instability.
2. The water depths at Site U1314 (2820 m) and the ability to derive a benthic stable isotope record from this region (see Chapman and Shackleton, 1999) will allow ice sheet–ocean interaction to be placed on a benthic isotopic record, and carbon

¹Expedition 306 Scientists, 2006. Site U1314. In Channell, J.E.T., Kanamatsu, T., Sato, T., Stein, R., Alvarez Zarikian, C.A., Malone, M.J., and the Expedition 303/306 Scientists. Proc. IODP, 303/306: College Station TX (Integrated Ocean Drilling Program Management International, Inc.). doi:10.2204/iodp.proc.303306.113.2006

²Expedition 306 Scientists' addresses.



- isotope data will allow high-resolution monitoring of NADW.
3. Sedimentation rates are as high as needed for the proposed high-resolution studies.
 4. Good preservation of foraminifers, nannofossils, and diatoms, and the potential for paleomagnetic and isotopic age control, means that the environmental record comprising sea-surface and bottom water characteristics and detrital (Heinrich-type) stratigraphy can be integrated into a paleointensity-assisted chronostratigraphy.

Operations

We arrived at Site U1314 (proposed Site GAR1B) early Thursday morning, 7 April 2005, after a 943 nmi transit from Site U1313. Positioning beacon SN 2199 (15.0 kHz, 211 dB) was deployed at 0330 h, and operations at Site U1314 officially began. See Table [T1](#) for the coring summary.

Hole U1314A

Hole U1314A was spudded at 0950 h on 7 April 2005. Core 1H recovered 1.95 m of sediment and established a rig floor-corrected seafloor depth of 2810.6 meters below rig floor (mbrf). Coring continued with the advanced piston corer (APC) without incident in Hole U1314A until Core 28H at a depth of 258.4 meters below seafloor (mbsf). The overshot pin sheared during the attempt to recover Core 28H. Unfortunately, the driller did not initially realize that the core barrel was not being recovered and proceeded to drill downhole in preparation for the next core. After recovering the core barrel on the second wireline run, the APC system was found to be heavily damaged, including overtorqued piston rod connections and other damage. Because it was going to take an hour or more to repair and rebuild the APC system, the Co-Chief Scientists elected to terminate coring in Hole U1314A and proceed with the next hole. After repairing the APC, the drill string was pulled clear of the seafloor at 1100 h on 8 April, officially ending operations in Hole U1314A.

Tensor core orientation was used for all cores beginning with Core 4H from a depth of 20.9 mbsf. Drill-over of stuck APC barrels was not required, and all core barrels fully stroked. Nonmagnetic core barrels were used to recover all 28 cores. Problems with swollen or imploded core liners were more prevalent in this hole than experienced previously at the other sites. Of 28 cores recovered, four liners suffered some swelling (Cores 12H, 15H, 16H, and 23H) and six core liners either shattered (Core 20H) or imploded (Cores 18H, 22H, 26H, 27H, and 28H). In addition, four barrels mechanically sheared during deploy-

ment (Cores 2H, 4H, 6H, and 11H). These problems were most likely heave induced and led to more disturbed and lower-quality core than normally experienced with the APC system. The cored interval for this hole was 258.4 m, and 267.34 m of sediment was recovered (103.5%).

Hole U1314B

The drillship was offset 25 m due north (000°) of Hole U1314A. The bit was positioned at a depth of 2806.0 mbrf, or 3.0 m deeper than Hole U1313A, to offset the core breaks between cores. Hole U1314B was spudded at 1220 h on 8 April 2005, and Core 1H recovered 4.02 m and established a rig floor-corrected seafloor depth of 2811.5 mbrf. APC coring with nonmagnetic core barrels continued without incident in Hole U1314B through Core 30H to a total depth of 279.5 mbsf. Tensor core orientation was used for all cores beginning with Core 4H from a depth of 23.0 mbsf. All core barrels fully stroked, and no drillover was required in this hole. The cored interval for this hole was 279.5 m, and 285.36 m of sediment was recovered (102.1%). The drill string was pulled clear of the seafloor at 1155 h on 9 April, officially ending operations in Hole U1314B. Although there still were some core liner incidents in this hole, core quality was improved. Of the 30 cores recovered, four liners were recovered swollen (Cores 15H, 21H, 22H, and 26H) and another three were imploded at the bottom end (Cores 9H, 19H, and 27H). The overshot pin sheared once on Core 6H, requiring a second wireline run to recover the core barrel.

Hole U1314C

The drillship was offset 25 m due east (90°) of Hole U1314B. The bit was positioned at a depth of 2809.0 mbrf, or 6.0 m deeper than Hole U1314A, again to offset the core breaks. Hole U1314C was spudded at 1320 h on 9 April 2005, and Core 1H recovered 8.22 m and established a rig floor-corrected seafloor depth of 2810.3 mbrf. APC coring with nonmagnetic core barrels continued in Hole U1314C through Core 22H to a total depth of 207.7 mbsf. During this period, the weather deteriorated as a major gale approached our location and brought high winds and steadily building seas and swells with it. By Sunday morning, we had long-period heave cycles in excess of 5 m and storm-force winds were forecast for the Site U1314 location by late Sunday or early Monday. Tensor core orientation was used for all cores beginning with Core 3H from a depth of 17.7 mbsf. All core barrels fully stroked, and no drillover was required in this hole. The cored interval for this hole was 207.7 m, and 212.93 m of sediment was recov-



ered (102.5%). The drill string was pulled clear of the seafloor at 0915 h on 10 April, and positioning beacon SN 2199 was recovered during the pipe trip, officially ending operations at Site U1314 at 1030 h. After we recovered and stored the drill string, the ship was secured for transit and all thrusters and hydrophones were pulled. At 1545 h on 10 April, the ship was switched from dynamic positioning to cruise mode and began the sea voyage to Site U1315 (Site 642 on the Vøring Plateau).

Lithostratigraphy

Three holes were drilled and cored at Site U1314, reaching a maximum depth of 279.91 mbsf in Hole U1314B. Sediments at Site U1314 are characterized by a strong presence of biogenic and terrigenous material, with varying proportions of nannofossils and detrital clay minerals that contain only minor amounts of biogenic silica and, to a lesser extent, foraminifers. Sediments are predominantly greenish gray with recurring variations in shade that occur in decimeter-scale bands. These color changes are primarily related to changes in the relative proportion of biogenic carbonate and detrital clay minerals in the sediments. Only one lithologic unit, spanning the Holocene–late Pliocene, was defined at Site U1314.

Description of units

Unit I

Intervals: Sections 306-U1314A-1H-1, 0 cm, through 28H-CC, 5 cm; 306-U1314B-1H-1, 0 cm, through 30H-CC, 23 cm; and 306-U1314C-1H-1, 0 cm, through 22H-CC, 23 cm

Depths: Hole U1314A: 0–257.58 mbsf, Hole U1314B: 0–279.91 mbsf, and Hole U1314C: 0–208.18 mbsf

Age: Holocene–late Pliocene

Unit I comprises nannofossil- and clay-rich sediments having varying proportions of diatoms and foraminifers (Fig. F5). In particular, two sets of lithologies can be identified: (1) predominantly nannofossil oozes enriched in biogenic (mainly diatoms and foraminifers) and terrigenous (principally clay minerals, quartz, opaque minerals, and calcite) components and (2) terrigenous silty clay with varying proportions of calcareous and siliceous organisms (see “[Site U1314 smear slides](#)” in “Core descriptions”). The sediment varies in color mainly from very dark gray (5Y 3/1) to light gray (5Y 7/1) to hues of greenish gray (5GY 6/1–4/1 and 5G 6/1–4/1). In contrast to these gray colors, the uppermost 9 cm of sediment in Hole U1314A and the uppermost 14 cm in Hole U1314B consist, respectively, of yellowish brown

(10YR 5/4) and dark yellowish brown (10YR 4/4) silty clay biosiliceous-nannofossil ooze. The yellowish color of this zone is probably due to the sediment being above the redox boundary and reflects the circulation of oxygen-rich seawater through the sediments.

Horizontal and parallel bedding planes and color contacts without erosional relief suggest that there is not visible evidence of significant sediment disturbance by natural processes. Most lithologic changes are gradual, spanning several decimeters, although more pronounced transitions sometimes occur within a decimeter. However, a very distinct, sharp contact between very dark gray (5Y 3/1) and gray (5Y 6/1) sediments was observed at 29.03 mbsf in Hole U1314B (Section 306-U1314B-4H-5, 3 cm) and 30.80 mbsf in Hole U1314C (Section 306-U1314C-4H-3, 60 cm). Here, a thick clay-rich interval with laminations at the base has a sharp basal contact with an underlying biogenic carbonate-rich layer (Fig. F6). This contact was not observed in Hole U1314A. Inferred depth by correlation with Hole U1314B and Hole U1314C suggests the contact might have been lost in the break between Cores 306-U1314A-4H and 5H. Micropaleontological analysis of core catcher 306-U1314A-4H-CC indicates a poor abundance of foraminifers and the presence of aggregates (see Table T8). This sharp contact, the scarcity of foraminifers, and the presence of aggregates suggest this abrupt change in lithologies may have been associated with distinct changes in current strength.

Disseminated pyrite staining on millimeter to centimeter scale is present in most of the sediment below the uppermost section of the holes. Intervals 1–5 cm thick, with distinct green coloration (grayish green: 5G 4/2 and 5G 5/2) and sometimes coarser texture, are also distributed throughout the core (Fig. F7). Preliminary X-ray diffraction data suggest that some glauconite may contribute to the green coloration within these lenses (Fig. F8).

Bioturbation is most obvious where there is a rapid change in lithology presenting contrasting colors, and it is mainly characterized by millimeter- to centimeter-scale mottling and blurred transitions (Fig. F9). Discrete pyritized worm burrows are also occasionally scattered through the sequence. Although bioturbation is often difficult to assess in the darkest sediments, the presence of faint mottling in most of the sections suggests that it is a quite pervasive process throughout the sedimentary succession.

Smear slides show most of the sediments to be in the clay size range (see “[Site U1314 smear slides](#)” in “Core descriptions”). However, some centimeter- to decimeter-scale intervals contain lenses of silt- and sand-sized grains. These intervals are more pro-



nounced in darker sediments. Calcium carbonate ranges from 7.48 to 70.43 wt%, with an average of 33.8 wt% throughout Unit I (see Fig. F26), reflecting varying proportions of clay and both biogenic and detrital carbonate. Calcareous nannofossils make up a significant proportion of the clay-sized fraction in carbonate-rich sediments (smear slides indicate up to 85%; see “[Site U1314 smear slides](#)” in “Core descriptions;” Fig. F10). Foraminifers also contribute a minor amount of calcium carbonate, generally up to 5%, as estimated from the smear slides. Slightly higher carbonate values are observed in the upper 50 m of the sedimentary succession (see Fig. F26).

Biogenic silica in the sediments is represented by diatoms, sponge spicules, radiolarians, silicoflagellates, and ebridians. Generally, biogenic silica abundances are <25% (see “[Site U1314 smear slides](#)” in “Core descriptions;” Fig. F10). In an isolated interval, however, diatom levels comprise 80% of the sediments (interval 306-U1314B-4H-2, 18–30 cm; 24.68–24.80 mbsf). Sponge spicules, radiolarians, silicoflagellates, and ebridians usually occur only in trace amounts to a few percent.

Terrigenous sediments are mainly represented by clay minerals, which range in abundance from 5% to 70% (see “[Site U1314 smear slides](#)” in “Core descriptions;” Fig. F10). Other terrigenous components, in decreasing order of abundance, include quartz, opaque minerals, detrital calcite, accessory minerals, glauconite, and feldspar. These components range in abundance from trace amounts to 55%. Volcanic glass occurs in trace and rare amounts throughout the sedimentary sequence of Site U1314, with some peak occurrences of 10%–80% (see “[Site U1314 smear slides](#)” in “Core descriptions”).

Gravel-sized dropstones are common at Site U1314, occurring from 0 to 240 mbsf (Table T2; Fig. F11). Preliminary analyses of these dropstones show that they range in size from 2 to 45 mm, are rounded to angular, and are of felsic and mafic igneous, (granite and basalt), metamorphic (gneiss and quartzite), or sedimentary/metasedimentary (sandstone and mudstone) origins (Table T2; Figs. F12, F13).

The magnetic susceptibility, color reflectance, and natural gamma ray records show an overall distinct short-term variability. In addition, long-term changes are centered between ~240 and 270 mcd and at ~70 mcd (Fig. F14). However, apart from darker sediment colors, no changes in lithologic characteristics and composition are clearly discernible from visual core description and smear slide examination. Therefore, at this preliminary stage, lithologic Unit I cannot be effectively divided into subunits.

Discussion

The sediments at Site U1314 consist of carbonate-rich and carbonate-poor intervals that alternate on decimeter to meter scale. Sediment types range from nannofossil oozes with biosilica and/or silty clay as minor components (the carbonate-rich intervals) to silty clay (the carbonate-poor intervals). Changes in the relative proportions of these two sediment types might reflect variable deposition rates rather than selective sediment removal, as suggested by the good preservation of calcareous and siliceous microfossils and by the visual absence of sedimentary structures related to erosion or winnowing.

Distribution of fine-grained sediments in this region is probably controlled by deepwater circulation (McCave and Tucholke, 1986). In particular, the Iceland-Scotland Overflow Water (ISOW), which travels south of Iceland along the eastern flank of the Reykjanes Ridge, plays an important role in producing and shaping the Gardar Drift (Johnson and Schneider, 1969; Jones et al., 1970).

Silt- and clay-sized terrigenous components from Site U1314 show the presence of volcanic products (see “[Site U1314 smear slides](#)” in “Core descriptions”). The finer fraction of volcanic material, mainly derived from the Icelandic ice sheet, was deposited on the continental slope south of Iceland and subsequently transported downslope by turbidity currents and further along slope by the southwest-flowing ISOW and Norwegian Sea Water (Davies and Laughton, 1972; Kissel et al., 1999). In addition, volcanioclastic sediments can also be transported in this region as tephra fallout (Lacasse et al., 1998).

Although high sedimentation rates at this site are mainly related to deep-sea sediment focusing, the presence of dropstones throughout the sedimentary succession recovered at Site U1314 indicates that ice-rafting played an important role (Figs. F11, F12, F13). Sand- and gravel-sized sediments, observed either during visual core descriptions or smear slide estimates, provide direct evidence of ice rafting and document the influence of the late Pliocene–Pleistocene glaciation in this region. The presence of gravel-sized grains downcore is coupled with an increased abundance of peaks of quartz and sand-sized sediment (Fig. F11), indicating several possible pulses of IRD input. Preliminary age estimates based on biostratigraphic and paleomagnetic data show that higher abundances occurred from 2.6 to 2.2 Ma, 1.7 to 0.8 Ma, and during the last 0.23 m.y., suggesting that these time intervals were probably characterized by higher IRD input.



Possible provenance areas for this terrigenous sediment include Iceland, Greenland, and the Canadian Shield (Bond and Lotti, 1995). More specifically, felsic igneous dropstones may be sourced from southeast Greenland, and mafic igneous dropstones may be derived from either Greenland flood basalts or Iceland's volcanic province (Krissek and St. John, 2002). Additionally, the presence of sand-sized, hematite-stained quartz, which was identified in smear slide estimates, is well documented in previous IRD studies in this region and might be sourced from the east central coast of Greenland (Bond and Lotti, 1995; Bond et al., 1999).

Sediment at Site U1314 is also supplied from surface biological production. Smear slide estimates suggest that the biogenic sediment component at this site is mainly composed of calcareous nannofossils. Fluctuations in the relative percentages of calcareous nannofossils may be related to dilution by high terrigenous sedimentation and also may reflect changes in sea-surface productivity. In general there is an inverse relationship between nannofossil abundance and the abundance of terrigenous components, such as clay minerals and quartz. This may suggest movement of the Polar Front to the east-southeast when nannofossil abundance decreased and terrigenous input increased (Andruleit and Baumann, 1998).

Biostratigraphy

Core catcher samples from Holes U1314A, U1314B, and U1314C contain rich assemblages of calcareous nannofossils, foraminifers, diatoms, and radiolarians that are well to moderately well preserved. A succession of biostratigraphic events provides a reliable chronological framework spanning the late Pliocene (~3 Ma) to the Holocene (Table T3).

Polar and subpolar calcareous and siliceous plankton assemblages are dominant throughout the Pliocene and Pleistocene, with a lower proportion of North Atlantic transitional species. Because this site is near the distribution limit of some temperate to subtropical species, some events that were very useful at the previous sites seem to be diachronous here, as the first and last occurrences of these species are probably not coincident with those in the mid-latitude North Atlantic. This may explain why some nannofossil events are somewhat depressed relative to foraminifer events in the late Pliocene (Figs. F15, F16, F17). Many of the samples analyzed at this site contain rare to abundant lithic grains of quartz, volcanic glass, basalts, and other rock fragments, including some gravel-sized rocks.

Sedimentation rates estimated using the approximate depth of biostratigraphic events defined in this

study are relatively constant throughout the Pleistocene (7.0–7.5 cm/k.y.), whereas late Pliocene sedimentation rates are closer to 11 cm/k.y. (Figs. F15, F16, F17).

Calcareous nannofossils

We examined all core catcher samples from Holes U1314A through U1314C for calcareous nannofossils. All samples yielded abundant to very abundant nannofossil assemblages. Preservation was good to moderately good throughout the section. Gephyrocapsids, small reticulofenestrids, and *Pseudoemiliania* species dominate most Pleistocene assemblages, although several core catcher samples yielded very high percentages of *Coccolithus* spp. These samples are typically coarser grained, with lower overall abundance. Reworked Cretaceous and Paleogene nannofossils are present throughout the section, although Cretaceous species are more predominant within the Pleistocene, whereas Paleogene species are more common in the upper Pliocene and lowermost Pleistocene sediments.

The sections recovered at Site U1314 yielded Pleistocene and upper Pliocene assemblages (Tables T4, T5, T6, T7). We identified 11 Pleistocene nannofossil datums defined by Sato et al. (1999) in most holes at Site U1314. We were unable to identify the last occurrence of *Helicosphaera inversa* (0.16 Ma) at this site. In fact, no occurrences of this species are found within Martini's (1971) nannofossil Zone NN21, although it does occur in other parts of the section. The first occurrence (FO) of *Emiliania huxleyi* (0.25 Ma), which marks the base of Zone NN21, is present in Samples 306-U1314A-3H-CC, 306-U1314B-3H-CC, and 306-U1314C-2H-CC. This event is problematic because *E. huxleyi* is very rare in the early stage of its evolution and difficult to recognize under the light microscope. Zone NN20, which spans the time period between the last occurrence (LO) of *Pseudoemiliania lacunosa* and the FO of *E. huxleyi*, occurs in Samples 306-U1314A-4H-CC, 306-U1314B-4H-CC, and 306-U1314C-3H-CC.

The LO of *P. lacunosa* (0.41 Ma), which defines the top of Zone NN19, occurs in Samples 306-U1314A-5H-CC, 306-U1314B-5H-CC, and 306-U1314C-4H-CC. The FO of *H. inversa* (0.51 Ma) is only identifiable in Samples 306-U1314A-5H-CC and 306-U1314C-6H-CC, as *H. inversa* is only found in one sample in Hole U1314B. The LO of *Reticulofenestra asanoi* (0.85 Ma) occurs in Samples 306-U1314A-8H-CC, 306-U1314B-8H-CC, and 306-U1314C-8H-CC. In Holes U1314A and U1314B, this event occurs in conjunction with the FO of *Gephyrocapsa parallela* (0.95 Ma). In Hole U1314C, the FO of *G. parallela* occurs in Sample 306-U1314C-8H-CC. The FO of *R.*



asanoi (1.16 Ma) occurs in Samples 306-U1314A-10H-CC, 306-U1314B-9H-CC, and 306-U1314C-9H-CC.

Large specimens of *Gephyrocapsa oceanica* and *Gephyrocapsa caribeanica* are quite prominent at this site. Specimens of these species range in size from small (<4 µm) to >6 µm. Careful measurements were required to identify the FO and LO of large *Gephyrocapsa* spp., which Sato et al. (1999) defines as those specimens >5 µm. Based on this size definition, the LO of large *Gephyrocapsa* spp. (1.21 Ma) occurs in Samples 306-U1314A-11H-CC, 306-U1314B-10H-CC, and 306-U1314C-10H-CC. The LO of *Helicosphaera sellii* (1.27 Ma) occurs with the LO of large *Gephyrocapsa* spp. in Sample 306-U1314C-10H-CC and in Samples 306-U1314A-12H-CC and 306-U1314B-12H-CC. The FO of large *Gephyrocapsa* spp. (1.45 Ma) is significantly more difficult to detect than the LO of this species, since larger specimens of this species grade from smaller specimens near its FO. Careful examination yielded the FO of this species in Samples 306-U1314A-13H-CC, 306-U1314B-12H-CC, and 306-U1314C-11H-CC.

The FOs of medium-sized (>4 µm) *G. oceanica* (1.65 Ma) and *G. caribeanica* (1.73 Ma) occur together in Holes U1314A and U1314B. We use the latter species to approximate the Pliocene/Pleistocene boundary. Rare occurrences of these species are present below their FO datum. Specimens of these older occurrences are usually <4 µm, although rare occurrences of specimens >4 µm can occur in the upper Pliocene. We placed the FOs of *G. oceanica* and *G. caribeanica* at the base of consistent occurrences of specimens >4 µm (Tables T4, T5, T6). The FOs of both species occur together in Samples 306-U1314A-14H-CC and 306-U1314B-15H-CC. In Hole U1314C, the FO of *G. oceanica* occurs in Sample 306-U1314-14H-CC, whereas the FO of *G. caribeanica* occurs in Sample 306-U1314-15H-CC.

Pleistocene sediments at Site U1314 contain scattered occurrences of reworked Cretaceous and Paleogene material throughout much of the interval. The number of reworked specimens present is generally very rare, although some samples contain few reworked specimens. These samples are typically coarser grained and likely contain higher amounts of IRD. Reworked specimens are typically more poorly preserved than the in situ assemblage at this site.

Four Pliocene events dated by Sato et al. (1999) that should occur within the sedimentary section at Site U1314 are difficult to identify. These events are based on the LOs of discoasters, which are considered warm-water species. Discoasters are present at higher latitudes during the Neogene, although in reduced numbers. Therefore, the latitude of Site U1314

made it challenging to identify these Pliocene datums, particularly within the time constraints of drilling operations. Additional study of samples following completion of drilling allowed us to more accurately identify the LOs of these events, although some are still depressed relative to foraminifer and paleomagnetic datums (Figs. F15, F16).

The LO of *Discoaster brouweri* (1.97 Ma), which marks the top of Zone NN18, occurs in Samples 306-U1314A-18H-CC, 306-U1314B-18H-CC, and 306-U1314C-18H-CC. This datum is in close agreement with the FO of the planktonic foraminifer *Globorotalia inflata* at 2.08 Ma (Table T3). The LO of *Discoaster pentaradiatus* (2.38 Ma), which marks the top of Zone NN17, occurs in Samples 306-U1314A-24H-CC and 306-U1314B-24H-CC. Hole U1314C terminated above the LO of this species. *D. pentaradiatus* is particularly rare within this section, and as a result, the position of its LO is somewhat deeper than datums of similar age. The LO of *Discoaster surculus* (2.54 Ma), which marks the top of Zone NN16, occurs in Samples 306-U1314A-26H-CC and 306-U1314B-26H-CC. The LO of this species also occurs slightly deeper than correlative events. The LO of *Discoaster tamalis* (2.74 Ma) occurs in Samples 306-U1314A-28H-CC and 306-U1314B-28H-CC, indicating that the total depth of Hole U1314A just reached 2.74 Ma, whereas Hole U1314B penetrated 19 m beyond this datum.

Planktonic foraminifers

The planktonic foraminifer assemblages were studied in all core catchers from Holes U1314A to U1314C (Tables T8, T9, T10). In addition, the washout from the top of Cores 306-U1314A-1H, 306-U1314B-1H, and 306-U1314C-1H, for which only the >150 µm fraction is available, was examined. Even after intensive washing of the samples, many clay aggregates remained in the residues of some samples, making observation of the foraminifers more difficult. Planktonic foraminifers are the dominant component of the >63 µm fraction in nearly all samples, with lower proportions of benthic foraminifers, ostracodes, radiolarians, sponge spicules, diatoms, and ice-raftered grains of different mineralogical composition. Foraminifers are rare and the residue is completely dominated by IRD in Sample 306-U1314C-15H-CC. In addition, diatoms and radiolarians are more abundant than foraminifers in the washout surface sample of Section 306-U1314B-1H-1.

Site U1314 is located within the subpolar plankton province, and the foraminifer assemblages are dominated by *Globigerina bulloides* along with other subpolar to transitional species, such as *Neogloboquadrina pachyderma* (dextral), *Turborotalia quinqueloba*, *Globigerinita glutinata*, and *G. inflata*. These species,



together with *N. pachyderma* (sinistral), *Neogloborotalia quadrina atlantica* (sinistral), and *Globorotalia puncticulata* are the main components of the assemblage throughout the upper Pliocene and Pleistocene.

As most subtropical and temperate species are absent in this region, only subpolar to transitional species are used for definition of biostratigraphic events. The first event observed at this site is the first abundant occurrence (FaO) of *N. pachyderma* (sinistral), which is recorded in Samples 306-U1314A-16H-CC, 306-U1314B-15H-CC, and 306-U1314C-15H-CC. This species is common to abundant in most of the samples from the middle and upper Pleistocene, but is absent or very rare in the lowermost Pleistocene, where *N. pachyderma* (dextral) becomes the dominant component of the assemblage. The FaO of this species has been dated at 1.78 Ma by Weaver and Clement (1987) and 1.8 Ma by Lourens et al. (1996).

We observed the FO of *G. inflata* within the interval of dominant *N. pachyderma* (dextral) and only two cores below the previous event, (Samples 306-U1314A-18H-CC, 306-U1314B-18H-CC, and 306-U1314C-18H-CC). This species, which is absent in the upper Pliocene, becomes a significant component of the assemblage near the Pliocene/Pleistocene boundary at ~2.09 Ma (Weaver and Clement, 1987; Lourens et al., 1996). *Globorotalia truncatulinoides* is rarely present at this site in the upper Pleistocene, and therefore its FO was not used to build the biostratigraphic framework.

An interval with no globorotalids of the *Globorotalia* (*Globoconella*) lineage is observed between Samples 306-U1314A-18H-CC and 306-U1314A-23H-CC, 306-U1314B-18H-CC and 306-U1314B-23H-CC, and 306-U1314C-18H-CC and the bottom of Hole U1314C. The base of this interval is defined by the LO of *G. puncticulata*, dated at 2.41 Ma in the Mediterranean (Lourens et al., 1996). This event is nearly isochronous with the LO of *N. atlantica* (sinistral), which is identified in Samples 306-U1314A-23H-CC, 306-U1314B-23H-CC, and 306-U1314C-22H-CC. This is a cold-water species and therefore we assume this event, dated at 2.41 Ma by Weaver and Clement (1987), is synchronous across the northern latitudes of the North Atlantic.

Sand- to small gravel-sized lithic grains, most of which are likely to be IRD, are present in numerous core catchers in all three holes, with higher abundances in the Pleistocene samples (Tables T8, T9, T10). Several of the core catcher samples, especially in Holes U1314B and U1314C, contain basaltic tephra and hematite-stained quartz grains, two of the tracers used by Bond and Lotti (1995) to study phasing in the surges from circum-North Atlantic ice sheets. The presence of these marker grains in sam-

ples at Site U1314 will allow us to extend the detailed study of Bond et al. (1999) back to at least the early Pleistocene.

Benthic foraminifers

Benthic foraminifer assemblages from Site U1314 were only studied in Hole U1314A. Few moderately well preserved benthic foraminifers occur throughout the Neogene sequence, except in eight samples (306-U1314A-4H-CC, 6H-CC, 14H-CC, 16H-CC, 18H-CC, 20H-CC, 26H-CC, and 27H-CC), which contain very rare, poorly preserved specimens (Table T11). Three assemblages are determined in Hole U1314A.

Assemblage I (*Epistominella exigua*-*Melonis pompilioides*)

E. exigua and *M. pompilioides* are predominant and *Cassidulina carinata* is subordinate between Samples 306-U1314A-1H-CC and 3H-CC, in 5H-CC, between 7H-CC and 13H-CC, and in 23H-CC, 24H-CC, and 28H-CC.

Assemblage II (*Nuttallides umboniferus*)

This assemblage, represented by abundant occurrences of *N. umboniferus*, is recognized in Samples 306-U1314A-19H-CC and 21H-CC.

Assemblage III (*Oridorsalis umbonatus*)

This assemblage is characterized by the abundant occurrence of *O. umbonatus* and co-occurrence of *M. pompilioides* and *Uvigerina peregrina* in Samples 306-U1314A-17H-CC and 22H-CC.

According to Murray (1991), the association of abundant of *E. exigua* and *O. umbonatus* suggests the influence of NADW in the depositional environment. In contrast, high frequencies of *N. umboniferus* in Samples 306-U1314A-19H-CC and 21H-CC suggest an increased influence of Antarctic Bottom Water (AABW) between 2.09 and 2.38 Ma.

The only benthic foraminifer biostratigraphic event recognized in Hole U1314A is the LO of *Stilostomella* spp., which occurs in Sample 306-U1314A-10H-CC. Most species of *Stilostomella* disappear between 1.0 and 0.6 Ma (Hayward, 2001). Thus, the age indicated by the benthic foraminifer coincides with the nanofossil results.

Diatoms

Diatoms were investigated in smear slides from 80 core catcher samples of Holes U1314A to U1314C (Tables T12, T13, T14). Diatoms are generally present within all holes, although in lower abun-

dances in the lower one-third of each hole. Also, abundances are highest in Hole U1314A and lowest in Hole U1314C.

The overall diatom assemblage is characterized by boreal and subarctic diatoms, such as *Actinocyclus curvatulus*, *Thalassionema nitzschioides*, and *Rhizosolenia hebetata* (Andersen et al., 2004). As a result, the relatively detailed diatom biostratigraphy of ODP Site 983 (Koç et al., 1999) must be used. Warm-water species like *Fragilariopsis doliolus*, *Fragilariopsis reinholdii*, and *Hemidiscus cuneiformis* are often present in lower numbers, so the low- to mid-latitude stratigraphy of Baldauf (1987) can be used as secondary datums when possible. This stratigraphy can also be applied to lower parts of the sedimentary successions.

The LO of *Proboscia curvirostris* (0.3 Ma), which marks the base of the *Thalassiosira oestrupii* Zone, is found in Samples 306-U1314A-4H-CC, 306-U1314B-3H-CC, and 306-U1314C-4H-CC. Koç et al. (1999) correlate this event to marine isotope Stage (MIS) 9.

The LO of *F. reinholdii* coincides with the LO of *Fragilariopsis fossilis* in Hole U1314A. In Hole U1314C, the same event coincides with the LO of *Neodenticula seminae*. In Hole U1314C, the LO of *F. reinholdii* occurs in Sample 306-U1314C-5H-CC, giving a secondary datum within the *P. curvirostris* Zone of Koç et al. (1999). The LO of *F. fossilis* is only present in Samples 306-U1314A-7H-CC and 306-U1314B-7H-CC. This event coincides with the FO of *N. seminae* in Hole U1314C.

The base of the *P. curvirostris* Zone is defined by the LO of *N. seminae*. This event occurs in Samples 306-U1314A-8H-CC, 306-U1314B-8H-CC, and 306-U1314C-7H-CC and marks the top of the *N. seminae* Zone. It occurs in MIS 21 at Site 983 (Koç et al., 1999).

The base of the *N. seminae* Zone, marked by the FO of *N. seminae*, is found in Samples 306-U1314A-11H-CC, 306-U1314B-10H-CC, and 306-U1314C-9H-CC. This suggests progressively lower sedimentation rates from Holes U1314A to U1314C in this interval. Koç et al. (1999) place this event somewhere between MIS 35 and 37 at Site 983.

Below the FO of *N. seminae*, the Koç et al. (1999) high-latitude stratigraphy merges with the lower-latitude stratigraphy of Baldauf (1987). The base of the *F. reinholdii* Zone is defined by the FO of *F. doliolus*. However, as this species is only sporadically present in trace numbers, it is not possible to constrain the base of the *F. reinholdii* Zone in any of the holes at Site U1314.

Thalassiosira convexa is utilized as a secondary datum in the *Alveus marinus* Zone of Baldauf (1987). It occurs in Sample 306-U1314A-25H-CC and below, as

well as in Sample 306-U1314B-26H-CC and below, suggesting that these holes reached an age of at least 2.4 Ma. The sporadic occurrences of this species in Samples 306-U1314C-3H-CC and 19H-CC are the result of reworking in either the sediment column or during coring. The shorter Hole U1314C does not reach this datum and therefore the age of the bottom of the hole is not much older than 2 Ma, as *F. doliolus* fragments seem to be present at least as far down as Sample 306-U1314C-21H-CC.

Fragilariopsis jouseae occurs in Sample 306-U1314B-27H-CC and below. This suggests an age of at least 2.7 Ma for Sample 306-U1314B-27H-CC, as the LO of *F. jouseae* indicates the top of the *F. jouseae* Zone (Baldauf, 1987).

Characteristic for this site is the high abundance of fragments of the long pennate diatom *Thalassiothrix longissima*. Other diatoms that occur frequently in large numbers are *Thalassionema nitzschioides* and *Thalassionema lineatum*. The *Thalassionema* species seems to be as abundant as *Thalassiothrix longissima* in the lower half of each hole (Tables T12, T13, T14). In addition, remains of large specimens of *Coscinodiscus* spp., resting spores of *Chaetoceros* spp. and *Rhizosolenia* spp., are often very abundant, especially in Hole U1314C.

The presence of large numbers of long pennate diatoms has previously been ascribed to intensification of oceanic circulation and the development of oceanic fronts (Kemp and Baldauf, 1993). The dominant diatom assemblage at this site is similar to that at Expedition 303, Site U1304, although so far only one interval of actual diatom ooze and possible mat-forming has been found at Site U1314 (see “[Lithostratigraphy](#)”).

Frequent low-abundance occurrences of benthic diatoms, neritic species such as *Paralia sulcata*, as well as ice-edge diatoms such as *Bacteriaprum* spp. suggest southward transport of sediment, possibly delivered to these latitudes from the Irminger Basin region by the East Greenland Current (Koç and Flower, 1998).

Radiolarians

We examined radiolarians in all core catcher samples from Holes U1314A, U1314B, and U1314C. In Hole U1314A, 4 of 28 core catcher samples (306-U1314A-4H-CC, 6H-CC, 20H-CC, and 21H-CC) contain rare to trace occurrences of poorly preserved radiolarians, whereas Sample 306-U1314A-16H-CC is barren (Table T15). Radiolarians are abundant to common and well preserved in the remaining samples from Hole U1314A. In Hole U1314B, radiolarians are generally abundant to common with good preservation throughout the hole. Only 3 of 30 core catcher sam-



ples (306-U1314B-16H-CC, 19H-CC, and 20H-CC) include rare specimens or traces of radiolarians that are of moderate to poor preservation (Table T16). Finally, abundant to common well-preserved radiolarians are generally observed throughout Hole U1314C. In 5 of 22 core catcher samples (306-U1314C-6H-CC, 13H-CC, 15H-CC, 20H-CC, and 21H-CC), moderate to poorly preserved radiolarians are rare or occur only as traces (Table T17).

We focused on the occurrence of *Cycladophora davisiana* at the previous sites and also found new, interesting information at this site. *C. davisiana* can be traced to the bottom of all three holes (Samples 306-U1314A-28H-CC, 306-U1314B-30H-CC, and 306-U1314C-22H-CC). Holes U1314A and U1314B date to 2.74–3.54 Ma, which results in an earlier than expected FO for *C. davisiana* (2.6 Ma), although this is synchronous with Site U1313. In addition, high abundances of *Cycladophora sakaii*, the ancestor of *C. davisiana* (Motoyama, 1997), are observed in Samples 306-U1314A-25H-CC and 306-U1314B-25H-CC. These samples are dated to 2.4 Ma by the LO of the diatom *T. convexa*, 2.41–2.54 Ma by the LOs of the planktonic foraminifers *N. atlantica* (sinistral) and *G. puncticulata*, and the LO of the nannofossil *D. surculus*, respectively. Motoyama (1997) demonstrated that the evolutionary transition from *C. sakaii* to *C. davisiana* occurs between 2.7 and 2.4 Ma, when the percentage of *C. davisiana* exceeds the percent of *C. sakaii* at Deep Sea Drilling Project (DSDP) Site 192 in the North Pacific. This may indicate that *C. davisiana* also evolved from *C. sakaii* in the North Atlantic and the evolutionary transition is synchronous with the North Pacific, although we have not encountered *C. sakaii* in any remaining samples, except for 306-U1314A-28H-CC.

The preliminary data obtained from core catcher studies show the radiolarian fauna depict different assemblages between the younger 100 k.y. cycle world and the 41 k.y. cycle world. The stronger and more prominent 100 k.y. cycle glacial periods have a stronger, more intense southern penetration of subpolar waters, as indicated by the presence of *Amphimelissa setosa*. This species is found in Samples 306-U1314B-3H-CC and 306-U1314C-1H-CC and 3H-CC. Today it inhabits cold arctic/subarctic water masses, so when present at Site U1314, it indicates a more intensive southward penetration of these water masses. Additionally, the numbers of different Spongodiscidae species, *Pseudodictyophimus gracilipes* (at least four varieties), and the percent of *C. davisiana* may help us gain new insight into how water masses changed through time over this site.

Discussion on radiolarian stratigraphy in the North Atlantic

The only stratigraphic scheme for radiolarians in the North Atlantic is proposed by Haslett (1994) based on samples from ODP Site 609. He suggests that the standard tropical radiolarian zones applied in the Indian, Atlantic, and Pacific Oceans can also be applied to the mid-latitude North Atlantic. “It is significant that this same zonation is also applicable to the Atlantic, thus offering a standard cosmopolitan Neogene zonation enabling correlation throughout the world’s ocean” (Haslett, 1994). We are of the opinion that the low-latitude radiolarian zonation cannot be applied to the high northern latitudes, due to missing key boundary markers, as discussed below. Haslett (1994) recognizes the following low-latitude zones mainly based on the biostratigraphic assemblages that occur within each zone and not on the presence of species that define the zonal boundaries.

RN17: *Buccinosphaera invaginata* Taxon Range Zone (Nigrini, 1971)

Base: FO *B. invaginata* (0.18 Ma)

Remarks: *B. invaginata* is very rare in the equatorial Atlantic and has so far not been observed in the North Atlantic sites studied.

RN16: *Collosphaera tuberosa* Interval Zone (Nigrini, 1971)

Top: FO *B. invaginata* (0.18 Ma)

Base: LO *Stylatractus universus* (0.42 Ma)

Remarks: *C. tuberosa* is present in the equatorial Atlantic but rare in the North Atlantic, as documented with our observation that only a few individuals of this species have been identified in the Expedition 306 material.

Haslett (1994) was not able to separate these two zones, as the species defining them were not present, which is in accordance to our Expedition 306 observations.

RN15: *S. universus* Concurrent Range Zone (Caulet, 1979)

Top: LO *S. universus* (0.42 Ma)

Base: FO *C. tuberosa* (0.47–0.61 Ma)

Remarks: Hays (1965) described *S. universus* and used it as a stratigraphic marker in the Antarctic. It has since been applied as a stratigraphic marker in most ocean basins due to its cosmopolitan distribution. *S. universus* was listed by Westberg-Smith and Riedel (1984) in their range chart (table 1) in the North Atlantic DSDP Site 552A (pl. 1, fig. 7). They did not suggest any radiolarian biostratigraphy for this site, but their



table 1 shows its LO in Sample 81-552A-2R-2, 122–123 cm. Similarly, Westberg-Smith et al. (1987) showed that the LO of *S. universus* was between Samples 94-609-3R-3, 40–42 cm, and 4H-2, 40–42 cm (0.25–0.56 Ma), thus marking the base of the RN16 Zone.

In the nine holes drilled during Expedition 306, we frequently observed “*Stylatractus universus*” as illustrated in Westberg-Smith and Riedel (1984). This is not *S. universus* as originally described by Hays (1965) and later used in North Pacific stratigraphy (Hays, 1970; Kling, 1973). The specimen illustrated by Westberg-Smith and Riedel (1984) is actually a *Druppatractus* species, probably *D. irregularis* (Popofsky).

RN14: Amphilhopalum *ypsilone* Interval Zone (Nigrini, 1971)

Top: LO *C. tuberosa* (0.47–0.61 Ma)

Base: LO *Anthocyrtidium angulare* (1.10–1.12 Ma)

Remarks: The species that defines the RN14 Zone are both absent in the Site 609 material, and we have not yet found them in our Expedition 306 material. Haslett (1994) states that the LO of *Anthocyrtidium nosicae* and the FO of *Lamprocyrtis hertwigi* occur in this zone, the latter close to the base of the *A. ypsilon* Zone. We therefore also question the application of this zone.

RN13: *A. angulare* Interval Zone (Nigrini, 1971)

Top: LO of *A. angulare* (1.10–1.12 Ma)

Base: LO of *Pterocanium prismaticum* (1.65–1.74 Ma)

Remarks: Again Haslett (1994) states that the key markers are missing in the Site 609 material, but the LO of *Lamprocyrtis neoheteroporus* was encountered, an event that occurs in this zone. This is also reflected in our preliminary Expedition 306 results, and we have no reason to believe that this zone can be defined, especially since its application seems vague.

RN12b: *P. prismaticum* Interval Subzone (Riedel and Sanfilippo, 1970)

Top: LO of *P. prismaticum* (1.65–1.74 Ma)

Base: LO of *Stichocorys peregrina* (2.74–2.78 Ma)

Remarks: Neither of these two zonal markers were found by Haslett (1994), so neither the top nor the base of the zone was defined. We could not document the presence of the key marker species of this zone in the Expedition 306 results.

Haslett (1994) applied the low-latitude radiolarian biostratigraphic scheme to the mid-latitude North Atlantic. His zonal scheme, however, has two prob-

lems. The first is most of the species used to define zonal boundaries are not present. The second is the occurrence of species living in low latitudes is strongly affected by paleoceanographic conditions in the mid-latitudes, so we cannot detect the real FO or LO of those species. At the three Expedition 306 sites, we encountered some age-diagnostic species in the lower-latitude sites (*Collospiraera tuberosa*, *P. hertwigi*, and *S. pregrina*); however, their occurrences are sparse and the FO or LO of these species is not reliable compared to other microfossils. The radiolarian stratigraphy proposed by Haslett (1994) has to be more carefully tested. The Expedition 306 results show that only trace and spotty occurrences of several key marker species for the Pliocene–Pleistocene radiolarian zones could be identified. We think that a local radiolarian zonation based on species that really occur in the sediments will give the best and most reliable results. During our shore-based study we will develop a biostratigraphy that is based on existing species, which will be directly calibrated to the geomagnetic polarity timescale (Cande and Kent, 1995).

Radiolarian zones, a comparison: North Pacific–North Atlantic

The standard low-latitude radiolarian biostratigraphy cannot be applied in the North Pacific and therefore Hays (1970) used the *Eucyrtidium tumidulum* Zone for the uppermost radiolarian zone, whereas Kling (1973) decided to use the *Artostrobium miralestensis* Zone and Foreman (1975) devised a third alternative, the *Artostrobium tumidulum* Zone. Each zone utilizes the same marker species. Nigrini (1977) ended the taxonomic discussion by introducing the *Botryostrobus aquilonaris* Zone (also using the same species). She stated that the base of this zone is defined by the morphotypic last appearance of *S. universus* and is coincident with the upper limit of the *S. universus* Zone. Robertson (1975) stated that at present *B. aquilonaris* is most abundant north of 40°N in the Pacific, whereas its abundance during the Last Glacial Maximum was significantly reduced. This species is also present in the North Atlantic and has been recovered in all of our Expedition 306 holes. The species is easy to recognize but probably has no stratigraphic application in the North Atlantic. It is present throughout the entire Pliocene–Pleistocene section recovered, and therefore it has no biostratigraphic potential. Its abundance through time may fluctuate, however, probably increasing in glacial times due to its cold-water affinity, in contrast to the Pacific, where it decreases in number during glacials. This has to be tested during our shore-based study.



We found it opportune to comment on the radiolarian stratigraphy that at present is available from the North Atlantic and stress that we had difficulties identifying the RN zones as suggested by Haslett (1994). These zones were redefined by Sanfilippo and Nigrini (1998). We agree with Sanfilippo and Nigrini (1998) that the North Atlantic requires a regional radiolarian zonation. For consistency we will follow the recommendation by Sanfilippo and Nigrini (1998) to use the following notation in our stratigraphic scheme for the North Atlantic: RN (N. Atl)–*Genus species* zone type. As we are only working with the uppermost part of the Neogene, it is not possible for us to allocate a zone number at this stage.

Above, we outlined the problems we are facing, but during shore-based studies we hope to provide a better understanding of radiolarian associations and how they reflect different paleoecological (paleoceanographical) conditions, as well as a stratigraphic scheme for the Pliocene–Pleistocene sediments recovered during Expedition 306.

Paleomagnetism

Archive halves of all cores recovered at Site U1314 were measured on the three-axis cryogenic magnetometer at 5 cm intervals. The natural remanent magnetization (NRM) was measured before (NRM step) and after stepwise alternating-field (AF) demagnetization in peak fields of up to 20 mT. Cores 306-U1314A-1H through 13H and 17H through 20H were AF demagnetized at peak fields of 10 and 20 mT. All other cores were AF demagnetized at a peak field of 20 mT.

Downcore variations in magnetic intensity in Holes U1314A–U1314C are shown in Figure F18. Data associated with intervals identified as physically disturbed were removed. NRM intensities after 20 mT AF demagnetization are in the range of 10^{-1} to 10^{-2} A/m. These values are much higher than at Sites U1312 and U1313, indicating a higher content of detrital magnetic minerals. Inclination and declination data (after 20 mT AF demagnetization) are shown in Figure F19. Declination values have been corrected using Tensor tool data, which were available starting with Cores 306-U1314A-4H, 306-U1314B-4H, and 306-U1314C-3H. All holes display similar directional changes.

The distribution of inclination values at Site U1314, after AF demagnetization at 20 mT, is composed of two log-normal distributions centered at -66° and $+68^{\circ}$. These values are close to the expected site values for a geocentric axial dipole ($I_{GAD} = \pm 71.6^{\circ}$). These results indicate that most of the drill string overprint was removed at 20 mT, although a small overprint

may remain in some intervals as the distributions are slightly skewed toward more positive values.

The magnetostratigraphy was constructed based on the succession of polarity reversals recorded at Site U1314 (Fig. F20). The Brunhes/Matuyama reversal, the Jaramillo and Olduvai Subchrons, and the Matuyama/Gauss reversal are well recorded in these sediments. Site U1314 also provides a good record of shorter geomagnetic events such as Cobb Mountain and Reunion. The Brunhes/Matuyama reversal occurs at 57.3 ± 0.1 mbsf in Hole U1314A, 56.6 ± 0.1 mbsf in Hole U1314B, and 57.7 ± 0.1 mbsf in Hole U1314C. The occurrence depths of the polarity transitions identified at Site U1314 and their possible correlation to the geomagnetic polarity timescale (Cande and Kent, 1995) are detailed in Table T18. The resulting age model is consistent with the biostratigraphy (see “[Biostratigraphy](#)”). The deepest magnetic polarity interval recorded at Site U1314 corresponds to the top normal interval of the Gauss Subchron (2An.1n). Core recovery could not reach the underlying polarity interval (Subchron 2An.1r, or Kaena, dated at 3.04 Ma), but extrapolation of the magnetostratigraphy-based age model suggests an age close to 3 Ma for the bottom of Hole U1314B.

Stratigraphic correlation

The upper 10–12 cores of all holes drilled at Site U1314 were measured for magnetic susceptibility at 5 cm resolution using the “Fast Track” magnetic susceptibility core logger (MSCL) soon after recovery. Initial correlation based on these data was used to monitor the coring breaks and ensure that they did not coincide for any two holes. It was confirmed that depth offsets between the holes were large enough to fill coring gaps, and subsequently, correlation based on MSCL measurements did not influence coring operations.

The final meters composite depth (mcd) scale (Table T19) and a spliced stratigraphic section (Table T20) were constructed after gamma ray attenuation (GRA) density, natural gamma radiation (NGR), magnetic susceptibility, magnetic intensity and inclination, and color reflectance data became available. Coring deformation as the result of large ship heave experienced during operations was severe in much of the upper portion of Hole U1314A, particularly in Cores 306-U1314A-2H, 5H, 6H, and 12H, but also in other intervals (Table T21). Weather conditions were more favorable during coring in Holes U1314B and U1314C, resulting in excellent core quality.

Prior to uploading the data into Splicer for correlation, we removed those intervals that contained coring disturbance or voids. Each of these cleaned data



sets shows prominent amplitude variations related to changes in lithology. For depth-shifting the cores from Site U1314, we relied mainly on between-hole correlation of distinctive magnetic susceptibility and NGR variations (Figs. F21, F22, F23). These correlations were confirmed to be consistent with geomagnetic polarity reversals recorded in the paleomagnetic inclination (Fig. F20).

Apart from a single problematic interval with a tenuous tie between Core 306-U1314C-3H and Core 306-U1314B-4H at 25.90 mcd, correlation was straightforward, the mcd scale was well resolved, and the spliced section was complete to 281 mcd. Because of the core disturbance in the upper part of Hole U1314A, the splice in the interval 0–188.30 mcd was built from Holes U1314B and U1314C, with the exception of a short interval (65.80–69.50 mcd), where an undisturbed section of Core 306-U1314A-8H was incorporated into the composite section (Table T20). From 188.30 to 300 mcd the splice was constructed from Holes U1314A and U1314B because Hole U1314C was drilled only to 222 mcd. The two deepest cores, 306-U1314B-29H and 30H (interval not cored in Holes U1314A and U1314C), were appended to the splice (Figs. F21, F22, F23). A growth factor of 1.08 is calculated by linear regression for the three holes at Site U1314, indicating an 8% increase in mcd relative to mbsf.

Unlike the previous two sites, the lightness variations do not correlate as well with the oxygen isotope stack of Lisiecki and Raymo (2005), nor do the sediments at Site U1314 have the large changes in lightness that were obvious at Sites U1312 and U1313. Instead, the color varies mainly through shades of greens and grays with some lighter intervals (cycles) occurring mainly in the upper 70 mcd.

Geochemistry

Inorganic geochemistry

Interstitial water chemistry

A total of seven interstitial water samples were extracted from 5 cm whole-round sediment sections from Hole U1314A with a resolution of one sample per core for the first five cores and thereafter one sample per core from Cores 306-U1314A-9H and 12H, covering a depth of 102.9 mbsf. Interstitial water samples were processed for routine shipboard geochemical analyses (see “[Geochemistry](#)” in the “Site U1312–U1315 methods” chapter). The concentrations of dissolved elements from Hole U1314A are given in Table T22, and their downhole profiles are illustrated in Figure F24. Three samples from Cores 306-U1314A-2H, 6H, and 12H appeared to be dis-

turbed by flow-in during coring (see “[Stratigraphic correlation;](#)” Table T21) and are identified by open circles in Figure F24. Like in Hole U1312A, the visually apparent disturbance in these sediment sections appears not to have affected the overall downhole pattern of the pore water chemistry. However, data from the undisturbed sections are the only ones used for the description.

Chlorinity, salinity, alkalinity, and pH

Chloride (Cl^-) concentrations in Hole U1314A range from ~540 to ~586 mM between 17.4 and 74.4 mbsf (Fig. F24A). The highest Cl^- value was measured at 74.4 mbsf.

The downhole salinity value of 34 g/kg prevails to 26.9 mbsf then decreases to 33 g/kg at 36.4 mbsf. The lowest salinity of 32 g/kg was measured at 74.4 mbsf (Fig. F24B).

Alkalinity increases from 5.38 to 7.46 mM between 17.4 and 74.4 mbsf (Fig. F24C). These values are similar to those reported from Site U1313 but lower than those reported from Site U1304 (see “[Geochemistry](#)” in the “Site U1304” chapter).

pH values in Hole U1314A range from 7.41 to 7.56 between 17.4 and 74.4 mbsf (Fig. F24D). These values are more or less similar to those reported from Sites U1312 and U1313 as well as from Site U1304 (see “[Geochemistry](#)” in the “Site U1304” chapter).

Sodium, potassium, magnesium, and calcium

Calcium (Ca^{2+}), potassium (K^+), and magnesium (Mg^{2+}) concentrations range from 8.4 to 5.2, 12.4 to 10.5, and 48.7 to 37.4 mM, respectively, and their downhole profiles show roughly similar decreasing trends with depth (Fig. F24F, F24G, F24H). Na^+ concentrations range from ~494 to ~446 mM throughout the profile and show a similar pattern as Cl^- (Fig. F24E).

Iron, boron, barium, lithium, manganese, and strontium

Iron (Fe^{2+}) concentrations in Hole U1314A increase from 25.5 to 31.8 μM between 17.4 and 26.9 mbsf and then decrease sharply to 6.5 μM at 36.4 mbsf (Fig. F24I). The lowest value of 6.5 μM is measured within a lithologic interval displaying darker and black streaks, suggesting the presence of diagenetic iron minerals. An Fe^{2+} concentration of 22.8 μM is measured at 74.4 mbsf.

Boron (B) concentrations, mostly as boric acid (H_3BO_3), increase between ~440 and 465 μM from 17.4 to 36.4 mbsf (Fig. F24J). A boron value of 457 μM is measured at 74.4 mbsf. Barium (Ba^{2+}) concentrations range from 17 to 18.3 μM throughout the



profile (Fig. F24K). Highest Ba²⁺ values are measured at this site in comparison to Sites U1312 and U1313. The lithium (Li⁺) and strontium (Sr²⁺) concentrations in Hole U1314 increase slightly with depth (Fig. F24L, F24N). Sr²⁺ is usually expelled in the pore water from the carbonate constituents in the sediments during their dissolution and reprecipitation. This is one hypothesis for the downhole increase of Sr²⁺ (Baker et al., 1982; De Carlo, 1992). It may be mentioned here that the Sr²⁺ values are 2–4 times lower than those measured at Sites U1312 and U1313, and in general the overall carbonate values are lower as well (see below).

Manganese (Mn²⁺) concentrations sharply decrease from 46.8 to 15.9 µM between 17.4 and 36.4 mbsf. However, they remain uniform from 36.4 to 74.4 mbsf (Fig. F24M).

Dissolved silica, sulfate, and ammonium

Dissolved silica (H₄SiO₄) concentrations show a downhole increasing trend (Fig. F24O). The highest dissolved silica concentration of 570 µM is measured at 74.4 mbsf and likely reflects the initial presence of biogenic silica in the sediments and its subsequent dissolution.

Sulfate (SO₄²⁻) concentrations range from 20.5 to 1.1 mM between 17.4 and 74.4 mbsf (Fig. F24P). However, both high and low SO₄²⁻ values of 20.5 and 1.1 mM are measured at 17.4 and 26.9 mbsf, respectively.

Ammonium (NH₄⁺) concentrations increase from 0 to 14.7 µM between 17.4 and 74.4 mbsf (Fig. F24P). These concentrations are almost 10 times lower than those measured in the pore water from Hole U1313A.

Organic geochemistry

Volatile hydrocarbons

A total of 27 headspace samples from Hole U1314A with a sample resolution of one sample per core were analyzed (Table T23). With the exception of one sample from 178.9 mbsf, methane was the only hydrocarbon gas detected in this hole. Concentrations of CH₄ in Hole U1314A range from 1.3 to 4.8 ppmv (average = 2.2 ppmv), which is slightly higher than atmospheric background level. Although overall low, a subsurface increase toward ~5 ppmv between 36.4 and 45.9 mbsf and a subsequent decrease to average values below ~50 mbsf is notable (Fig. F25). CH₄ concentrations slightly above the average also occur at 178.9 and ~250 mbsf. At 178.9 mbsf, ethane (C₂ = 1.9 ppmv) and ethene (C₂₌ = 1.95 ppmv) were also detected.

Sedimentary bulk geochemistry

Sediment samples for the analysis of solid-phase inorganic carbon, total organic carbon (TOC), and total nitrogen (TN) were collected from the working halves in Hole U1314A at a resolution of two samples per core. In addition, splits of squeeze cakes from interstitial water samples were also used for bulk measurements to investigate solvent-extractable organic matter (see below). Data for the bulk geochemical analysis were performed on a total number of 62 samples as shown in Table T24 (see “Geochemistry” in the “Site U1312–U1315 methods” chapter for analytical methods and the derivation of TOC values).

CaCO₃ contents in Hole U1314A range from 3.7 to 70.5 wt% (average = 34.1 wt%). A ±20–30 wt% variability around the average persists throughout the profile. Overall, the average carbonate concentration increased from ~20 wt% at 250 mbsf to a mean of ~40 wt% CaCO₃ at the seafloor (Fig. F26A). The comparison of CaCO₃ and color reflectance data (L*) at expanded depth scale (Fig. F26B) shows a nearly perfect correlation between these two, implying that the carbonate content is mainly controlling the variability in the lightness profile.

TOC and TN contents range from 0 to 0.5 wt% and 0.09 to 0.22 wt%, respectively, in sediments of Hole U1314A (Fig. F27). Overall, TOC contents from Hole U1314A are slightly higher compared to Sites U1312 and U1313, even though the maximum TOC is lower at Site U1314. Fluctuations in TOC of 0.2 wt% are present throughout the downcore profile. It appears that these fluctuations might be superimposed on an overall variability at low frequency as shown by the shaded area in Figure F27 (left panel). Furthermore, a correlation between TOC and magnetic susceptibility data is obvious (Fig. F28). The relatively high susceptibility is explained by the presence of more magnetic minerals probably caused by increased terrigenous input (see “Physical properties”). Thus, the covariance of TOC and susceptibility can be explained by the dominance of terrigenous organic matter. Indeed, this explanation is in accordance with molecular analysis of extractable organic compounds (see below), at least as observed for the upper ~100 m of the hole.

Extractable organic matter sources

In Hole U1314A, eight samples were used for an initial investigation of the solvent-extractable matter (Table T25). As for Site U1313, the flame ionization detector (FID) installed on the gas chromatograph had to be used for compound detection instead of the mass spectrometer. However, the use of the FID allowed us to obtain a visual overview of the extract-



able compound inventory and to identify its major constituents (see “Geochemistry” in the “Site U1312–U1315 methods” chapter). Extractable organic matter (EOM) from Hole U1314A consists mainly of the same compounds as found at Site U1313, namely a series of *n*-alkanes in a carbon atom number range of ~C₂₀–C₃₃ and homologs of C₃₇–C₃₉ unsaturated methyl and ethyl ketones (alkenones). Differences in relative proportions of these compound classes, as illustrated in Figure F29, can be used for an initial organic matter characterization in terms of terrigenous versus marine sources. See “Geochemistry” in the “Site U1313” chapter for details on the origin of these compound classes and the derivation of marine and terrigenous EOM proportions, and “Geochemistry” in the “Site U1312–U1315 methods” chapter for methodology. From this initial characterization it appears that all Pleistocene samples from Hole U1314A show relatively high proportions (~65%–90%) of terrigenous EOM except a single sample from the late Pliocene that shows a relatively higher marine proportion (Fig. F30).

Alkenone-derived sea-surface temperatures

As for Site U1313, alkenone-derived sea-surface temperatures (SSTs) were calculated for Hole U1314A. The available preliminary SSTs range from 9.7° to 13.5°C (Table T25) and are comparable to modern ocean-atlas annual mean SSTs in the relevant area. However, these initial SST data show a lower temperature variability (3.8°C) than the ~6°C difference between modern and Last Glacial Maximum SST obtained by foraminiferal transfer functions in this area of the North Atlantic (Pflaumann et al., 2003). One possible explanation for this discrepancy could be that none of the limited (and randomly chosen) shipboard samples originates from a full glacial interval.

Physical properties

Physical property measurements were carried out at Site U1314 following the procedures described in “Physical properties” in the “Site U1312–U1315 methods” chapter. These measurements provide important information about processes related to lithology and stratigraphic correlation. Magnetic susceptibility measurements were made with both the MSCL and the multisensor track (MST) system. Additionally, GRA density and NGR were measured with the MST. Discrete *P*-wave velocities were measured (*P*-wave sensor number 3 [PWS3]—measuring perpendicular to the core axis) on each section, and moisture and density measurements were measured on

two discrete samples per core, usually at the bottom of the first and sixth sections.

Whole-core magnetic susceptibility measurements

The magnetic susceptibility records derived during coring operations at Site U1314 (Fig. F31) show a highly variable record attributed to lithologic and/or mineralogic changes and show multiple excursions toward high values generally associated with IRD layers. Values of magnetic susceptibility are generally between 100 and 500 (0 and 0.03 SI units). These relatively high values are due to a higher magnetic content of these cores associated with the high fraction of terrigenous material. Values increase somewhat downhole. Below ~230 mbsf there is a distinctive change in the frequency content of the signal in Holes U1314A and U1314B.

GRA density

Sediments from Site U1314 show a general increase in bulk density downcore, consistent with a downcore increase in compaction and decrease in water content (Fig. F32). GRA density values vary between 1.3 and 1.5 g/cm³ and are consistent with discrete bulk density values (Fig. F33). Superimposed on this downhole increase in bulk density are fluctuations that may correspond to pebble layers or large clasts (>2 cm) in the core (see “Lithostratigraphy”).

Density and porosity

Bulk and grain density and porosity values estimated from Hole U1314A are shown in Figure F33. Grain density values are relatively uniform with an average value of ~2.7 g/cm³. Porosity decreases downcore from ~80% to 70%. Bulk density and porosity are inversely correlated consistent with the effects of compaction and decreasing water content.

P-wave velocity

P-wave velocities range between 1460 and 1564 m/s (Fig. F34). In Hole U1314A, velocity records from the MST (*P*-wave logger) and the split-core measurements (PWS3) are in general agreement except for a section between 90 and 120 mbsf, which is not understood.

Natural gamma radiation

Natural gamma radiation provides a means of evaluating the relative clay content of the sediments. NGR counts range from 15 to 30 cps, (Fig. F35). NGR counts are positively correlated with trends observed in magnetic susceptibility and GRA density data.



Discussion

Sediments cored at Site U1314 are composed of both terrigenous and biogenic material (see “[Lithostratigraphy](#)”). Changes in physical properties generally reflect variations in the relative amounts of these components. NGR counts, *P*-wave velocity, bulk density, and magnetic susceptibility are positively correlated. Large positive excursions in these properties may be attributed to IRD layers.

References

- Andersen, C., Koç, N., and Moros, M., 2004. A highly unstable Holocene climate in the subpolar North Atlantic: evidence from diatoms. *Quat. Sci. Rev.*, 23:2155–2166. [doi:10.1016/j.quascirev.2004.08.004](https://doi.org/10.1016/j.quascirev.2004.08.004)
- Andruleit, H.A., and Baumann, K.-H., 1998. History of the Last Deglaciation and Holocene in the Nordic seas as revealed by coccolithophore assemblages. *Mar. Micropaleontol.*, 35:179–201. [doi:10.1016/S0377-8398\(98\)00021-8](https://doi.org/10.1016/S0377-8398(98)00021-8)
- Baker, P.A., Gieskes, J.M., and Elderfield, H., 1982. Diagenesis of carbonates in deep-sea sediments—evidence from Sr²⁺/Ca²⁺ ratios and interstitial dissolved Sr²⁺ data. *J. Sediment. Petrol.*, 52:71–82.
- Baldauf, J.G., 1987. Biostratigraphic and paleoceanographic interpretation of lower and middle Miocene sediments, Rockall Plateau Region, North Atlantic Ocean. In Ruddiman, W.F., Kidd, R.B., Thomas, E., et al., *Init. Repts. DSDP*, 94 (Pt. 2): Washington (U.S. Govt. Printing Office), 1033–1043.
- Bond, G.C., and Lotti, R., 1995. Iceberg discharges into the North Atlantic on millennial time scales during the last glaciation. *Science*, 276:1005–1010.
- Bond, G.C., Showers, W., Elliot, M., Evans, M., Lotti, R., Hajdas, I., Bonani, G., and Johnson, S., 1999. The North Atlantic’s 1–2 kyr climate rhythm: relation to Heinrich events, Dansgaard/Oeschger cycles and the Little Ice Age. In Clark, P.U., Webb, R.S., and Keigwin, L.D. (Eds.), *Mechanisms of Global Climate Change at Millennial Time Scales*. Geophys. Monogr., 112:35–58.
- Cande, S.C., and Kent, D.V., 1995. Revised calibration of the geomagnetic polarity timescale for the Late Cretaceous and Cenozoic. *J. Geophys. Res.*, 100:6093–6095. [doi:10.1029/94JB03098](https://doi.org/10.1029/94JB03098)
- Caulet, J.-P., 1979. Les dépôts à radiolaires d’âge Pliocène supérieur à Pleistocene dans l’océan Indien central: nouvelle zonation biostratigraphique (Radiolarian upper Pliocene–Pleistocene deposits in the central Indian Ocean; new biostratigraphic zonation). *Mem. Mus. Natl. Hist. Nat. Ser. C*, 43:119–141.
- Channell, J.E.T., Hodell, D.A., McManus, J., and Lehman, B., 1998. Orbital modulation of the Earth’s magnetic field intensity. *Nature (London, U.K.)*, 394:464–468. [doi:10.1038/28833](https://doi.org/10.1038/28833)
- Channell, J.E.T., Sato, T., Kanamatsu, T., Stein, R., Malone, M.J., and the Expedition 303/306 Project Team, 2004. North Atlantic climate. *IODP Sci. Prosp.*, 303/306. [doi:10.2204/iodp.sp.303306.2004](https://doi.org/10.2204/iodp.sp.303306.2004)
- Chapman, M.R., and Shackleton, N.J., 1999. Global ice-volume fluctuations, North Atlantic ice-raftering events, and deep-ocean circulation changes between 130 and 70 ka. *Geology*, 27:795–798. [doi:10.1130/0091-7613\(1999\)027<0795:GIVFNA>2.3.CO;2](https://doi.org/10.1130/0091-7613(1999)027<0795:GIVFNA>2.3.CO;2)
- Davies, T.A., and Laughton, A.S., 1972. Sedimentary processes in the North Atlantic. In Laughton, A.S., Berggren, W.A., et al., *Init. Repts. DSDP*, 12: Washington (U.S. Govt. Printing Office), 905–934.
- De Carlo, E.H., 1992. Geochemistry of pore water and sediments recovered from the Exmouth Plateau. In von Rad, U., Haq, B.U., et al., *Proc. ODP, Sci. Results*, 122: College Station, TX (Ocean Drilling Program), 295–308.
- Flower, B.P., Oppo, D.W., McManus, J.F., Venz, K.A., Hodell, D.A., and Cullen, J., 2000. North Atlantic intermediate to deep water circulation and chemical stratification during the past 1 Myr. *Paleoceanography*, 15:388–403. [doi:10.1029/1999PA000430](https://doi.org/10.1029/1999PA000430)
- Foreman, H.P., 1975. Radiolaria from the North Pacific, Deep Sea Drilling Project, Leg 32. In Larson, R.L., Moberly, R., et al., *Init. Repts. DSDP*, 32: Washington (U.S. Govt. Printing Office), 579–676.
- Haslett, S.K., 1994. Plio–Pleistocene radiolarian biostratigraphy and paleoceanography of the mid-latitude North Atlantic (DSDP Site 609). *Geol. Mag.*, 131:57–66.
- Hays, J.D., 1965. Radiolaria and late Tertiary and Quaternary history of Antarctic seas. In Llano, G.A. (Ed.), *Biology of the Antarctic Seas II*. Antarct. Res. Ser., 5:125–184.
- Hays, J.D., 1970. Stratigraphy and evolutionary trends of radiolaria in North Pacific deep sea sediments. In Hays, J.D. (Ed.), *Geological Investigations of the North Pacific*. Mem.—Geol. Soc. Am., 126:185–218.
- Hayward, B.W., 2001. Global deep-sea extinctions during the Pleistocene ice-ages. *Geology*, 29:599–602. [doi:10.1130/0091-7613\(2001\)029<0599:GDSEDT>2.0.CO;2](https://doi.org/10.1130/0091-7613(2001)029<0599:GDSEDT>2.0.CO;2)
- Jansen, E., Raymo, M.E., Blum, P., et al., 1996. *Proc. ODP Init. Repts.*, 162: College Station, TX (Ocean Drilling Program).
- Johnson, G.L., and Schneider, E.D., 1969. Depositional ridges in the North Atlantic. *Earth Planet. Sci. Lett.*, 6:416–422. [doi:10.1016/0012-821X\(69\)90110-1](https://doi.org/10.1016/0012-821X(69)90110-1)
- Jones, E.J.W., Ewing, M., Ewing, J., and Eittreim, S.L., 1970. Influence of Norwegian Sea overflow water on sedimentation in the northern north Atlantic and Labrador Sea. *J. Geophys. Res.*, 75:1655–1680.
- Kemp, A.E.S., and Baldauf, J.G., 1993. Vast Neogene laminated diatom mat deposits from the eastern equatorial Pacific Ocean. *Nature (London, U.K.)*, 362:141–144. [doi:10.1038/362141a0](https://doi.org/10.1038/362141a0)
- Kissel, C., Laj, C., Labeyrie, L., Dokken, T., Voelker, A., and Blamart, D., 1999. Rapid climatic variations during marine isotopic Stage 3: magnetic analysis of sediments from Nordic Seas and North Atlantic. *Earth Planet. Sci. Lett.*, 171:489–502. [doi:10.1016/S0012-821X\(99\)00162-4](https://doi.org/10.1016/S0012-821X(99)00162-4)



- Kleiven, H.F., Jansen, E., Curry, W.B., Hodell, D.A., and Venz, K., 2003. Atlantic Ocean thermohaline circulation changes on orbital to suborbital timescales during the mid-Pleistocene. *Paleoceanography*, 18. doi:[10.1029/2001PA000629](https://doi.org/10.1029/2001PA000629)
- Kling, S.A., 1973. Radiolaria from the eastern North Pacific, Deep Sea Drilling Project, Leg 18. In: Kulm, L.D., von Huene, R., et al., *Init. Repts. DSDP*, 18: Washington (U.S. Govt. Printing Office), 617–671.
- Koç, N., and Flower, B.P., 1998. High-resolution Pleistocene diatom biostratigraphy and paleoceanography of Site 919 from the Irminger Basin. In: Saunders, A.D., Larsen, H.C., and Wise, S.W., Jr. (Eds.), *Proc. ODP, Sci. Results*, 152: College Station, TX (Ocean Drilling Program), 209–219. [PDF]
- Koç, N., Hodell, D.A., Kleiven, H., and Labeyrie, L., 1999. High-resolution Pleistocene diatom biostratigraphy of Site 983 and correlations with isotope stratigraphy. In: Raymo, M.E., Jansen, E., Blum, P., and Herbert, T.D. (Eds.), 1999. *Proc. ODP, Sci. Results*, 162: College Station, TX (Ocean Drilling Program), 51–62. [HTML]
- Krissek, L.A., and St. John, K.E.K., 2002. Pleistocene iceberg production from East Greenland: synchronous between source areas, but distinct from global ice volume. *Bull. Geol. Soc. Denmark*, 49:79–89.
- Lacasse, C., Carey, S., and Sigurdsson, H., 1998. Volcanogenic sedimentation in the Iceland Basin: influence of subaerial and subglacial eruptions. *J. Volcanol. Geotherm. Res.*, 83:47–73. doi:[10.1016/S0377-0273\(98\)00015-8](https://doi.org/10.1016/S0377-0273(98)00015-8)
- Lisiecki, L.E., and Raymo, M.E., 2005. A Pliocene–Pleistocene stack of 57 globally distributed benthic $\delta^{18}\text{O}$ records. *Paleoceanography*, 20. doi:[10.1029/2004PA001071](https://doi.org/10.1029/2004PA001071)
- Lourens, L.J., Antonarakou, A., Hilgen, F.J., Van Hoof, A.A.M., Vergnaud-Grazzini, C., and Zachariasse, W.J., 1996. Evaluation of the Plio–Pleistocene astronomical timescale. *Paleoceanography*, 11:391–413. doi:[10.1029/96PA01125](https://doi.org/10.1029/96PA01125)
- Martini, E., 1971. Standard Tertiary and Quaternary calcareous nannoplankton zonation. In: Farinacci, A. (Ed.), *Proc. 2nd Int. Conf. Planktonic Microfossils Roma*: Rome (Ed. Tecnosci.), 2:739–785.
- McCave, I.N., and Tucholke, B.E., 1986. Deep current-controlled sedimentation in the western North Atlantic. In: Vogt, P.R., and Tucholke, B.E. (Eds.), *The Western North Atlantic Region*. Geol. Soc. Am., Geol. of North Am. Ser., M:451–468.
- Motoyama, I., 1997. Origin and evolution of *Cycladophora davisiiana* Ehrenberg (Radiolaria) in DSDP Site 192, Northwest Pacific. *Mar. Micropaleontol.*, 30:45–63. doi:[10.1016/S0377-8398\(96\)00047-3](https://doi.org/10.1016/S0377-8398(96)00047-3)
- Murray, J.W., 1991. *Ecology and Palaeoecology of Benthic Foraminifera*: London (Longman).
- Nigrini, C., 1971. Radiolarian zones in the Quaternary of the equatorial Pacific Ocean. In: Funnell, B.M., and Riedel, W.R. (Eds.), *The Micropalaeontology of Oceans*: Cambridge (Cambridge Univ. Press), 443–461.
- Nigrini, C., 1977. Tropical Cenozoic Artostrobidae (Radiolaria). *Micropaleontology*, 23:241–269.
- Pflaumann, U., Sarnthein, M., Chapman, M., de Abreu, L., Funnell, B., Huels, M., Kiefer, T., Maslin, M., Schulz, H., Swallow, J., van Kreveld, S., Vautravers, M., Vogelsang, E. and Weinelt, M., 2003. Glacial North Atlantic: Sea-surface conditions reconstructed by GLAMAP 2000. *Paleoceanography*, 18(3). doi:[10.1029/2002PA00074](https://doi.org/10.1029/2002PA00074)
- Raymo, M., Ganley, K., Carter, S., Oppo, D.W., and McManus, J., 1998. Millennial-scale climate instability during the early Pleistocene epoch. *Nature (London, U.K.)*, 392:699–702. doi:[10.1038/33658](https://doi.org/10.1038/33658)
- Riedel, W.R., and Sanfilippo, A., 1970. Radiolaria, Leg 4, Deep Sea Drilling Project. In: Bader, R.G., Gerard, R.D., et al., *Init. Repts. DSDP*, 4: Washington (U.S. Govt. Printing Office), 503–575.
- Robertson, J.H., 1975. Glacial to interglacial oceanographic changes in the northwest Pacific, including a continuous record of the last 400,000 years [Ph.D. dissertation]. Columbia Univ., New York.
- Ruddiman, W.F., 1977. Late Quaternary deposition of ice rafted sand in the subpolar North Atlantic (Lat 40°N to 65°N). *Geol. Soc. Am. Bull.*, 88:1813–1827.
- Sanfilippo, A., and Nigrini, C., 1998. Code numbers for Cenozoic low latitude radiolarian biostratigraphic zones and GPTS conversion tables. *Mar. Micropaleontol.*, 33:109–117. doi:[10.1016/S0377-8398\(97\)00030-3](https://doi.org/10.1016/S0377-8398(97)00030-3)
- Sato, T., Kameo, K., and Mita, I., 1999. Validity of the latest Cenozoic calcareous nannofossil datums and its application to the tephrochronology. *Earth Sci.*, 53:265–274.
- Tiedemann, R., Sarnthein, M., and Shackleton, N.J., 1994. Astronomic timescale for the Pliocene Atlantic $\delta^{18}\text{O}$ and dust flux records of Ocean Drilling Program Site 659. *Paleoceanography*, 9:619–638.
- Weaver, P.P.E., and Clement, B.M., 1987. Magnetobiostratigraphy of planktonic foraminiferal datums, DSDP Leg 94, North Atlantic. In: Ruddiman, W.F., Kidd, R.B., Thomas, E., et al., *Init. Repts. DSDP*, 94: Washington (U.S. Govt. Printing Office), 815–829.
- Westberg-Smith, M.J., and Riedel, W.R., 1984. Radiolarians from the western margin of the Rockall Plateau: Deep Sea Drilling Project Leg 81. In: Roberts, D.G., Schnitker, D., et al., *Init. Repts. DSDP*, 81: Washington (U.S. Govt. Printing Office), 479–501.
- Westberg-Smith, M.J., Tway, L.E., and Riedel, W.R., 1987. Radiolarians from the North Atlantic Ocean, Deep Sea Drilling Project Leg 94. In: Ruddiman, W.E., Kidd, R.B., and Thomas, E., et al. (Eds.), *Init. Repts. DSDP*, 94: Washington (U.S. Govt. Printing Office), 763–777.

Publication: 9 September 2006
MS 306-113



Figure F1. Location of Site U1314 (proposed Site GAR-1B) on the southern Gardar Drift, North Atlantic. In addition, locations of ODP Sites 983 and 984 and Expedition 306 Sites U1312 and U1313 are shown in the overview map.

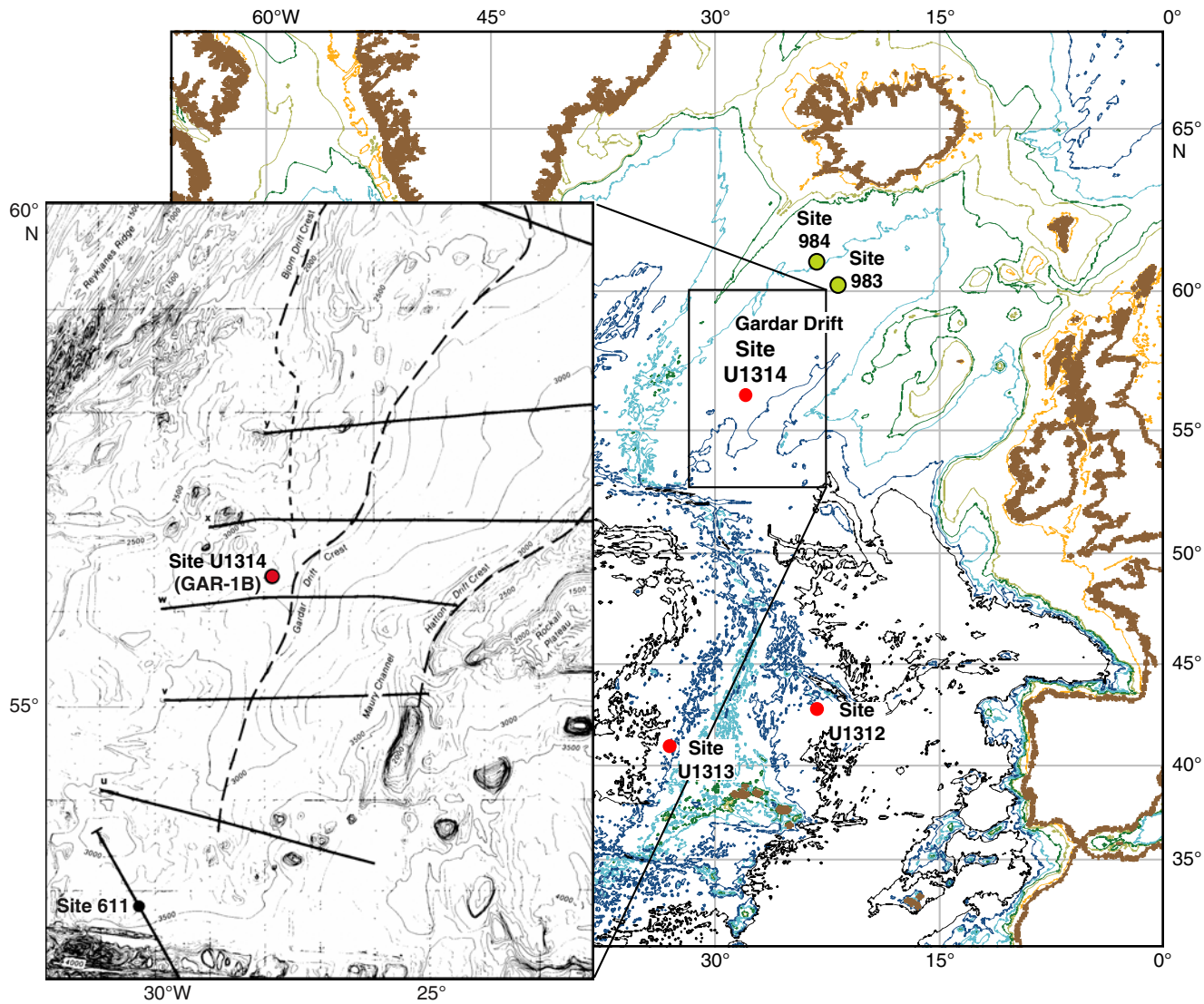


Figure F2. Southeast–northwest multichannel seismic profile across location of Site U1314 (from Channell et al., 2004). CDP = common depth point.

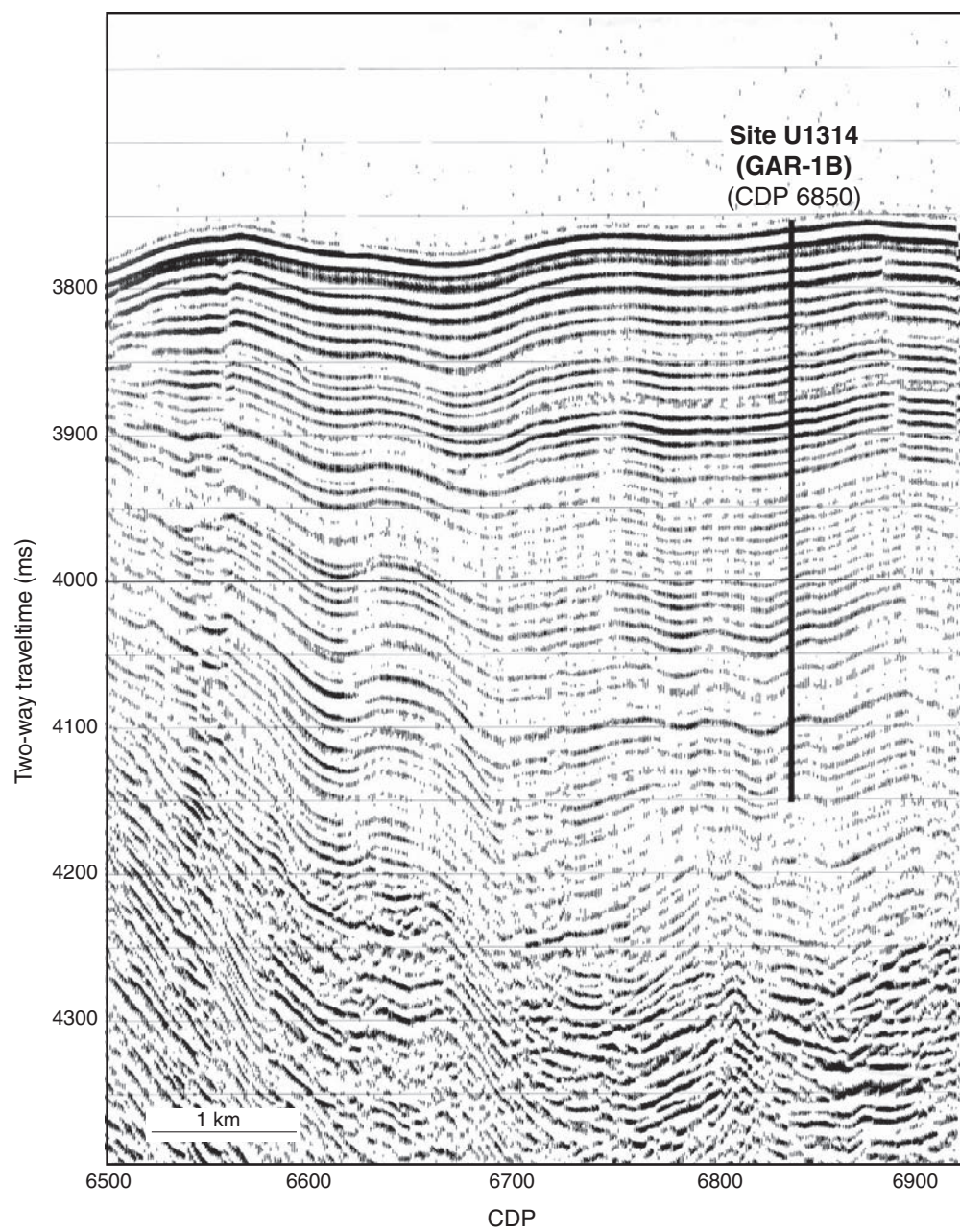


Figure F3. 3.5 kHz high-resolution profile across the location of Site U1314 (from Channell et al., 2004).

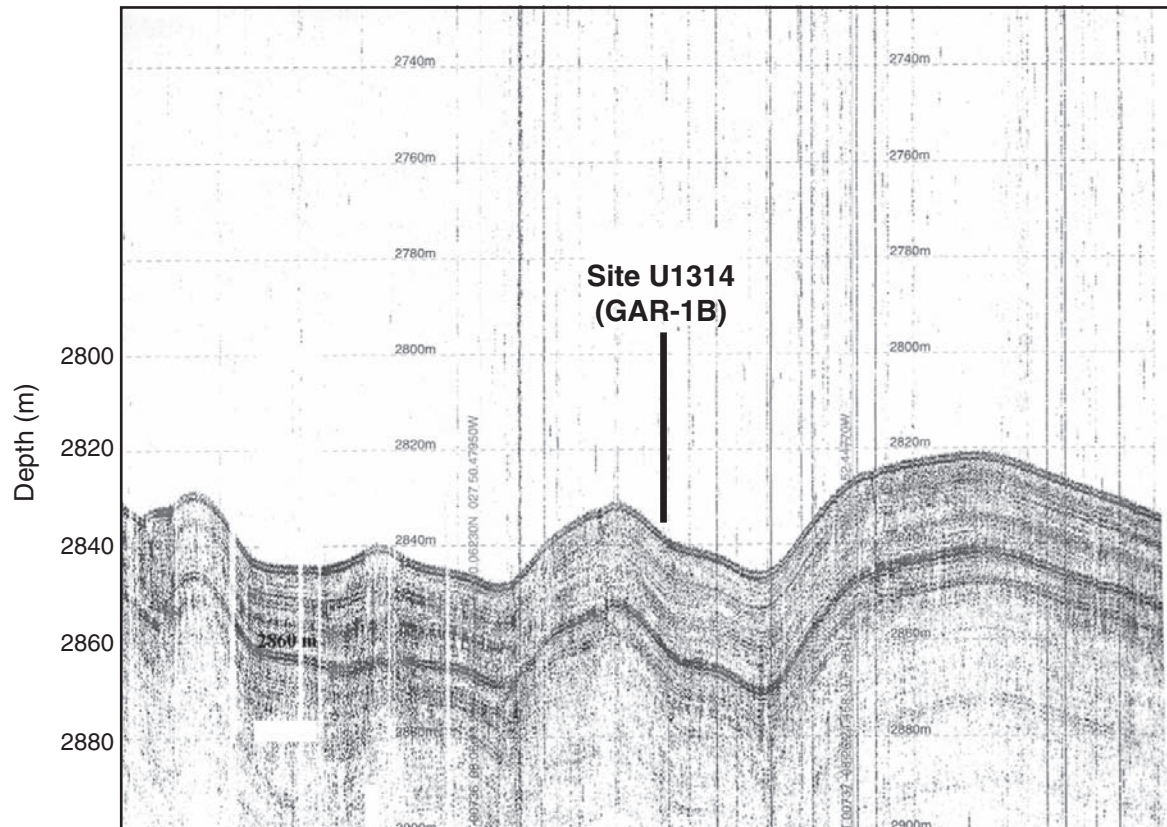


Figure F4. A. Benthic $\delta^{18}\text{O}$ record of Tiedemann et al. (1994) from ODP Site 659 in the eastern equatorial Atlantic; a proxy for paleoclimate and sea level fluctuations for the past 5 m.y. Pliocene and Pleistocene climate transitions are highlighted by shading. B. New high-resolution benthic $\delta^{18}\text{O}$ record from ODP Site 983 (solid line) plotted vs. the benthic $\delta^{18}\text{O}$ record from Site 659 (dashed line) for comparison across the mid-Pleistocene (0.7–1.2 Ma). Interglacial stages are labeled (from Kleiven et al., 2003). C. *wuellerstorffi* = *Cibicidoides wuellerstorffi*.

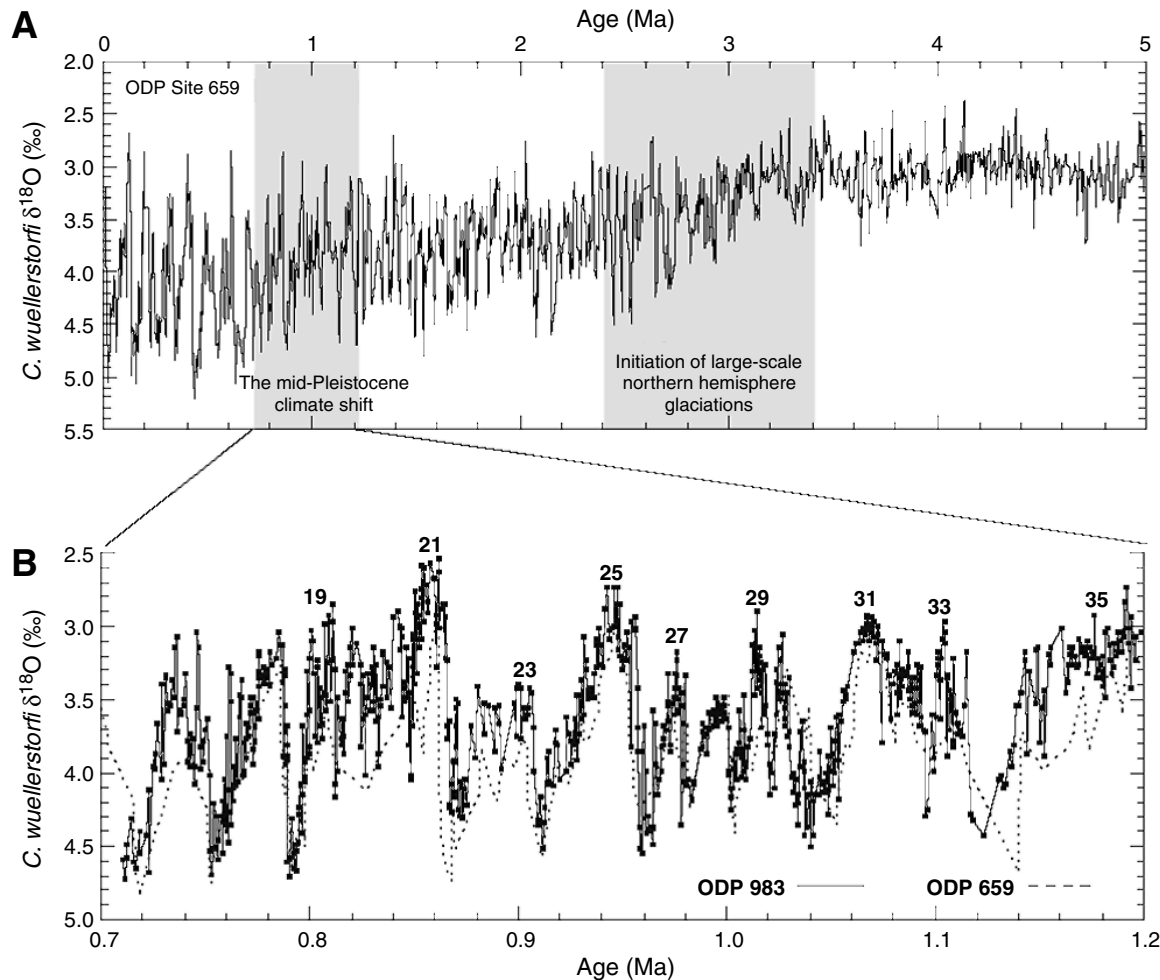


Figure F5. Schematic summary of core recovery at Site U1314 along with the lithologic unit and the lithologies recovered.

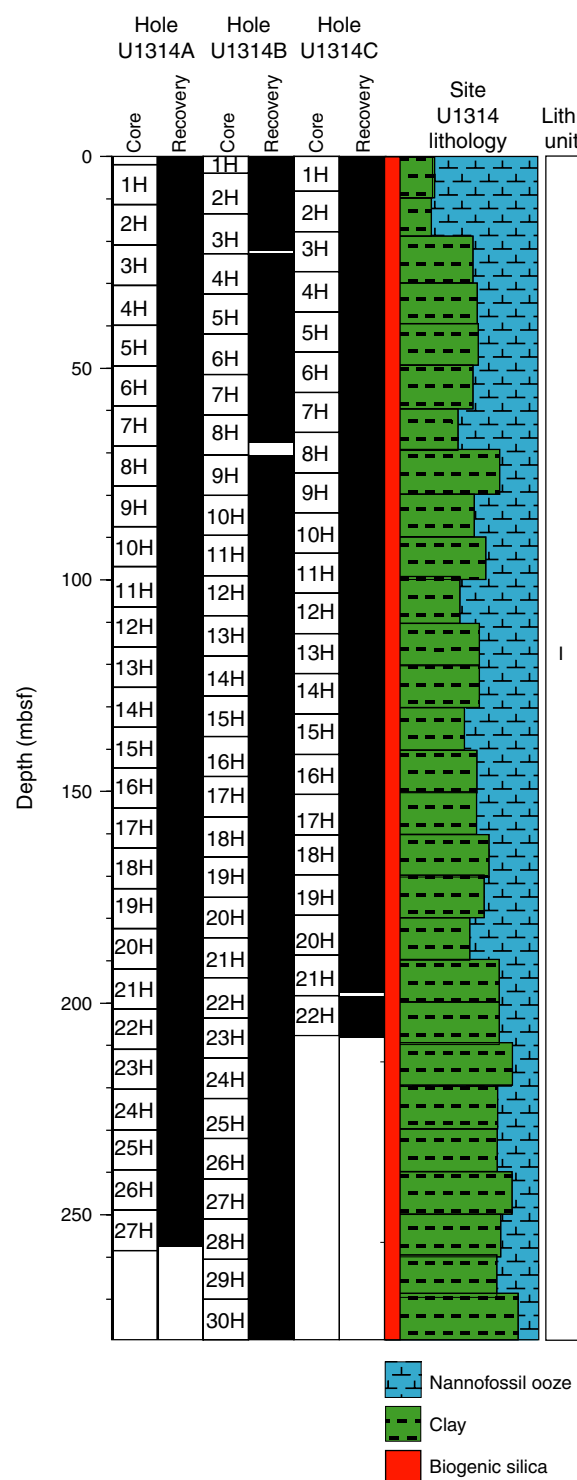


Figure F6. Clay-rich sediment having sharp basal contact with the underlying biogenic carbonate-rich layer (interval 306-U1314C-4H-3, 48–72 cm; 30.68–30.92 mbsf).

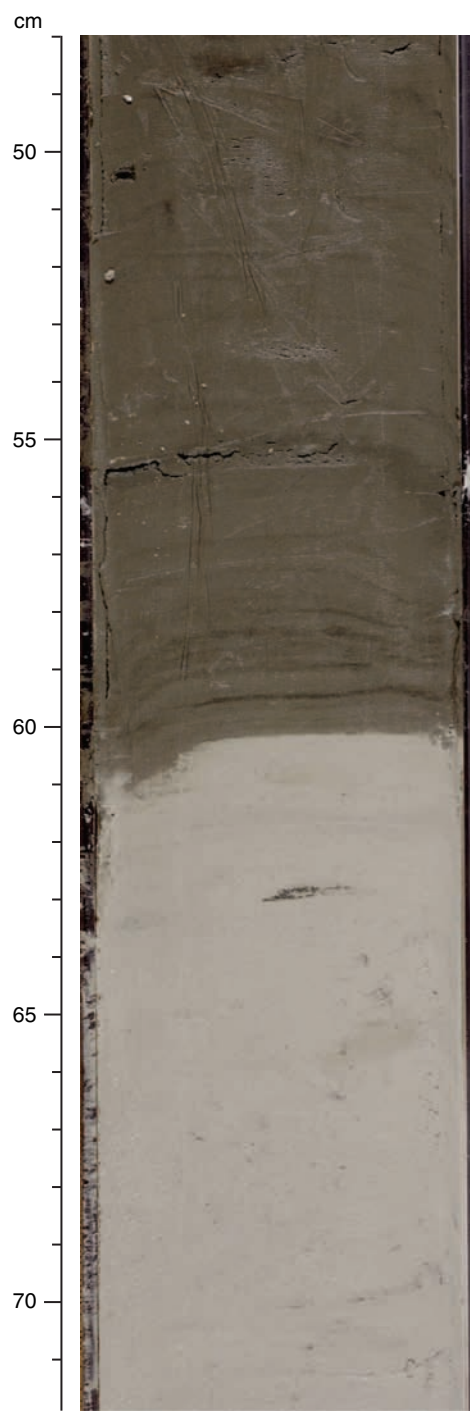


Figure F7. Typical green layer showing characteristic mottling and bioturbated contact found throughout Site U1314 (interval 306-U1314B-18H-3, 13–36 cm; 159.13–159.36 mbsf).

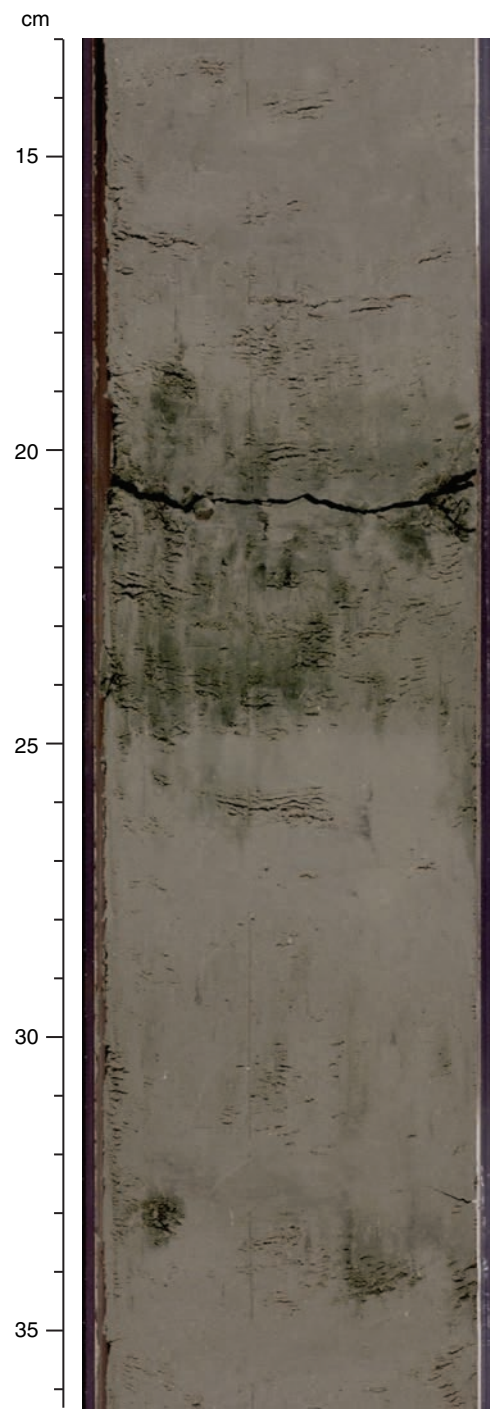


Figure F8. X-ray diffractogram for Sample 306-U1314A-1H-1, 140–141 cm.

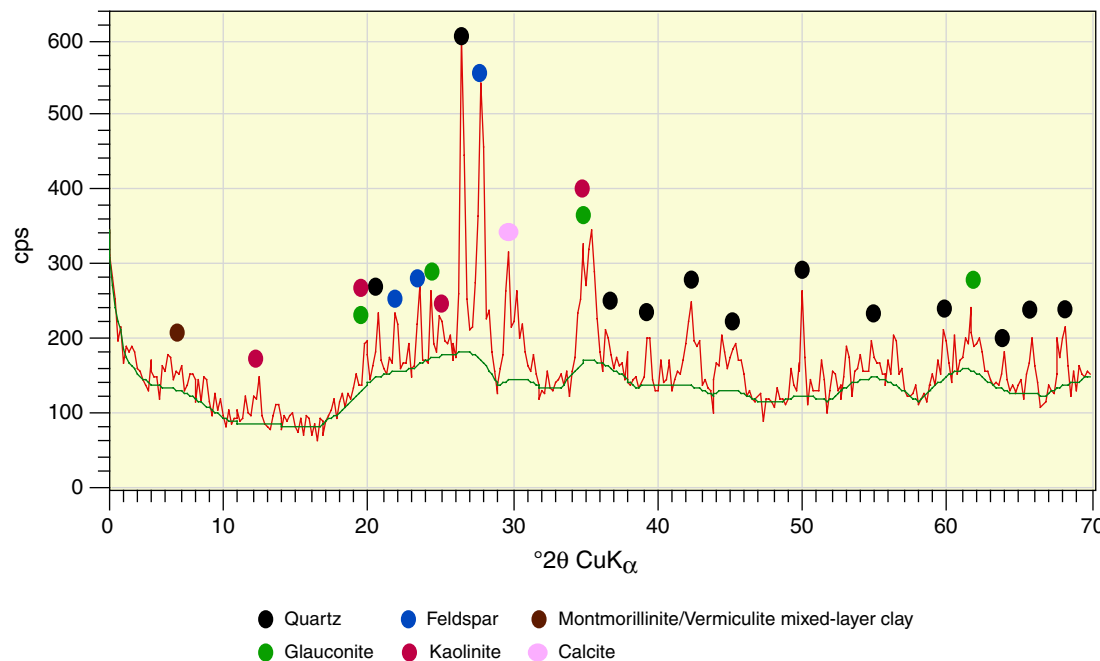


Figure F9. Typical bioturbated color contact in Site U1314 sediments (interval 306-U1314C-4H-2, 97–126 cm; 29.67–29.96 mbsf).

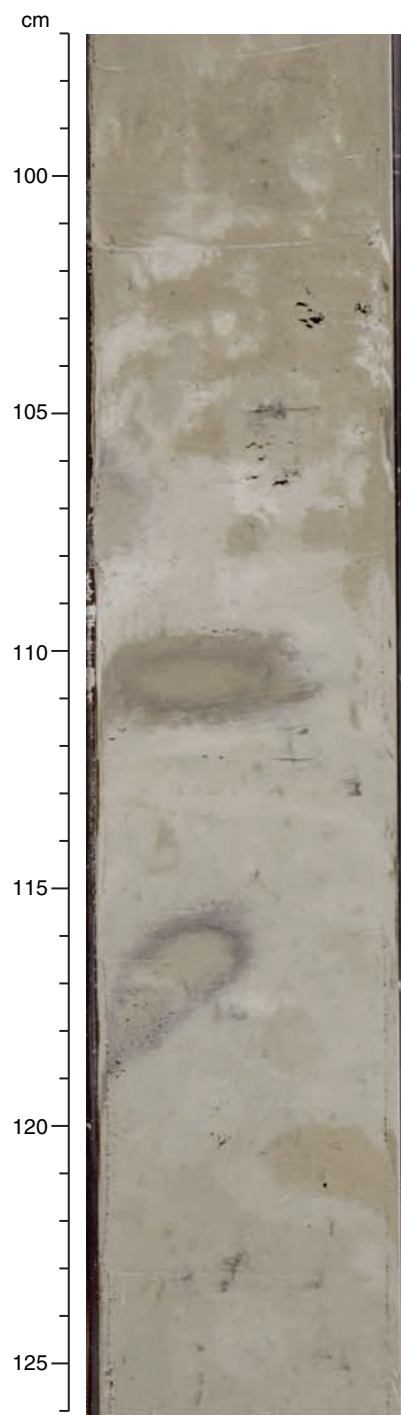


Figure F10. Relative abundances of calcareous nannofossils, diatoms, clay minerals, and quartz from dominant lithologies in Hole U1314B.

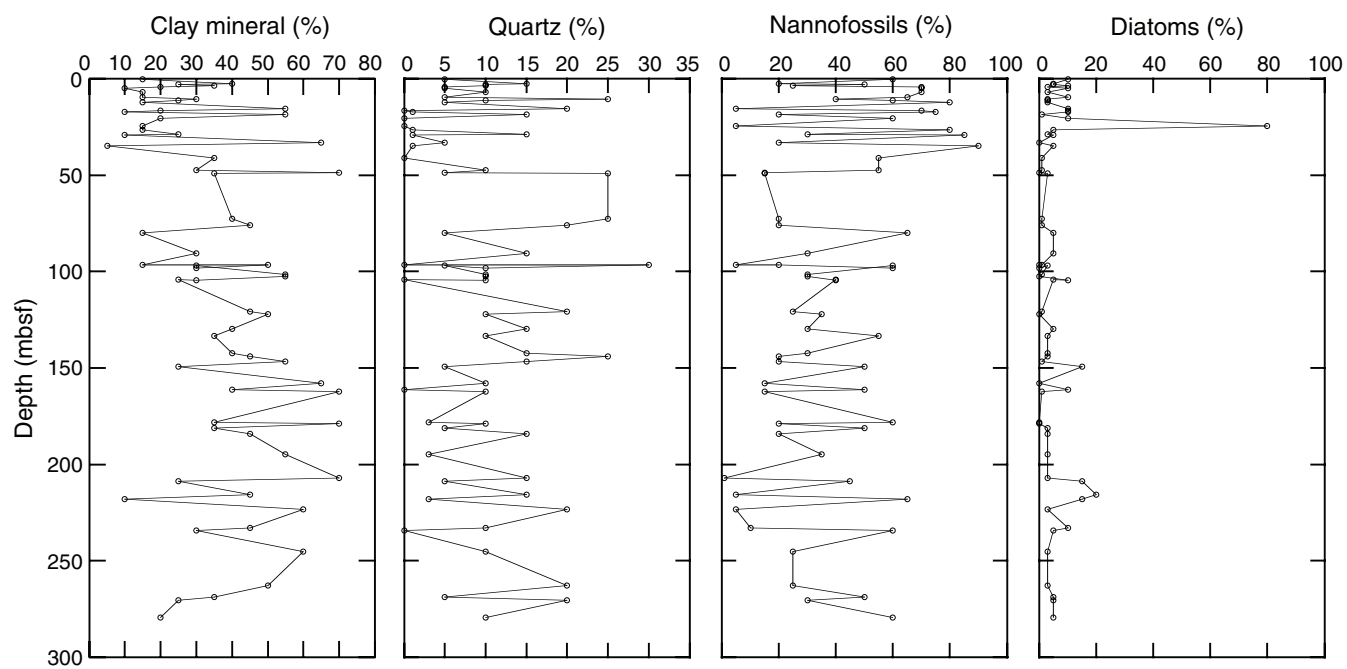


Figure F11. Relative abundances of sand-sized sediments and quartz from dominant lithologies in Hole U1314B. The occurrence of gravel-sized grains (dropstones) in Hole U1314B is shown as solid circles.

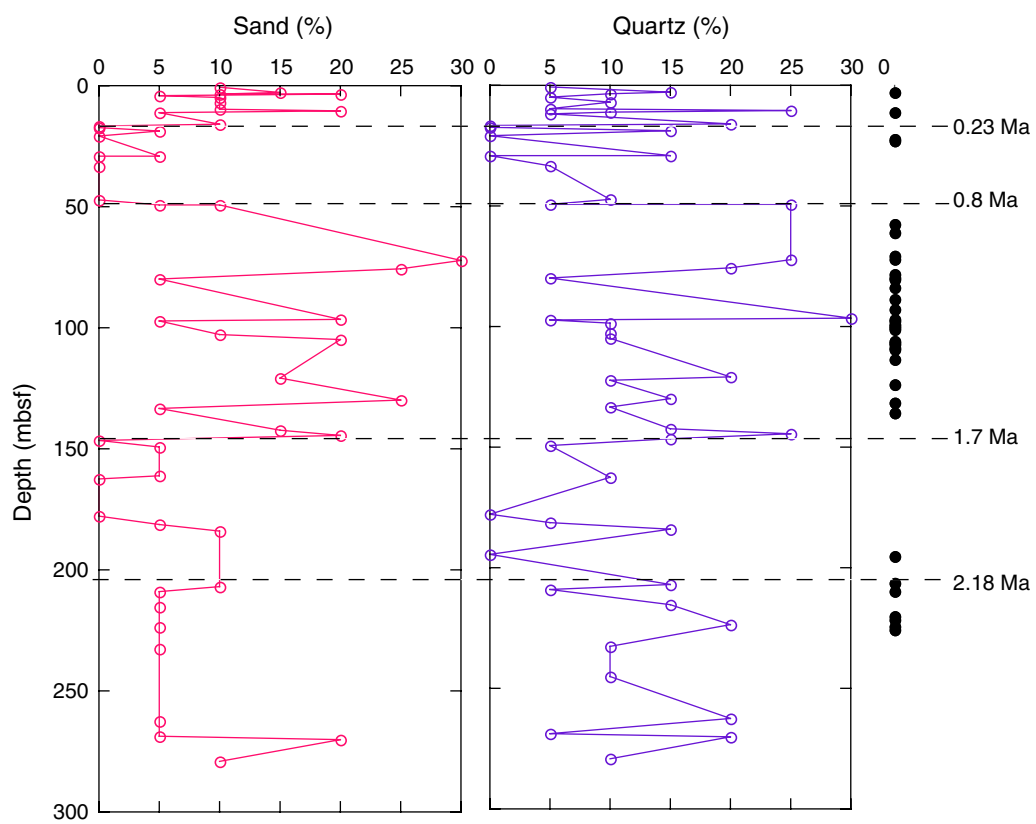


Figure F12. Basaltic dropstone (interval 306-U1314C-3H-4, 48–72 cm; 22.68–22.92 mbsf).

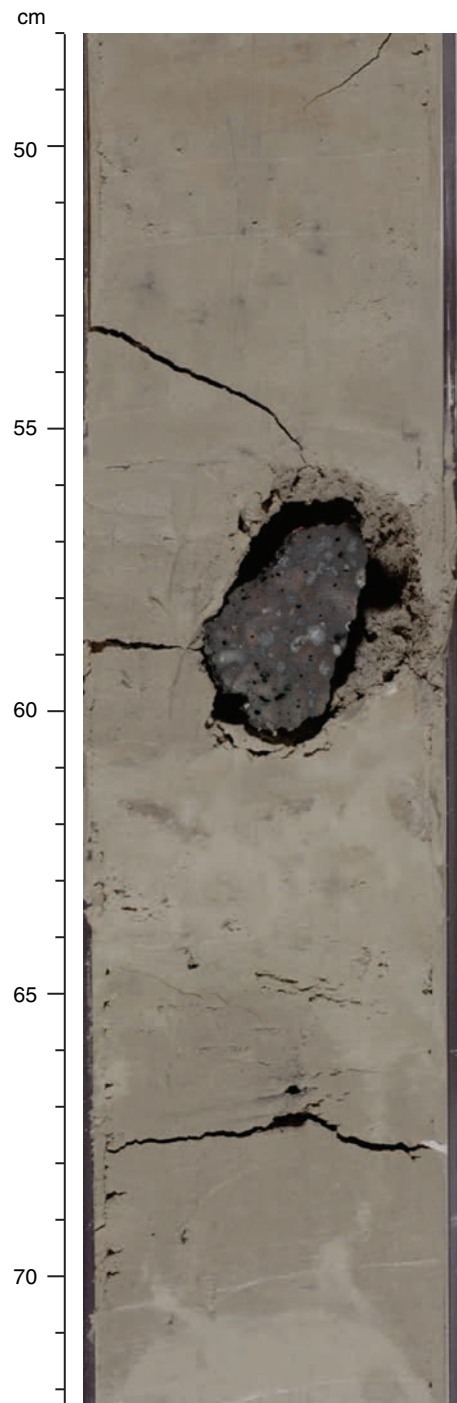


Figure F13. Metamorphic dropstone (interval 306-U1314A-22H-1, 67–85 cm; 192.57–192.75 mbsf).

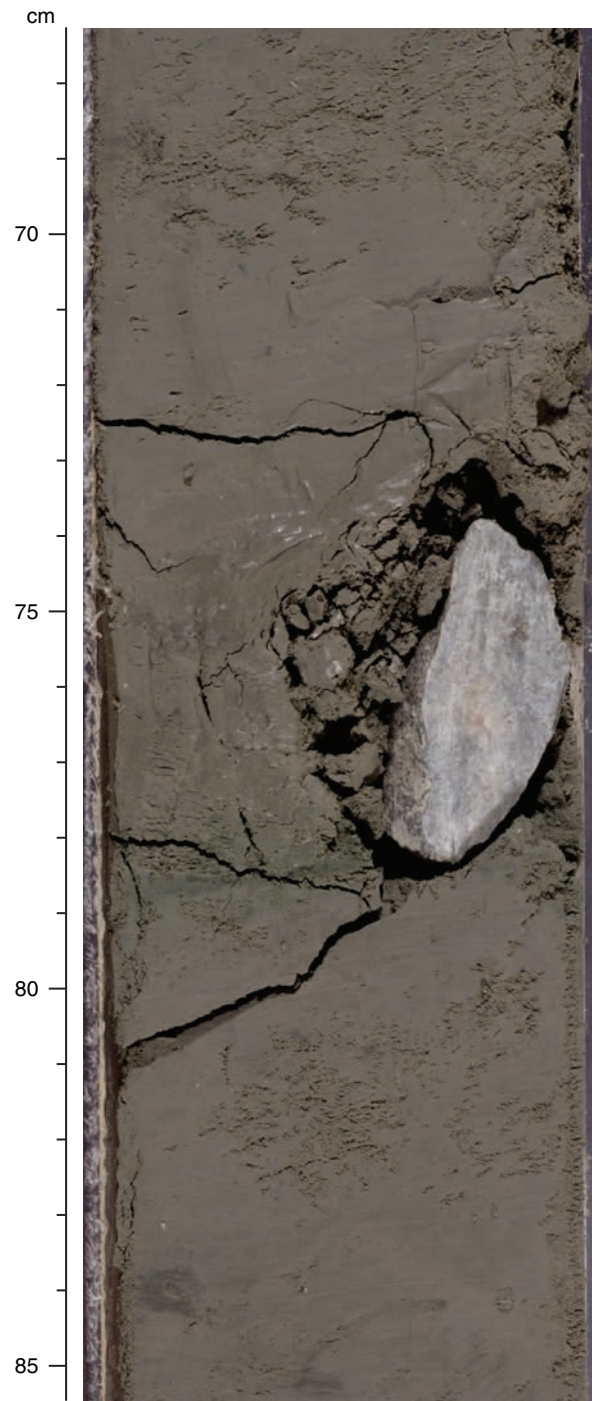


Figure F14. Smoothed lightness (L^*), redness (a^*), magnetic susceptibility, and natural gamma radiation data in the spliced record from Site U1314.

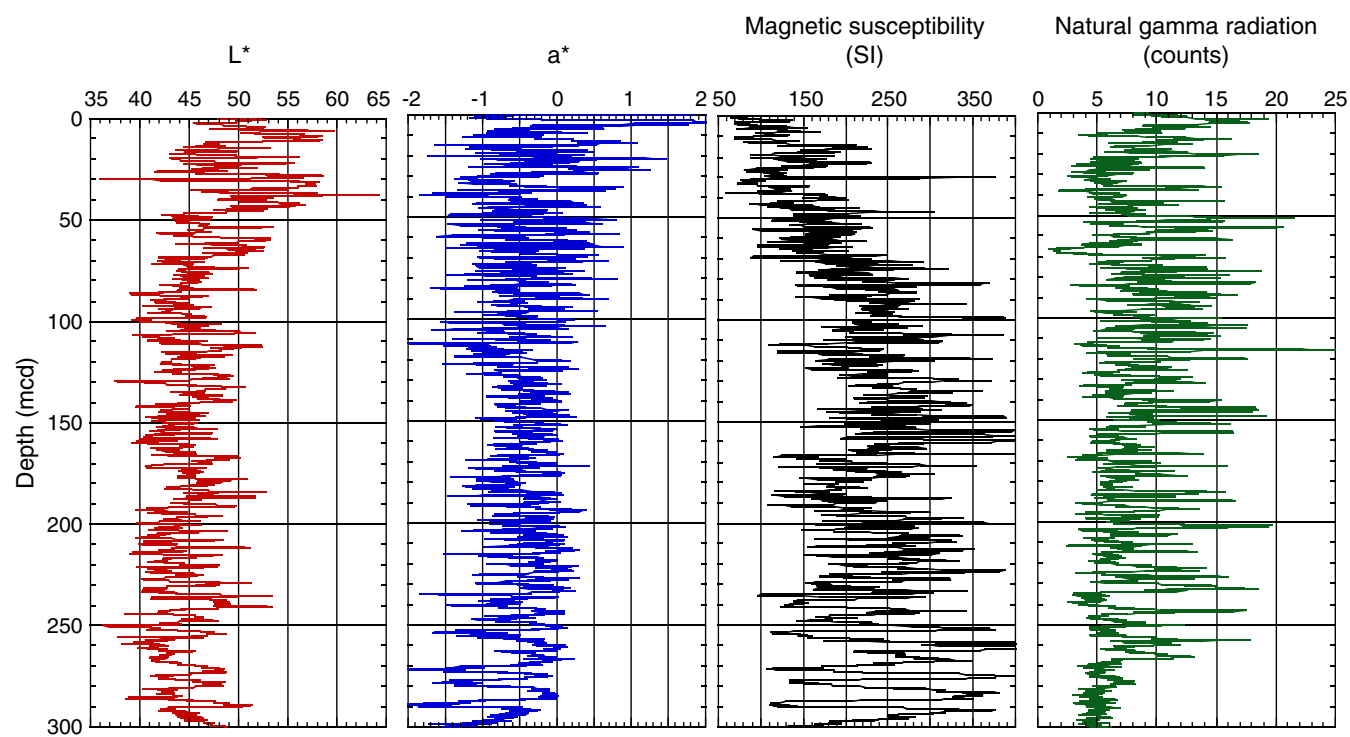


Figure F15. Age vs. depth plot and average sedimentation rates for different intervals of time in Hole U1314A. Biostratigraphic events used to construct the curve are given in Table T3. Paleomagnetism data for the curve are given in Table T18. Potentially problematic *Discoaster* datums are circled (see text for explanation).

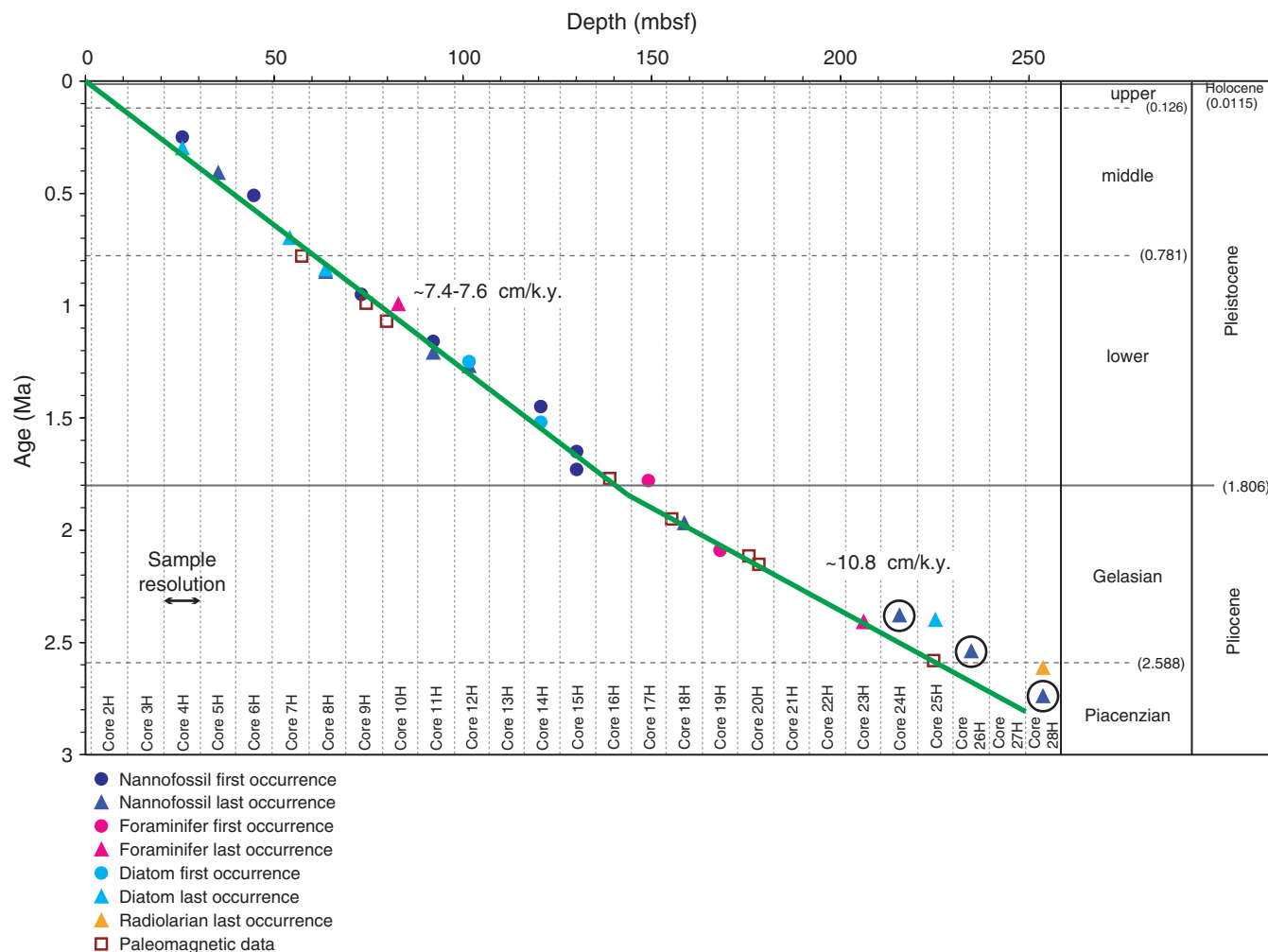


Figure F16. Age vs. depth plot and average sedimentation rates for different intervals of time in Hole U1314B. Biostratigraphic events used to construct the curve are given in Table T3. Paleomagnetism data for the curve are given in Table T18. Potentially problematic *Discoaster* datums are circled (see text for explanation).

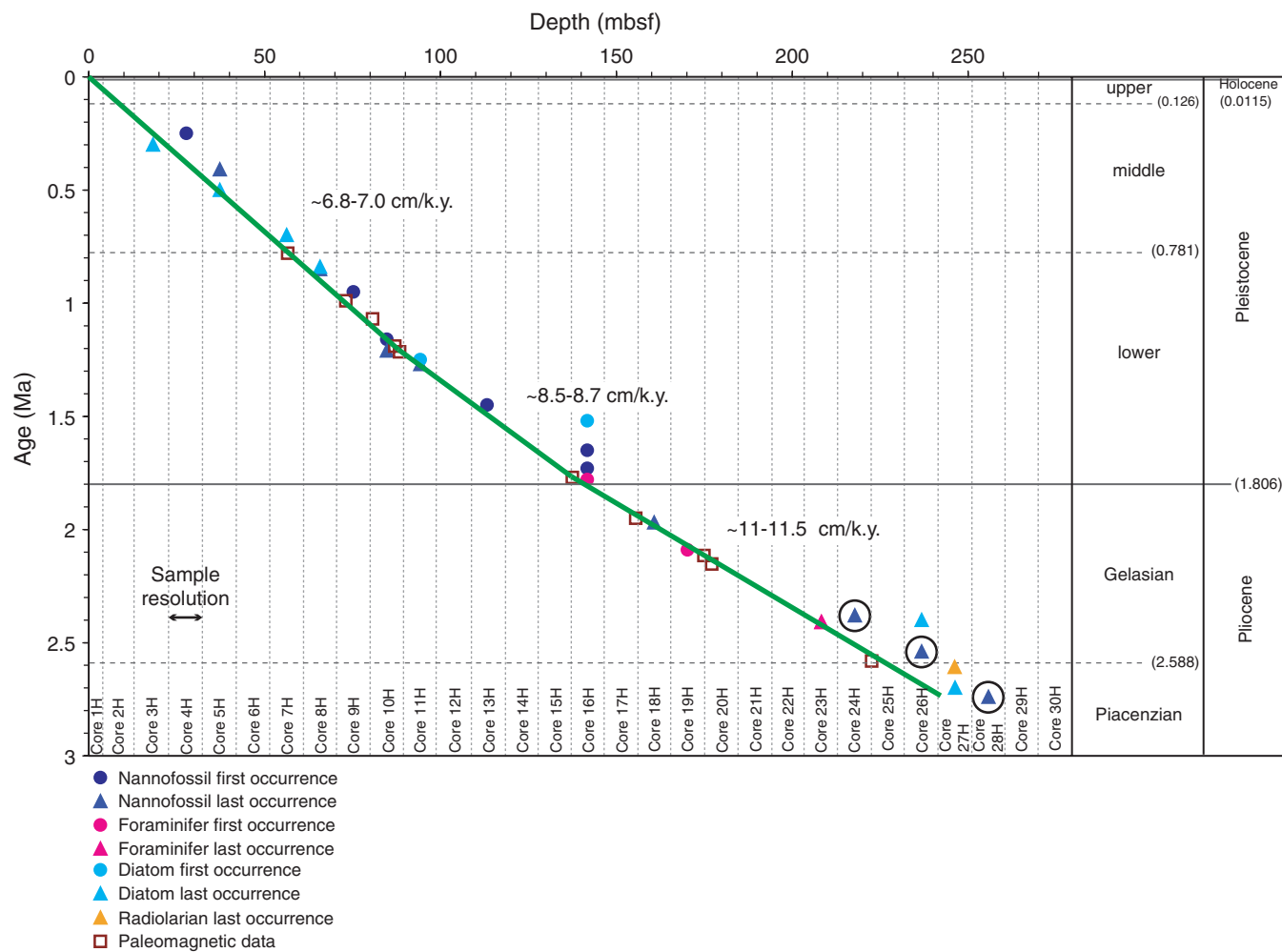


Figure F17. Age vs. depth plot and average sedimentation rates for different intervals of time in Hole U1314C. Biostratigraphic events used to construct the curve are given in Table T3. Paleomagnetism data for the curve are given in Table T18.

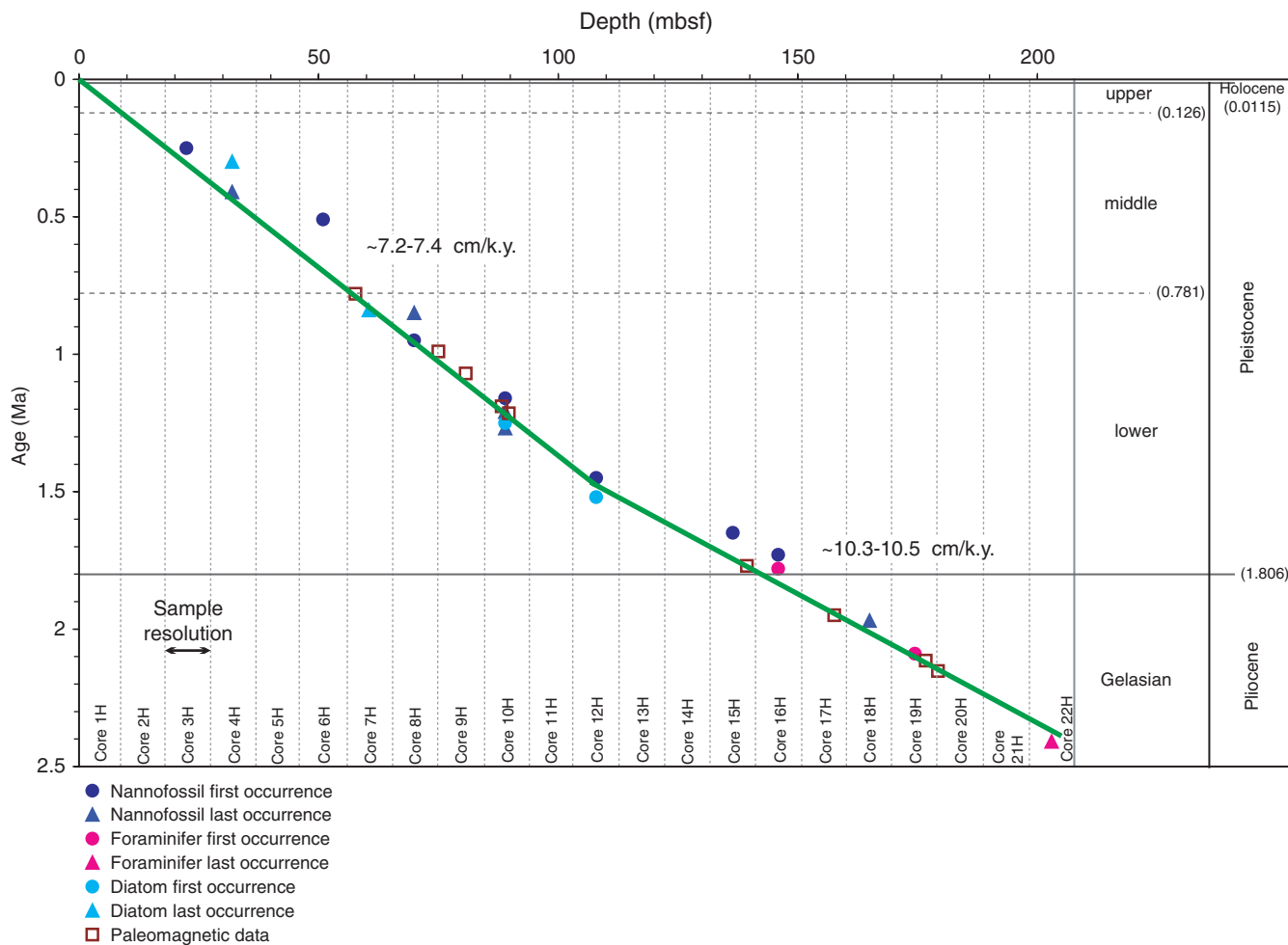


Figure F18. NRM intensity before (green) and after (red) AF demagnetization at 20 mT.

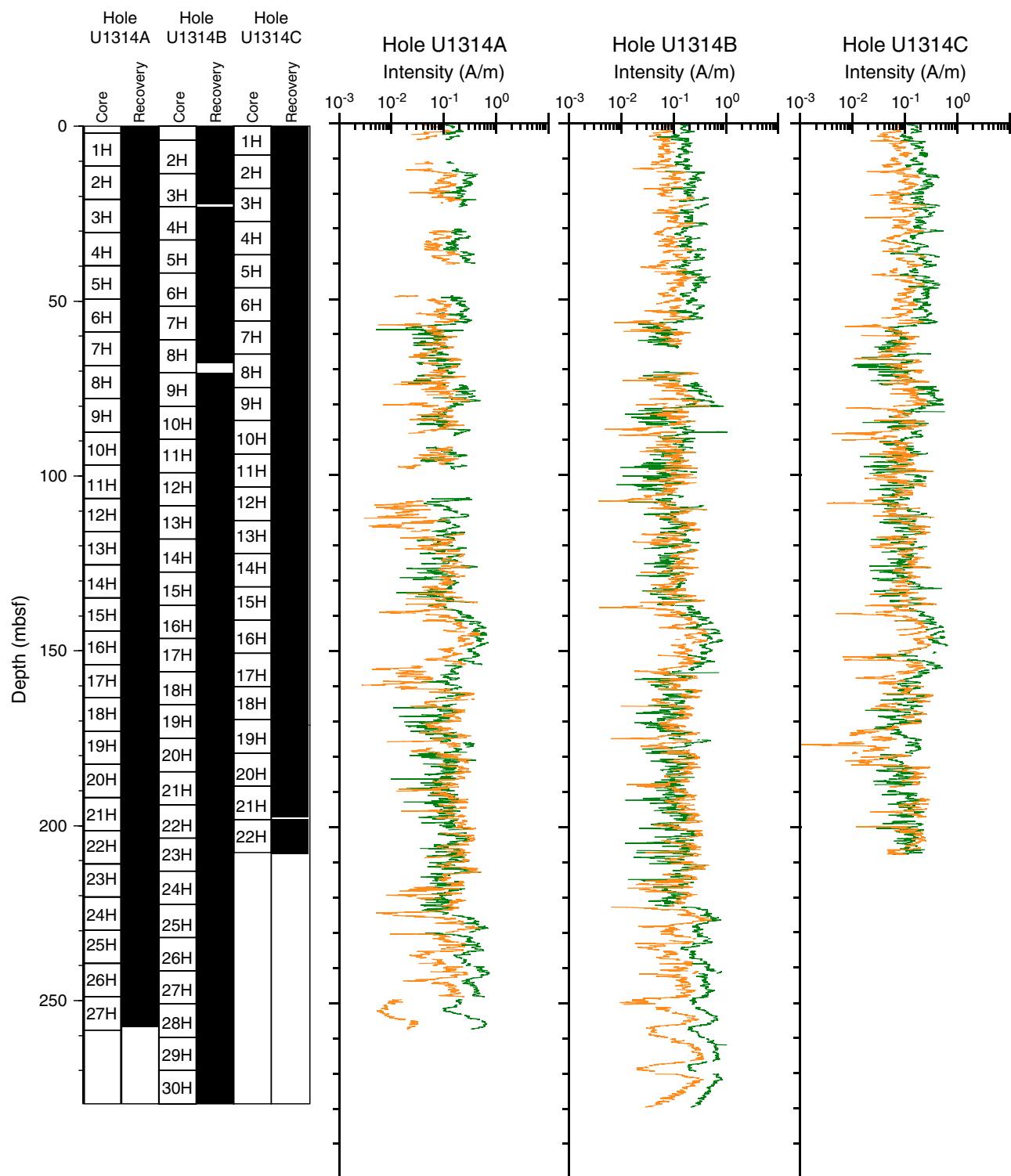




Figure F19. Inclination and declination of remanent magnetization after 20 mT AF demagnetization. Declination values have been corrected using Tensor tool data.

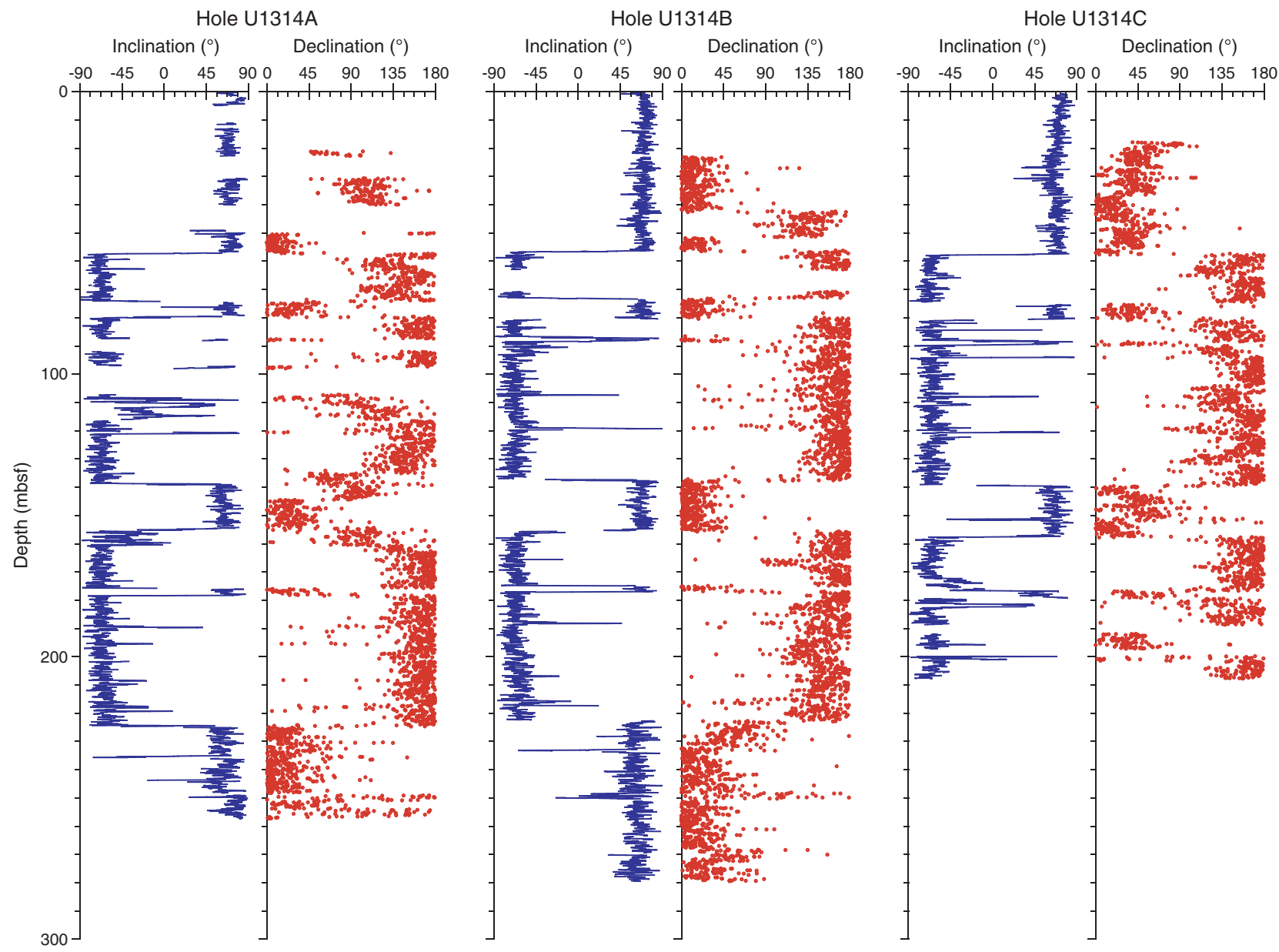


Figure F20. Inclination after 20 mT AF demagnetization. The paleomagnetic polarity interpretation (black = normal polarity, white = reversed polarity) is displayed on the right side of the figure along with the reference geomagnetic polarity timescale (Cande and Kent, 1995).

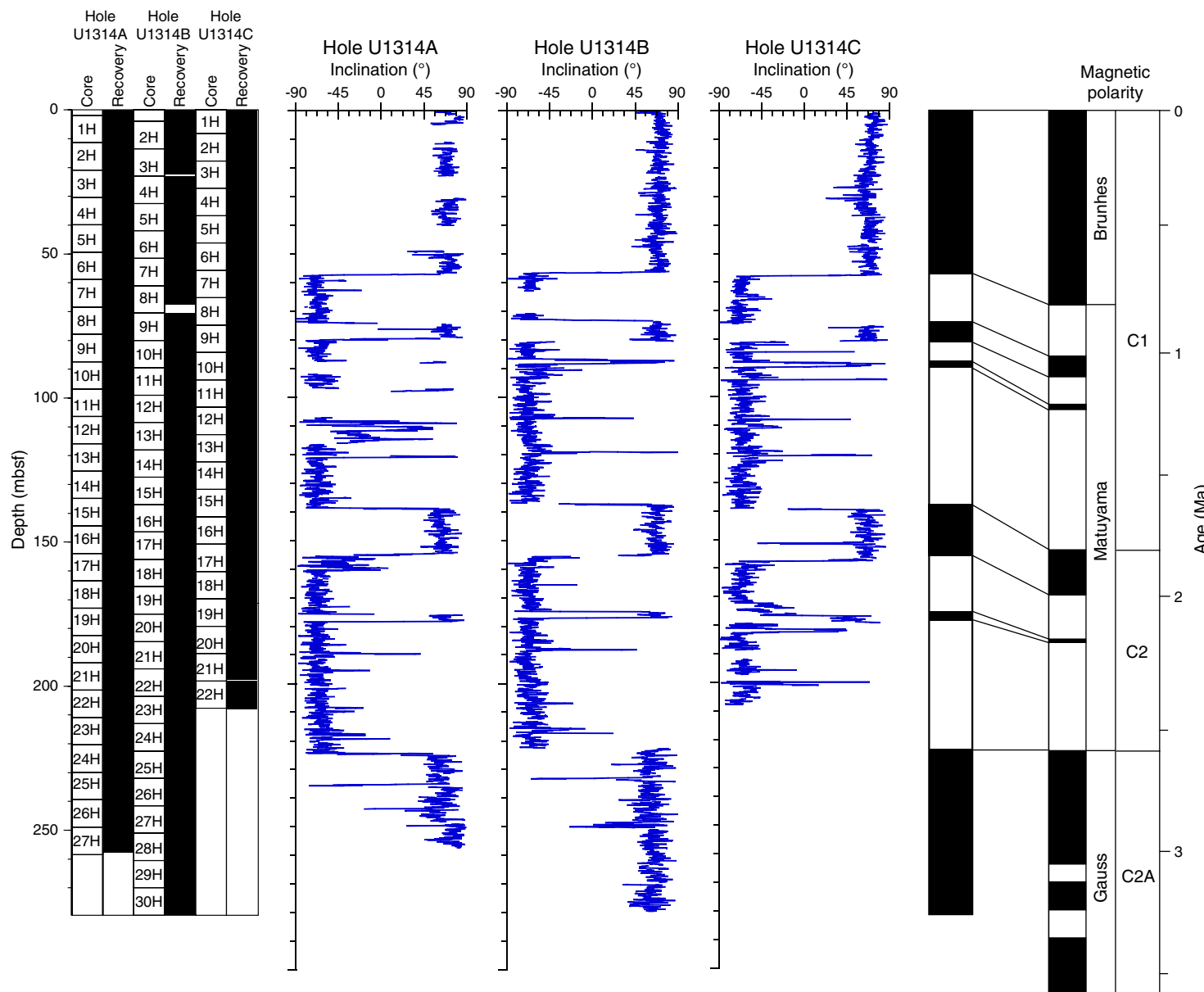


Figure F21. Magnetic susceptibility vs. mcd for each hole. Upper panels show composite magnetic susceptibility record indicating which hole was used to form the primary sampling splice. Numbers in lower panel indicate core numbers. A. 0–80 mcd. (Continued on next three pages.)

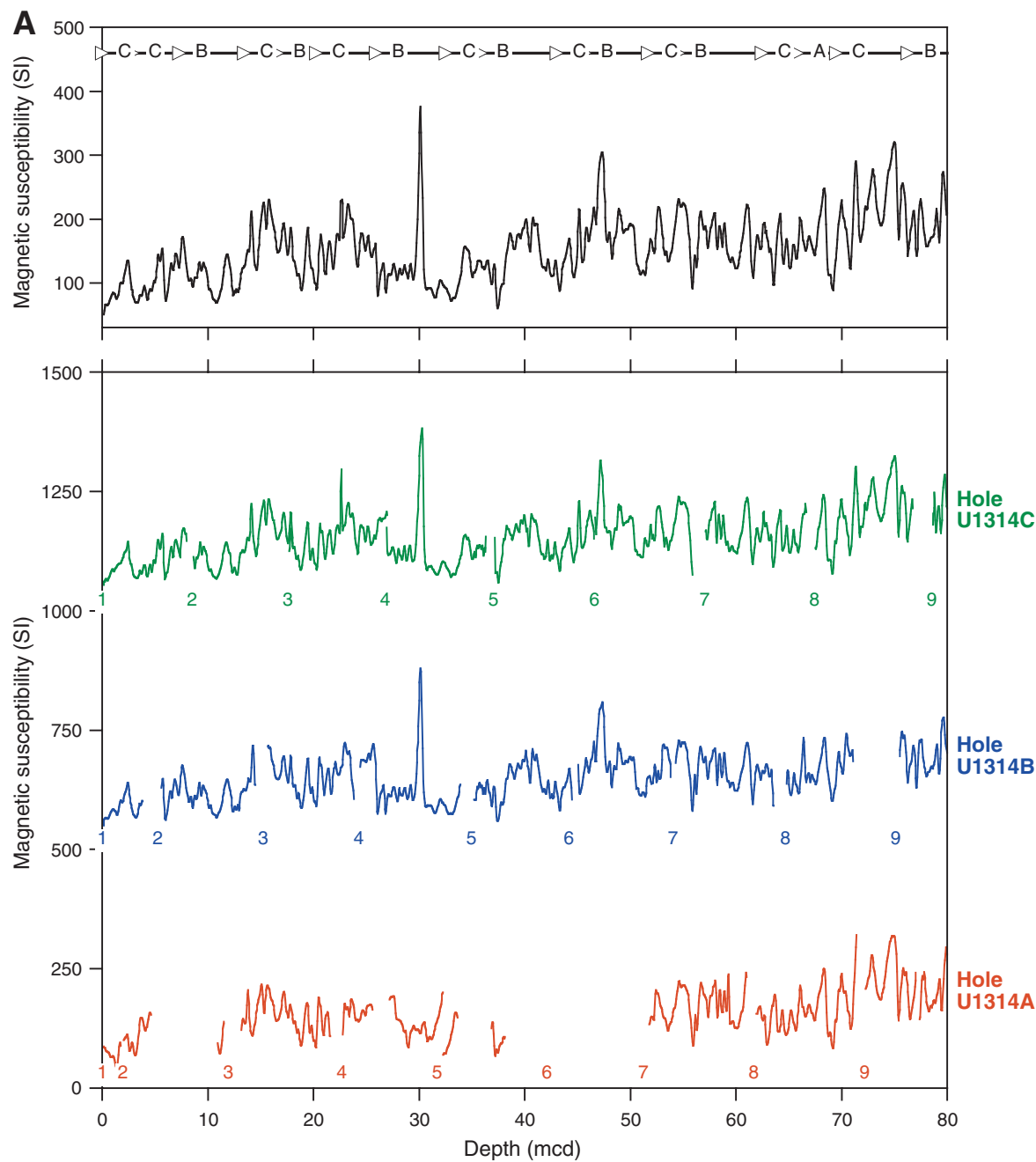


Figure F21 (continued). B. 80–160 mcd.

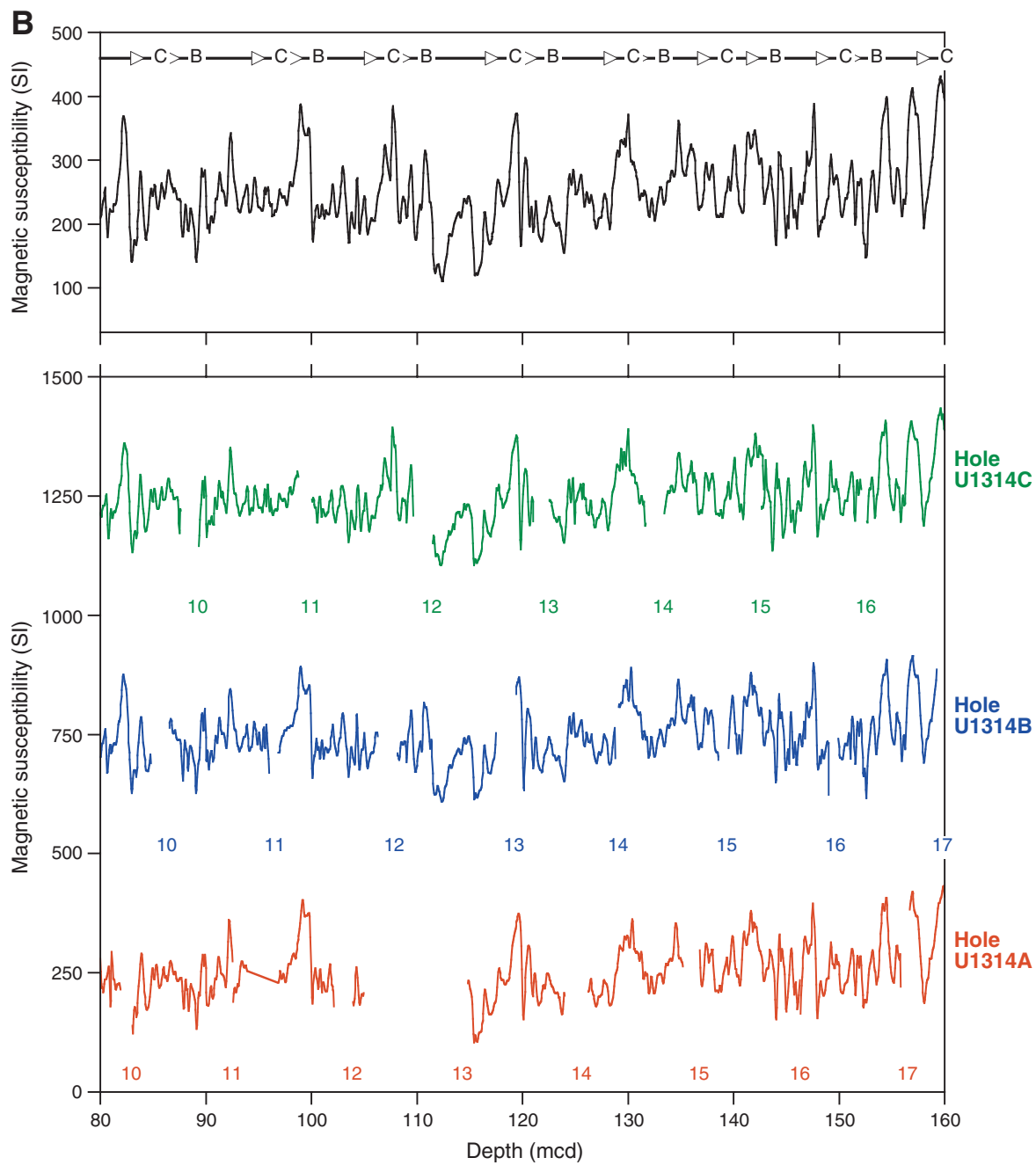


Figure F21 (continued). C. 160–240 mcd.

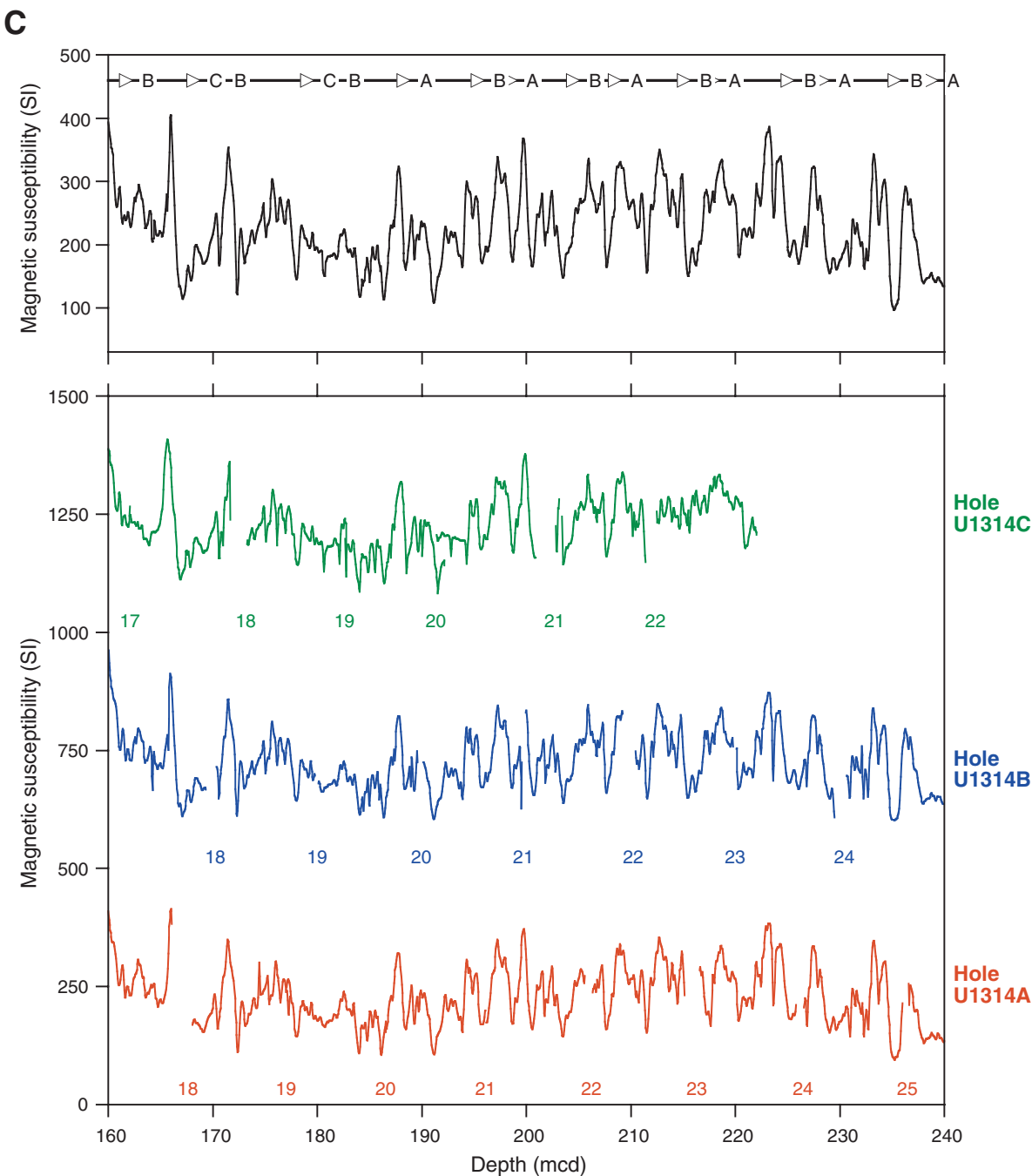


Figure F21 (continued). D. 240–320 mcd.

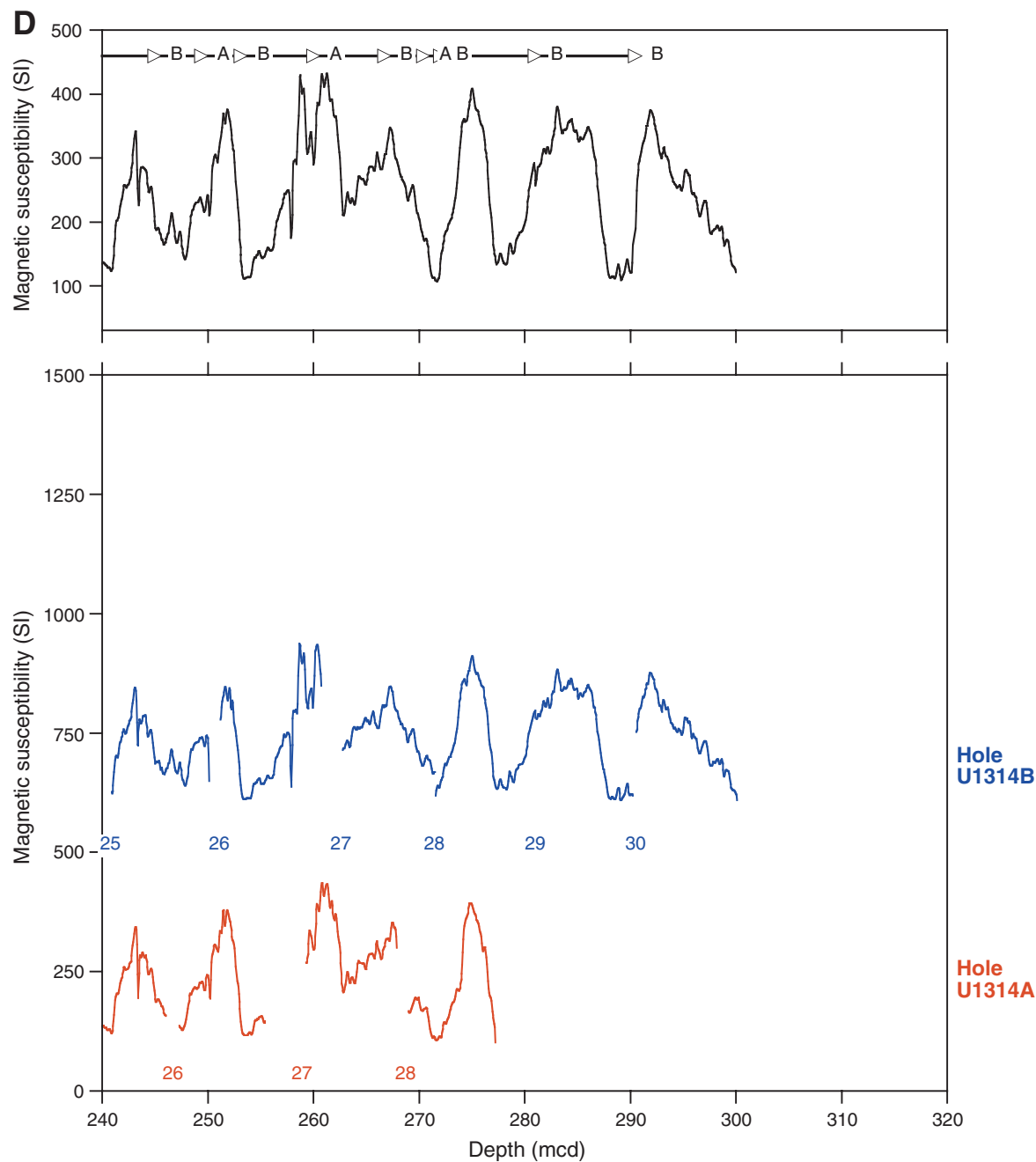


Figure F22. Natural gamma radiation (NGR) vs. mcd for each hole. Upper panels show composite NGR record indicating which hole was used to form the primary sampling splice. Numbers in lower panel indicate core numbers. A. 0–80 mcd. (Continued on next three pages.)

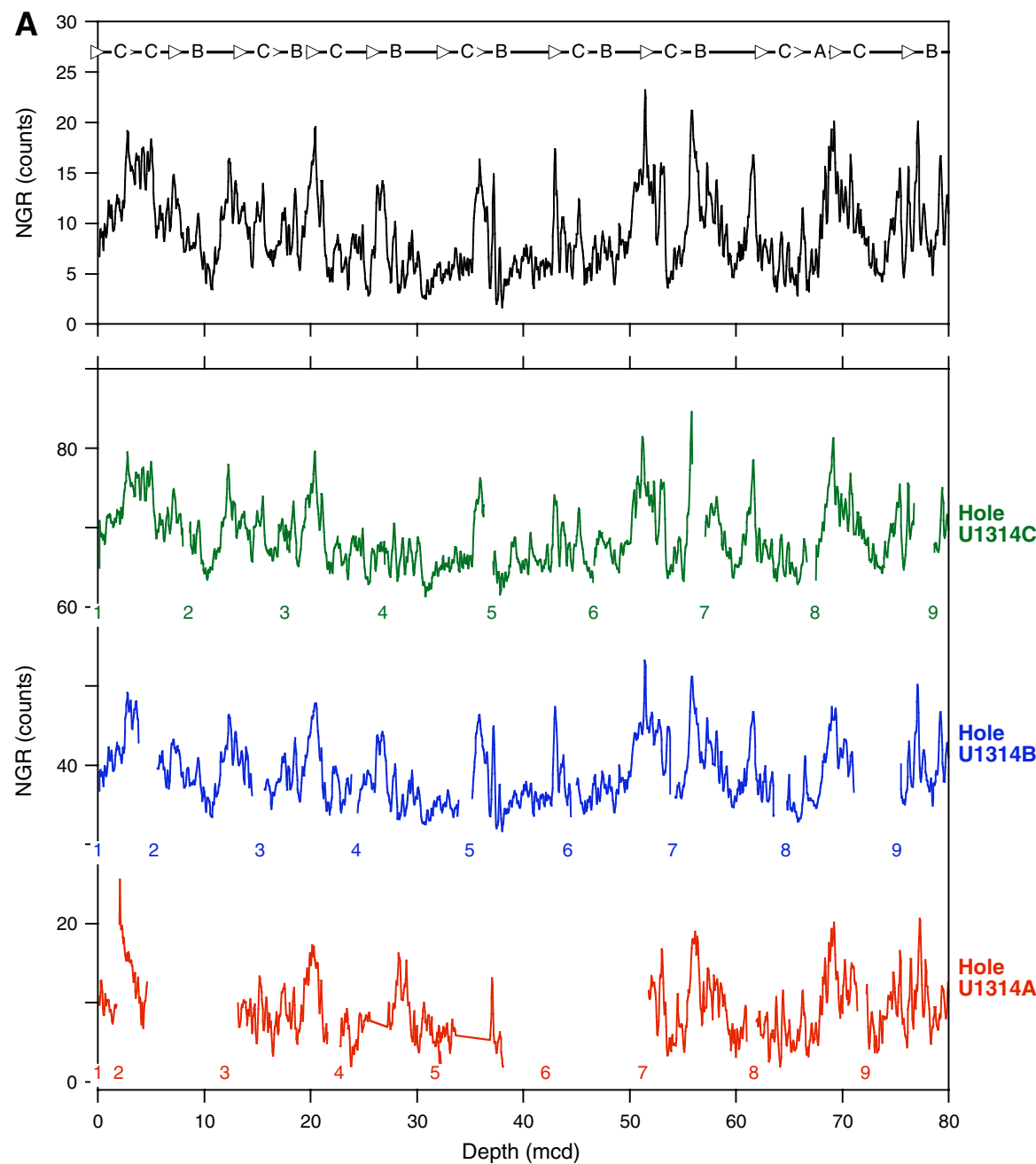


Figure F22 (continued). B. 80–160 mcd.

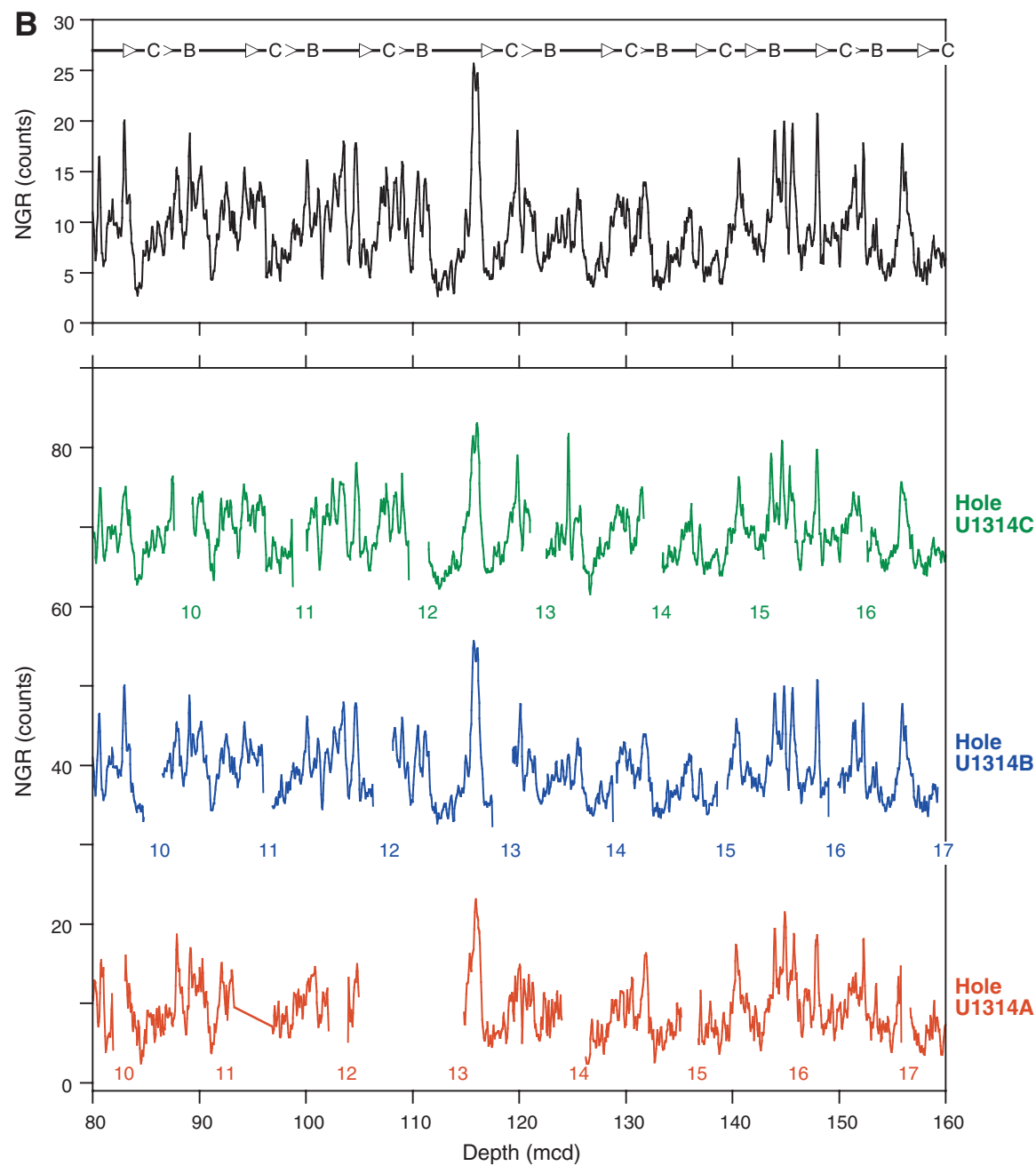


Figure F22 (continued). C. 160–240 mcd.

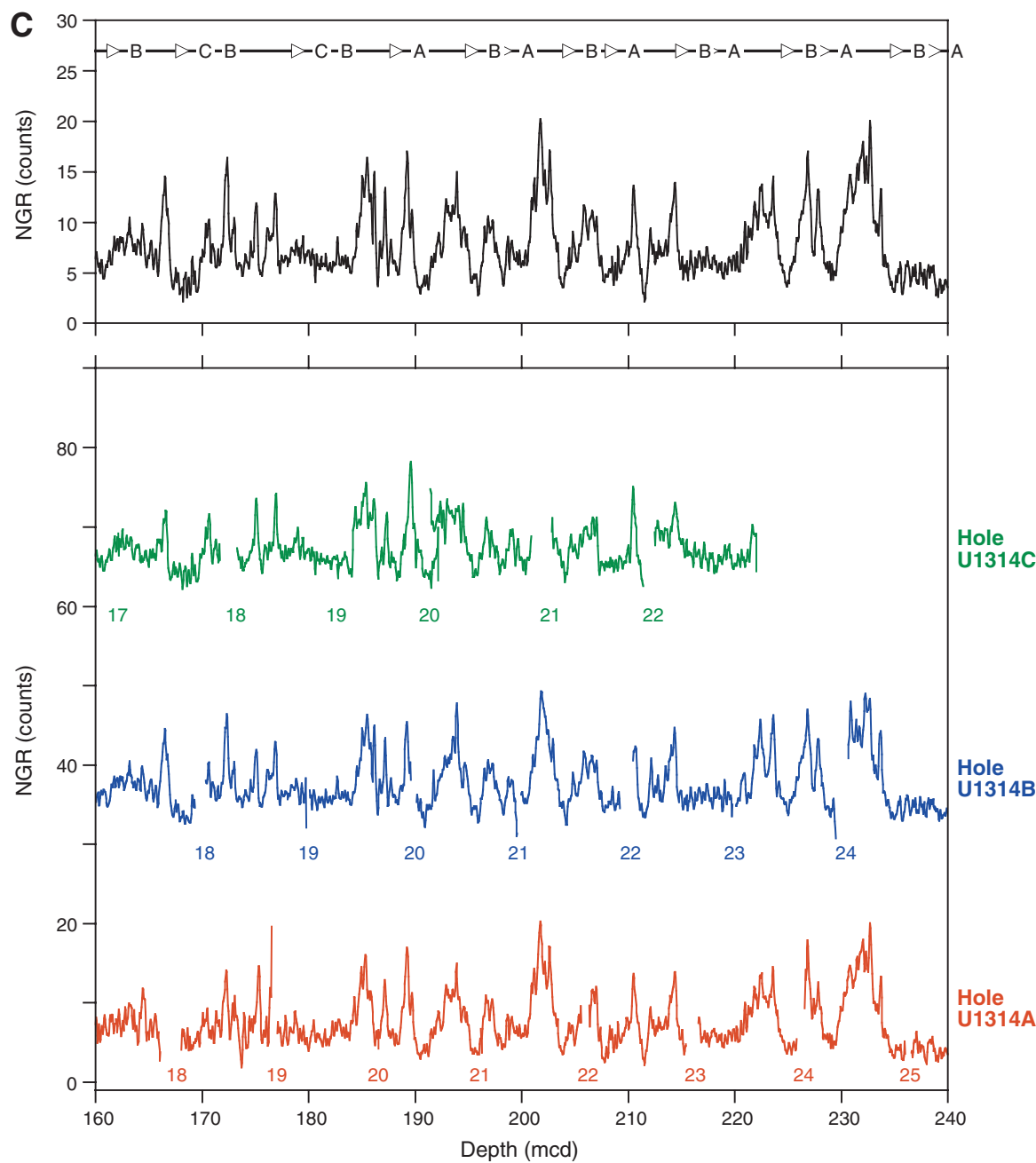


Figure F22 (continued). D. 240–320 mcd.

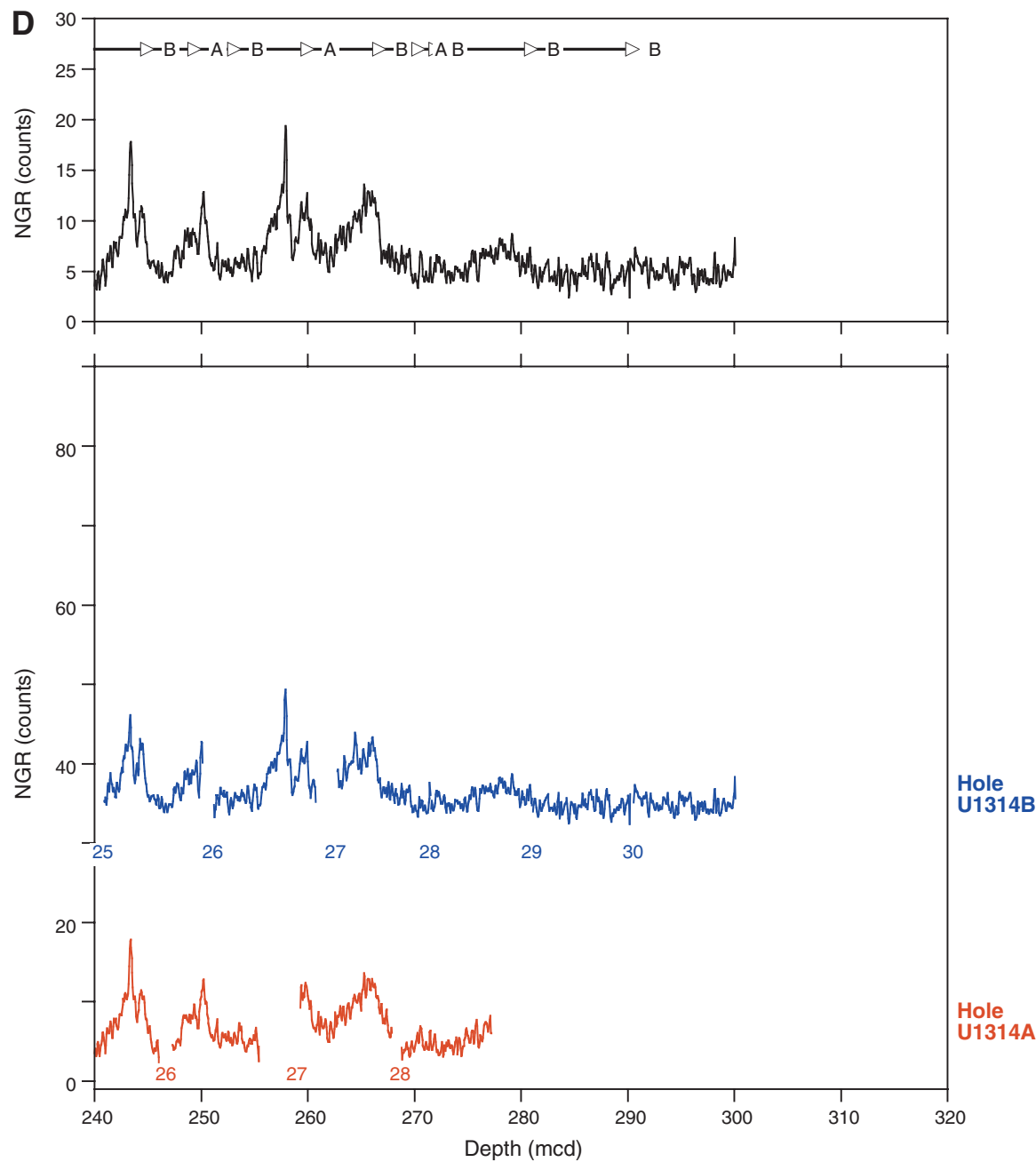


Figure F23. Inclination vs. mcd for each hole. Upper panels show composite inclination record indicating which hole was used to form the primary sampling splice. Numbers in lower panel indicate core numbers. A. 0–80 mcd. (Continued on next three pages.)

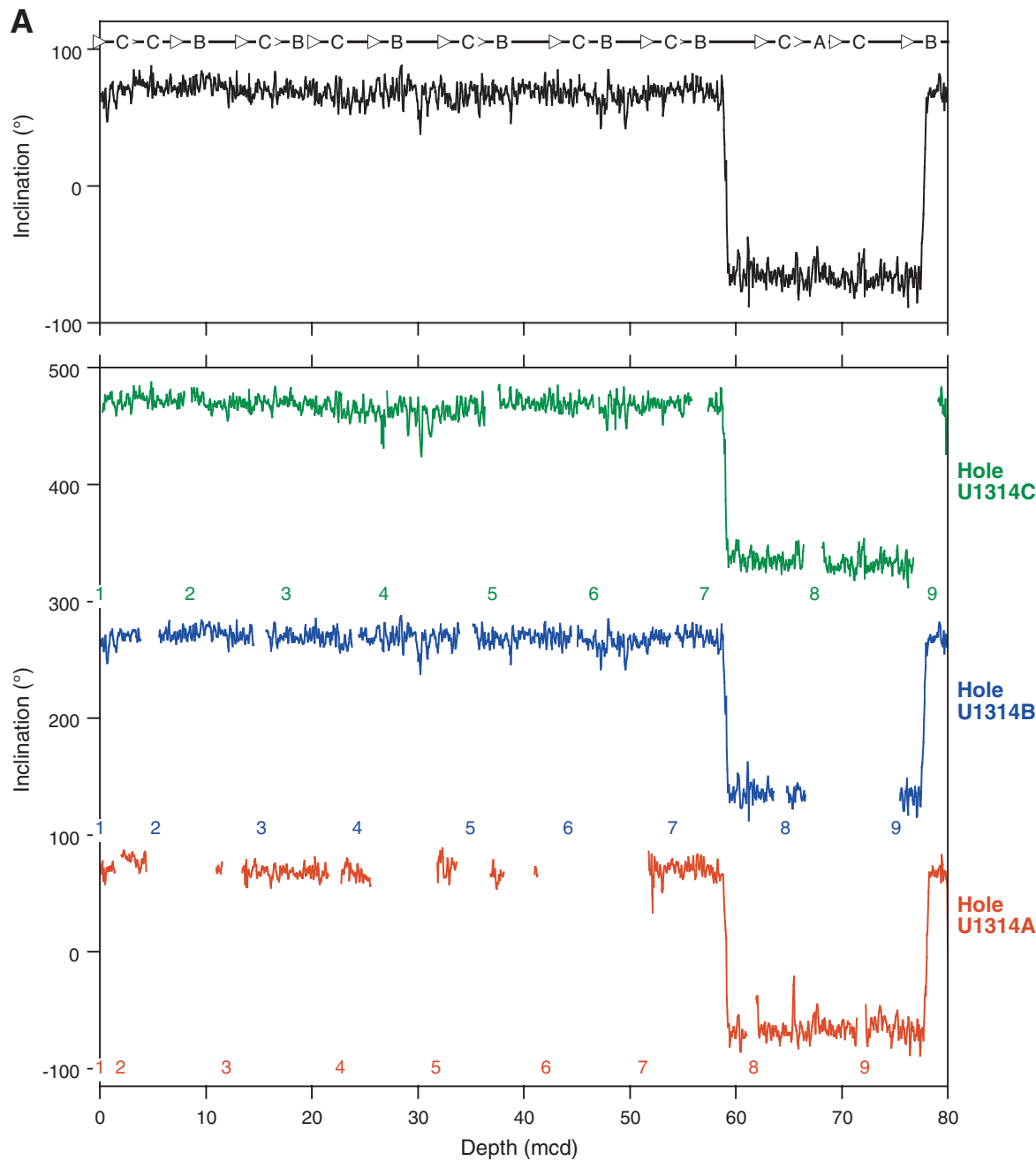


Figure F23 (continued). B. 80–160 mcd.

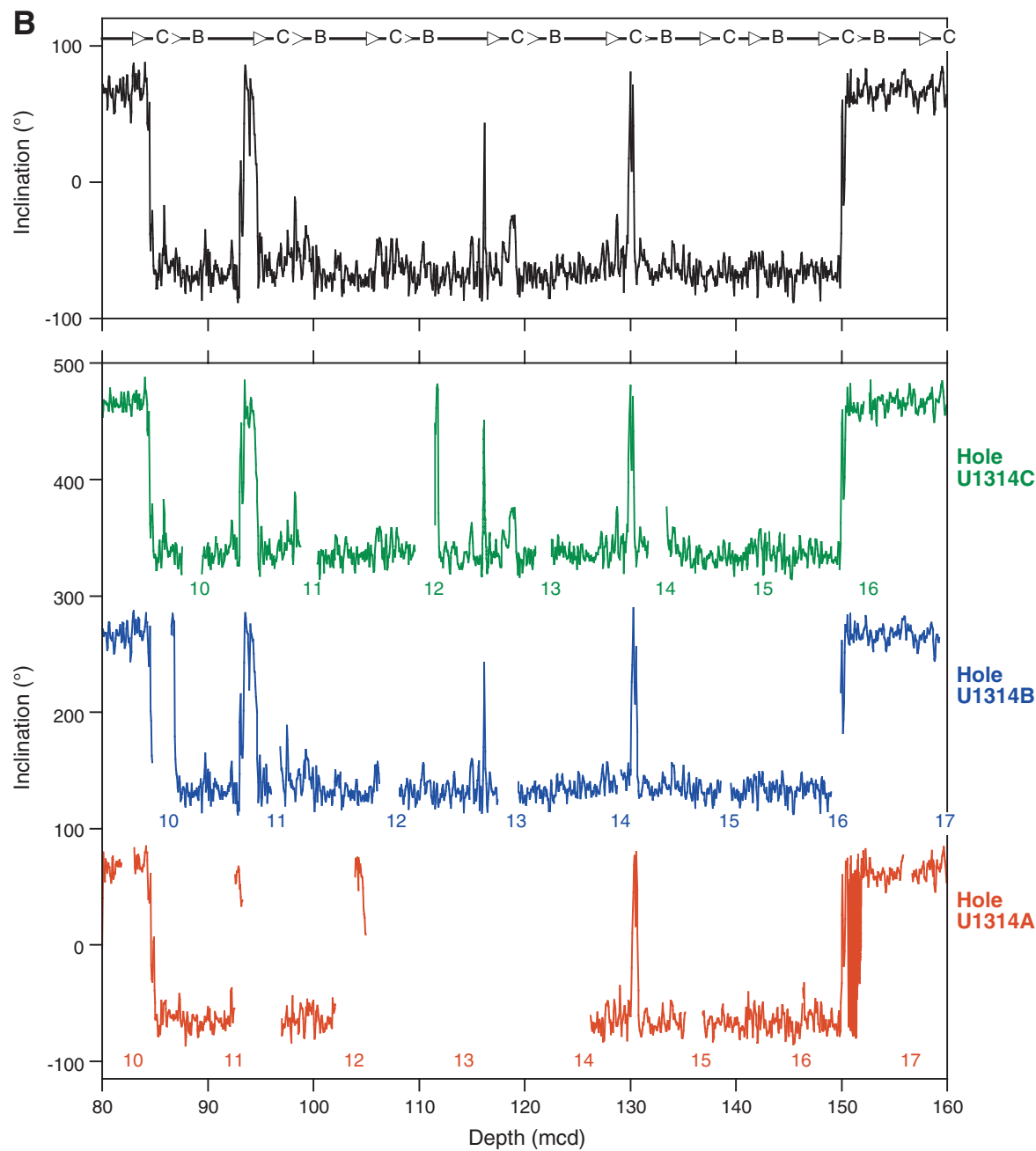


Figure F23 (continued). C. 160–240 mcd.

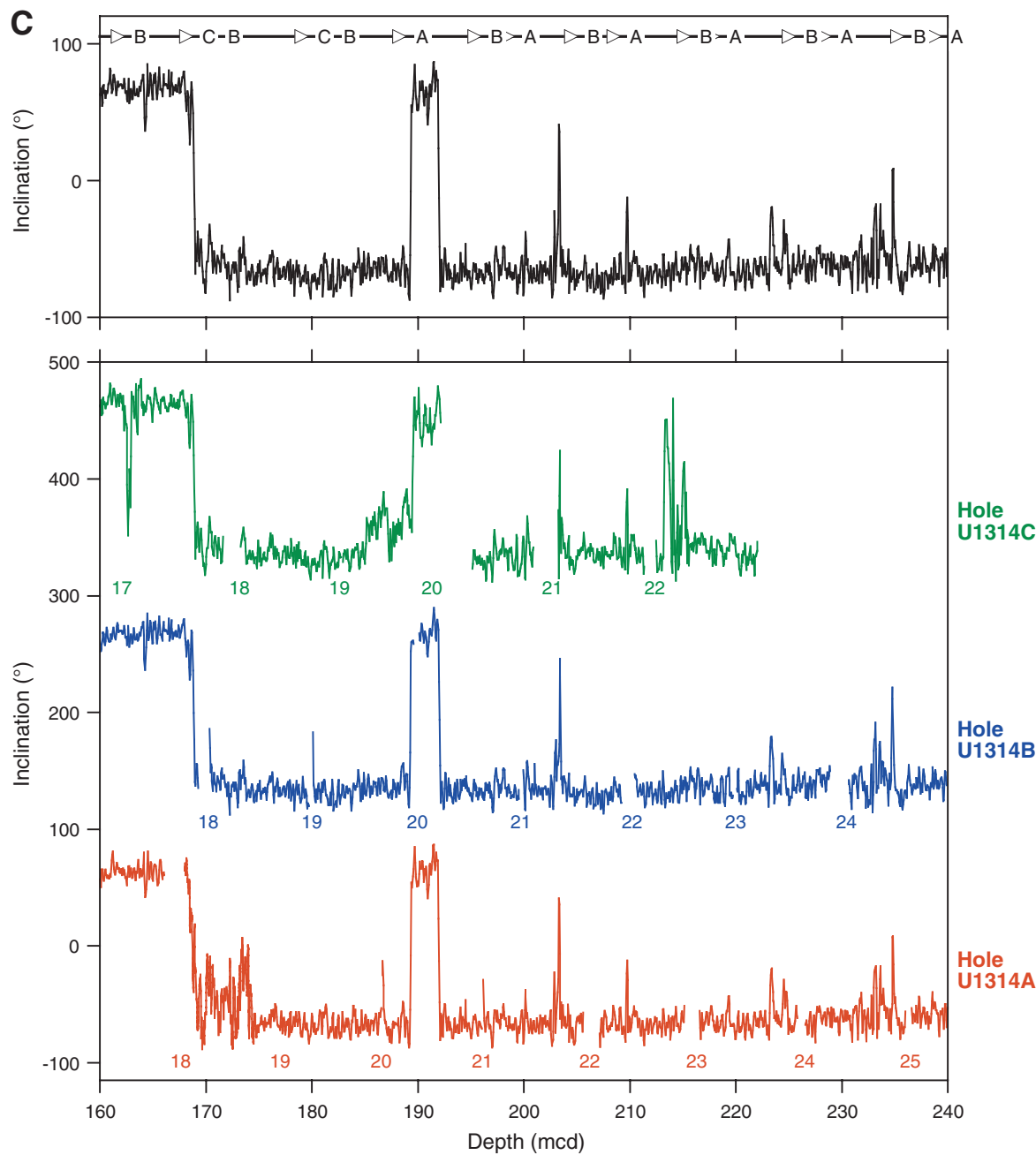


Figure F23 (continued). D. 240–320 mcd.

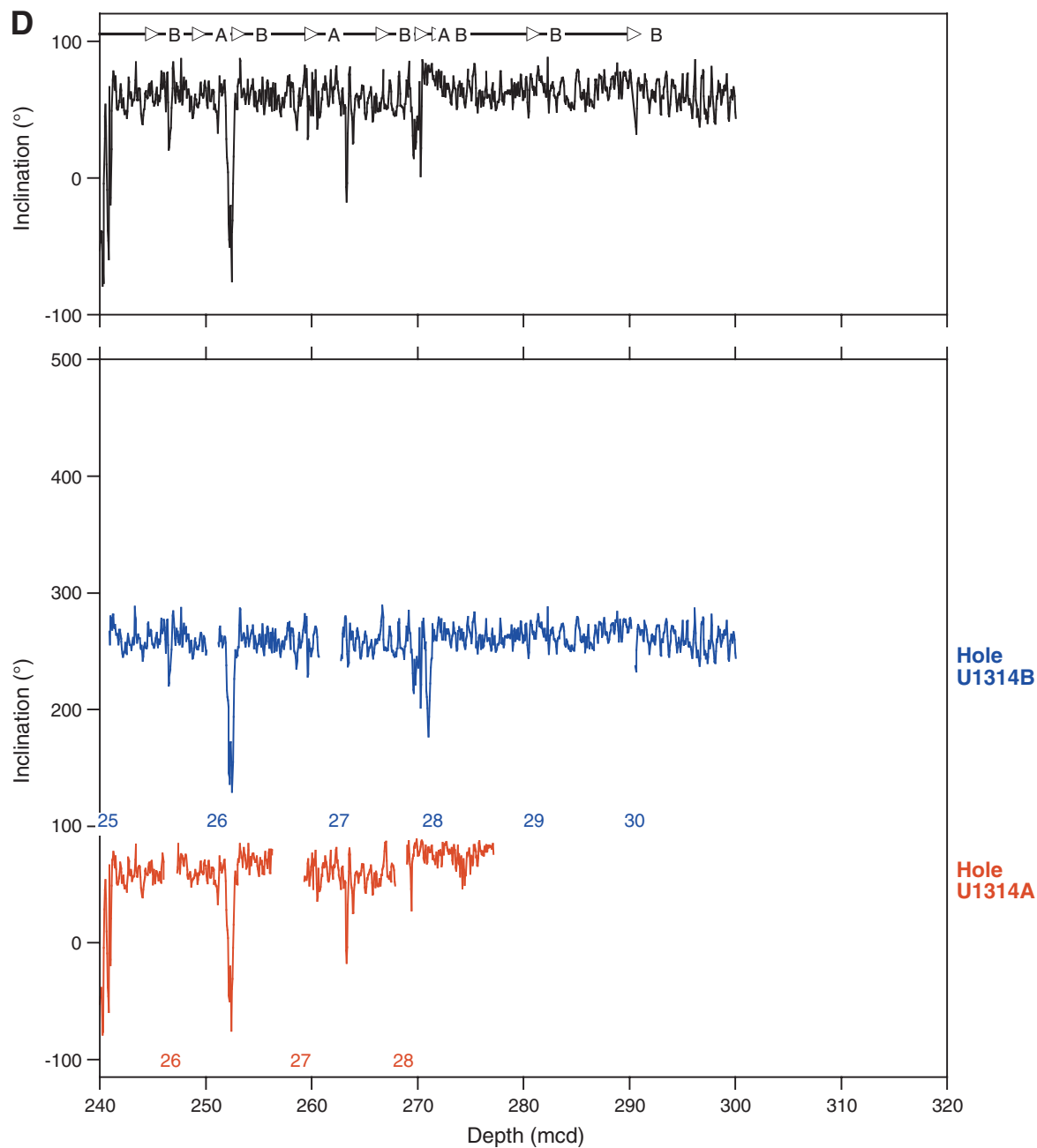


Figure F24. Downhole profiles of chemical constituents in interstitial waters from Hole U1314A. A. Chloride. B. Salinity. C. Alkalinity. D. pH. E. Sodium. F. Potassium. G. Magnesium. H. Calcium. I. Iron. J. Boron. K. Barium. L. Lithium. M. Manganese. N. Strontium. O. Silica. P. Sulfate and ammonium. Open symbols = samples obtained from cores showing flow-in.

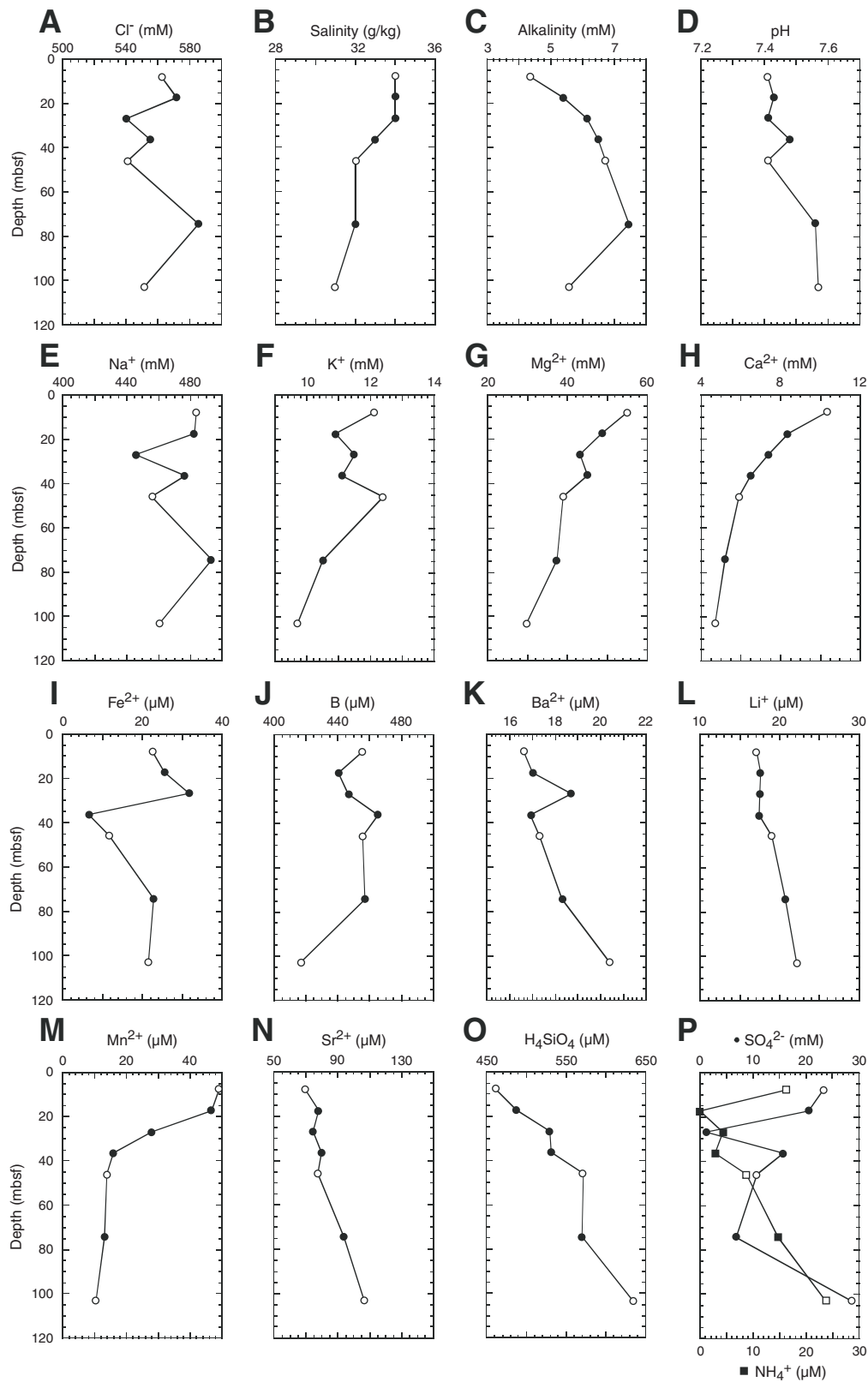


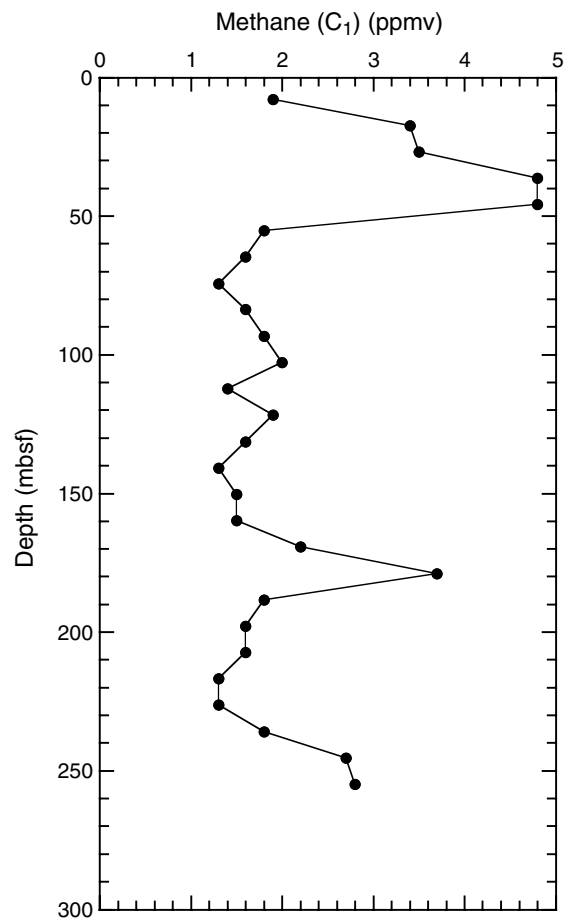
Figure F25. Headspace gas concentrations for Hole U1314A.

Figure F26. Calcium carbonate content for Hole U1314A. A. Gray line indicates the general trend from lower mean CaCO_3 abundance at the bottom toward a higher average at the top. B. CaCO_3 (blue dots) compared to color reflectance (L^* ; gray line).

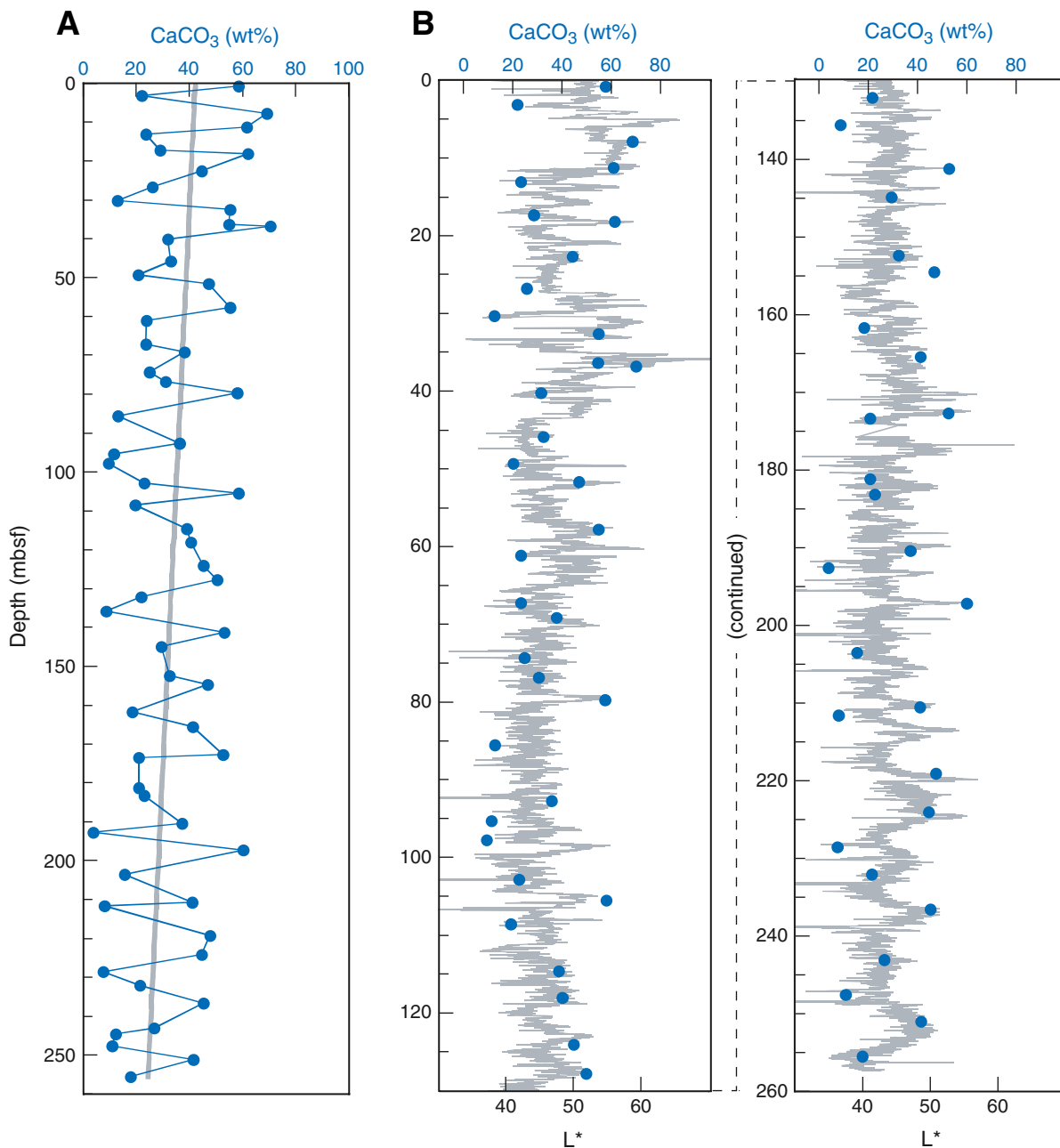


Figure F27. Total organic carbon (TOC) and total nitrogen (TN) for Hole U1314A. The shaded area shows the assumed long-term variability in TOC.

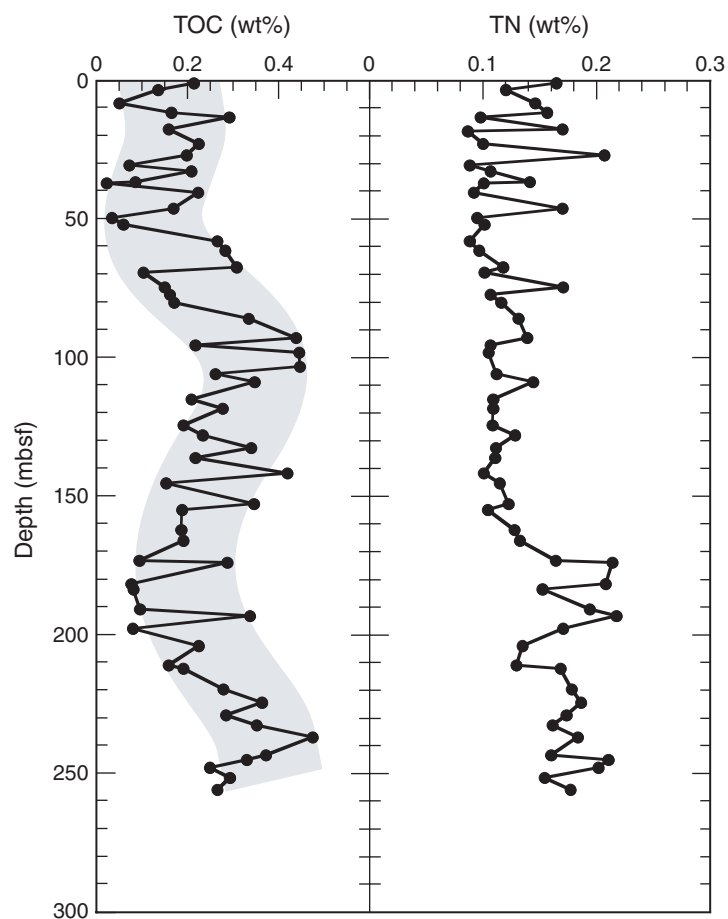


Figure F28. Total organic carbon (TOC; blue dots) for Hole U1314A compared to the magnetic susceptibility splice from Site U1314 (multiply susceptibility by 6×10^{-5} to obtain SI units). Green triangles = positions of samples used for extractable organic matter analysis.

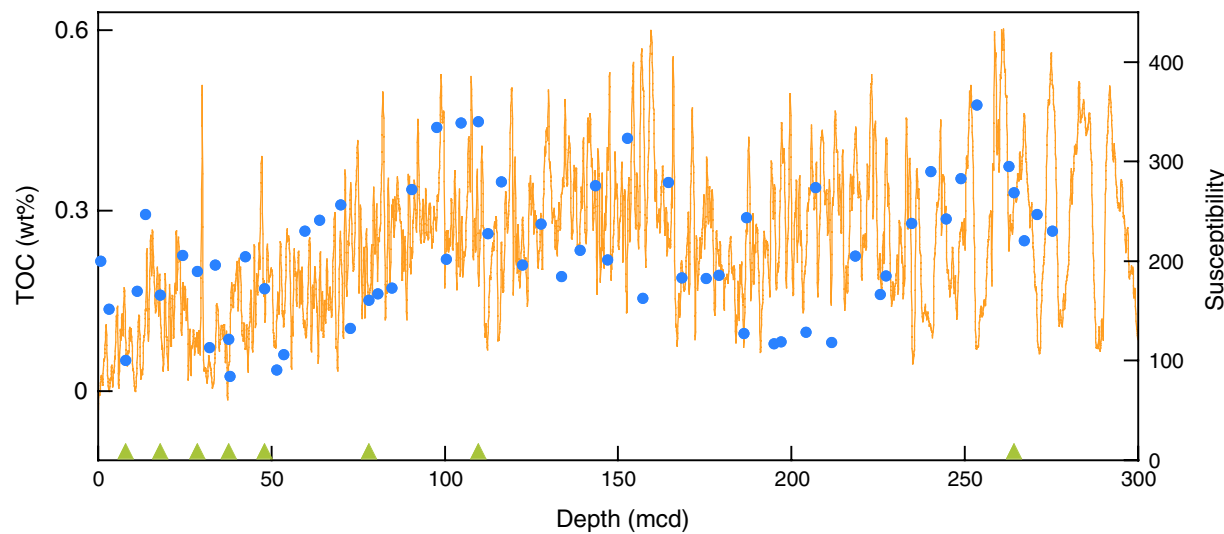


Figure F29. Gas chromatography FID traces of solvent-extractable compounds for Samples 306-U1314A-4H-4, 145–150 cm, and 27H-4, 82–84 cm, showing the difference of extractable organic matter with a predominant terrigenous nature (top panel) and EOM dominated by a marine source (bottom panel). Numbers above or below peaks refer to carbon atom numbers of *n*-alkanes and long-chain alkenones, respectively. Number of double bonds for C₃₇ alkenones are given as :4, :3, and :2. X = contaminant.

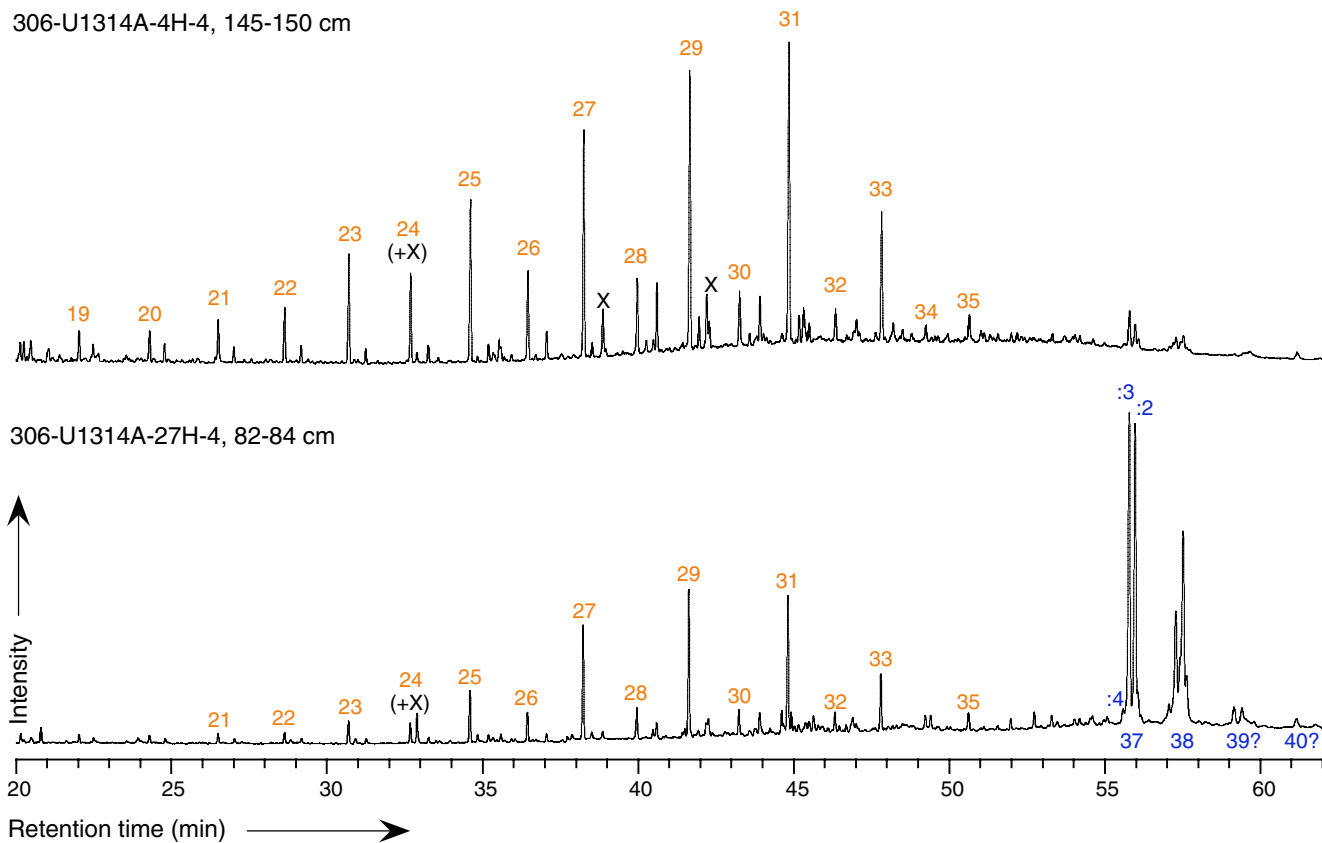


Figure F30. Proportions of marine (blue) and terrigenous (green) extractable organic matter (EOM) at Site U1314 as estimated from the ratios of C_{27} , C_{29} , and C_{31} *n*-alkanes to C_{37} alkenones. Note that the distance between bars does not represent the actual sample position in the depth profile.

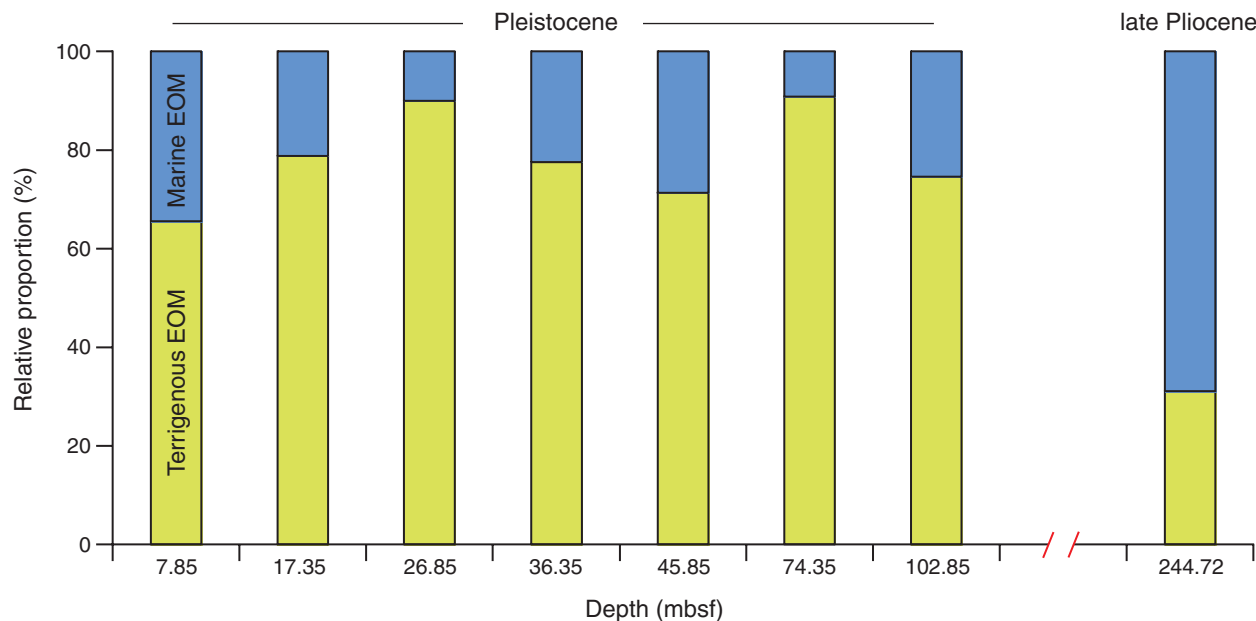


Figure F31. Magnetic susceptibility records from the MST. Multiply values by 6×10^{-5} to obtain SI units.

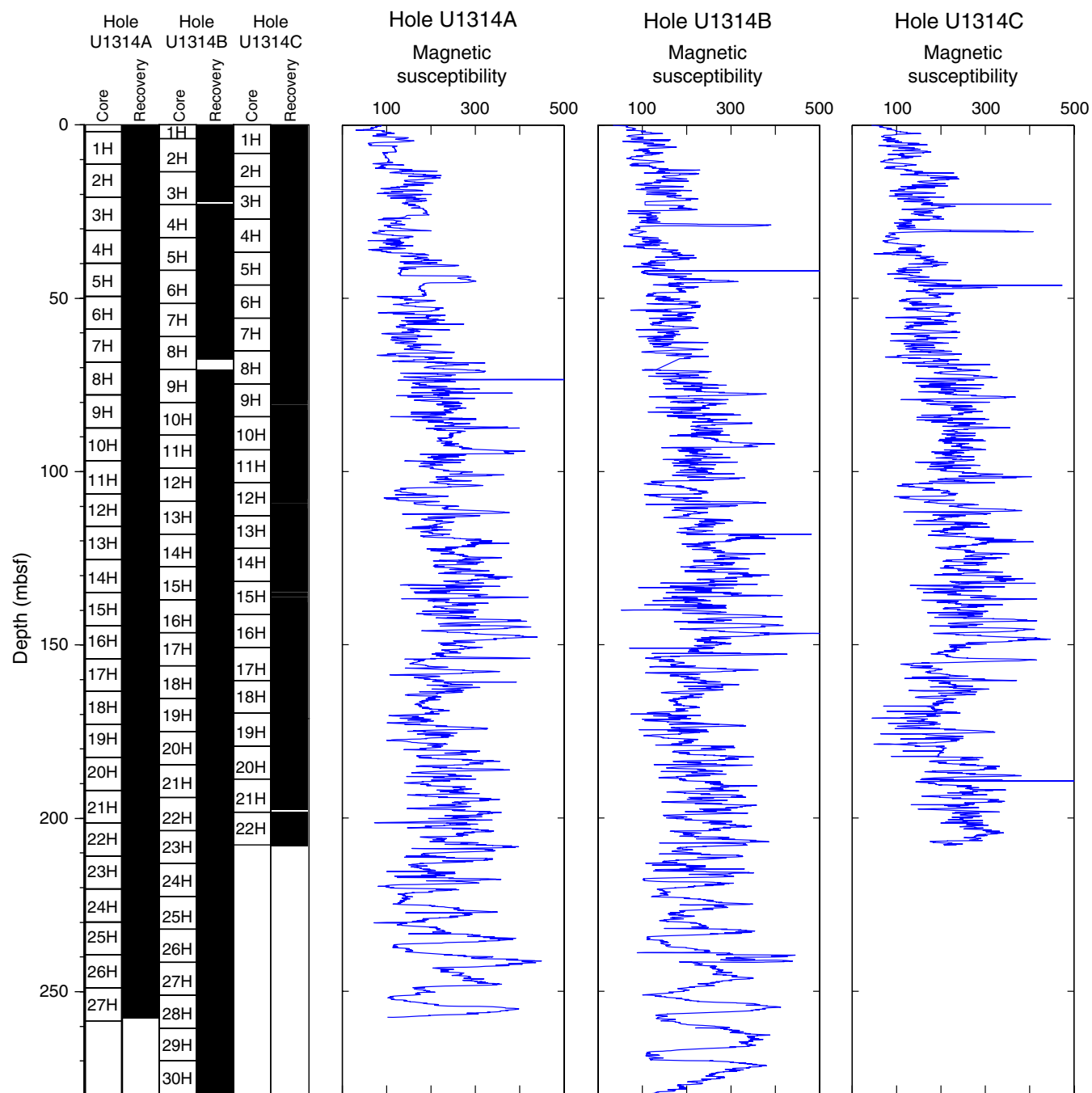


Figure F32. Combined GRA density measurements from the MST and bulk density from discrete measurements (red circles).

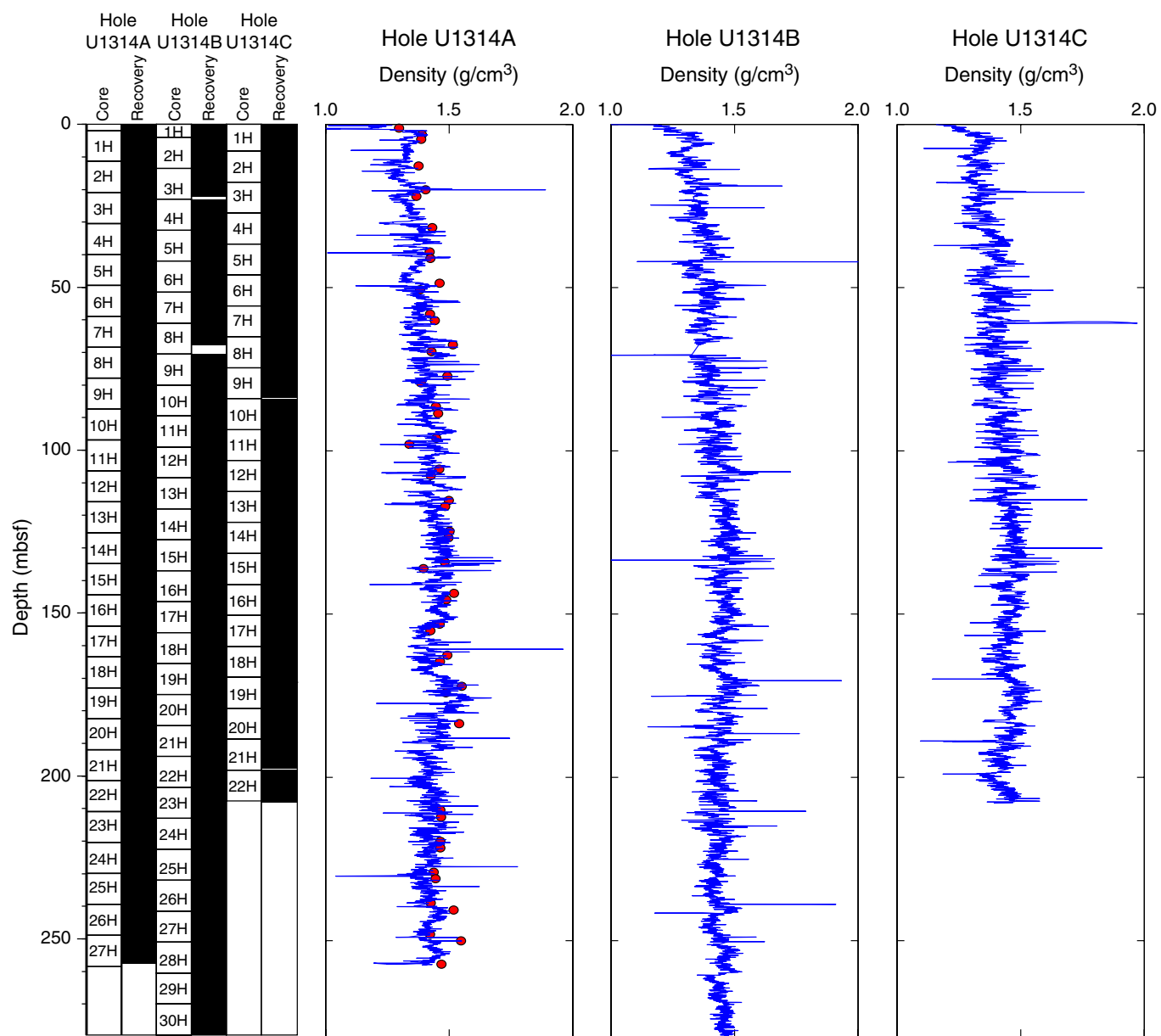


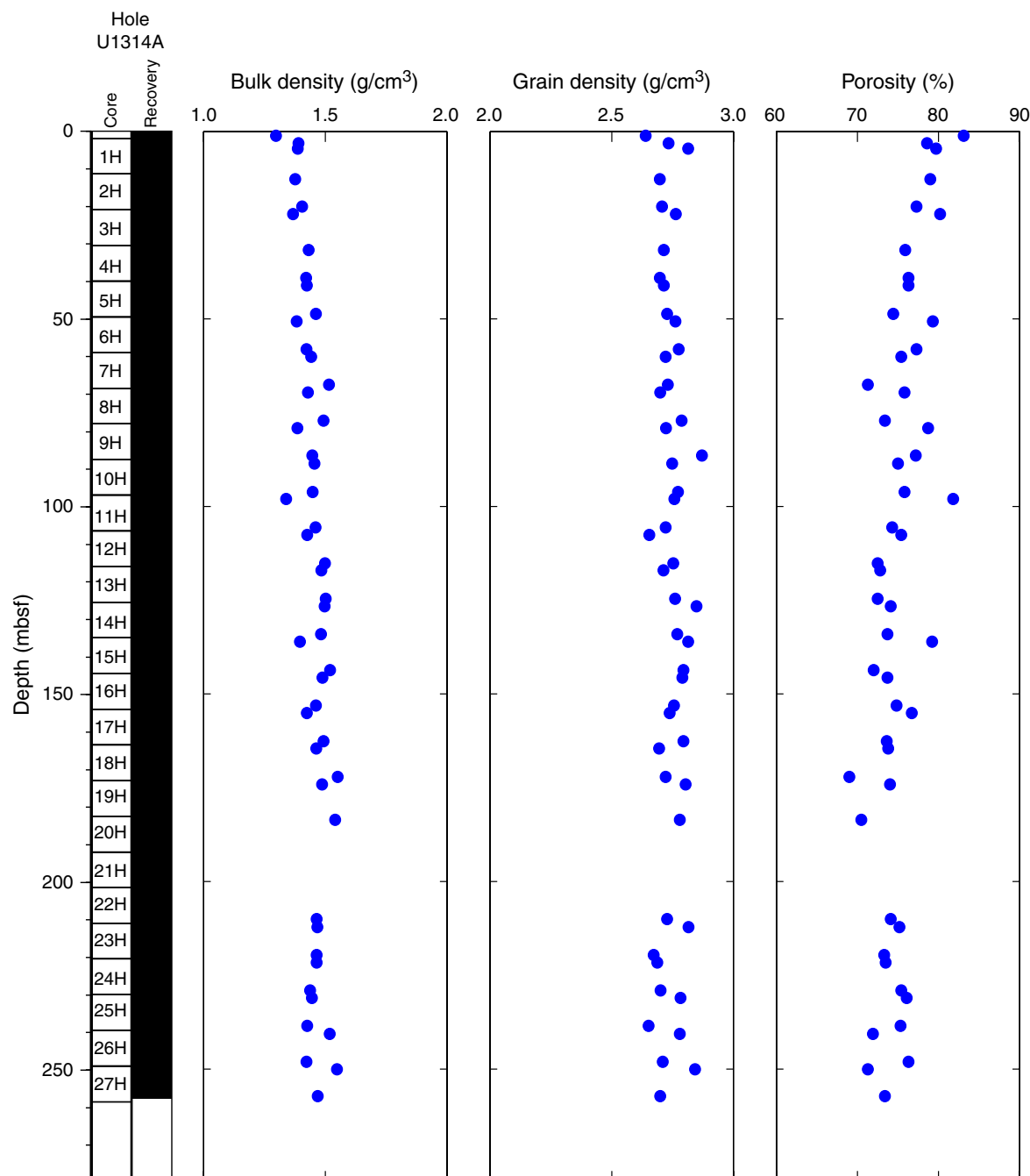
Figure F33. Bulk and grain density and porosity values from Hole U1314A.

Figure F34. Downcore PWL velocity records. Discrete PWS3 measurements from Hole U1314A are shown in red.

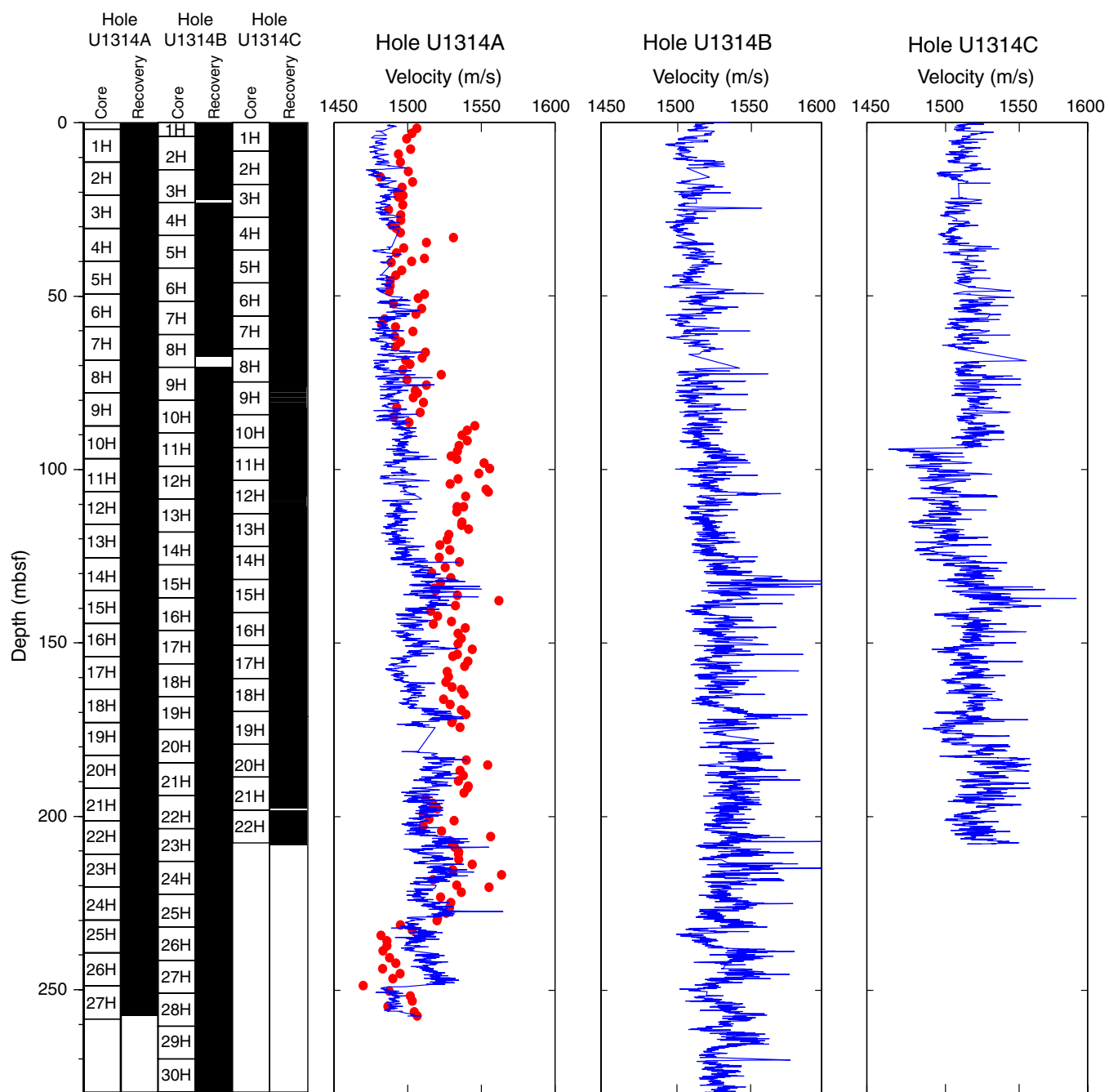


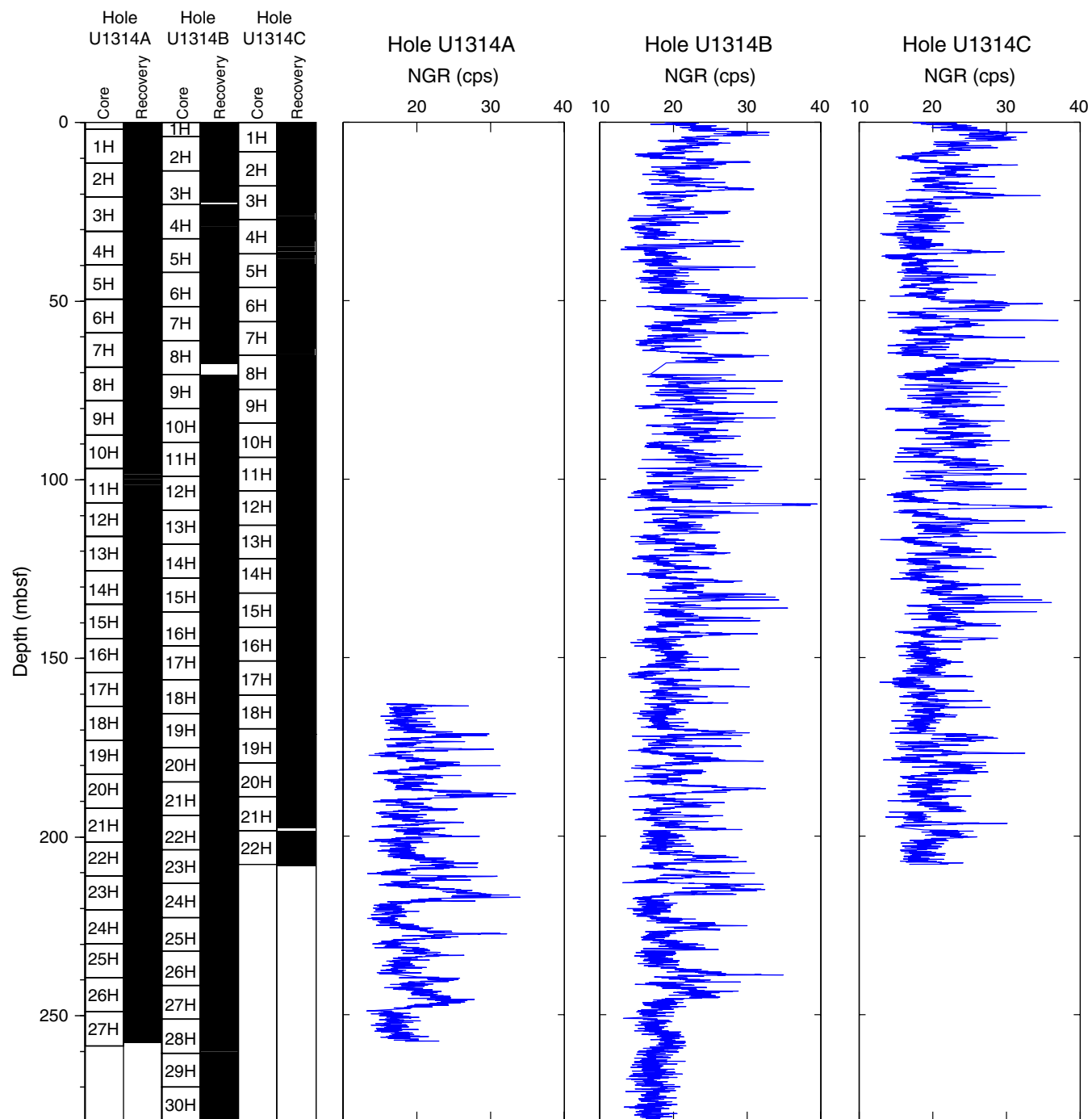
Figure F35. Natural gamma radiation (NGR) counts from the MST.

Table T1. Coring summary, Site U1314. (See table note. Continued on next page.)**Hole U1314A**

Latitude: 56°21.8826'N
 Longitude: 27°53.3091'W
 Time in hole (h): 31.5
 Seafloor (drill pipe measurement from rig floor, mbrf): 2810.6
 Distance between rig floor and sea level (m): -11.2
 Water depth (drill pipe measurement from sea level, m): 2799.4
 Total depth (drill pipe measurement from rig floor, mbrf): 3069
 Total penetration (mbsf): 258.4
 Total length of cored section (m): 258.4
 Total core recovered (m): 267.34
 Core recovery (%): 103.46
 Total number of cores: 28

Hole U1314B

Latitude: 56°21.8964'N
 Longitude: 27°53.3107'W
 Time in hole (h): 25
 Seafloor (drill pipe measurement from rig floor, mbrf): 2811.5
 Distance between rig floor and sea level (m): -11.2
 Water depth (drill pipe measurement from sea level, m): 2800.3
 Total depth (drill pipe measurement from rig floor, mbrf): 3091
 Total penetration (mbsf): 279.5
 Total length of cored section (m): 279.5
 Total core recovered (m): 285.36
 Core recovery (%): 102.1
 Total number of cores: 30

Hole U1314C

Latitude: 56°21.8957'N
 Longitude: 27°53.2867'W
 Time in hole (h): 27.75
 Seafloor (drill pipe measurement from rig floor, mbrf): 2810.3
 Distance between rig floor and sea level (m): -11.2
 Water depth (drill pipe measurement from sea level, m): 2799.1
 Total depth (drill pipe measurement from rig floor, mbrf): 3018
 Total penetration (mbsf): 207.7
 Total length of cored section (m): 207.7
 Total core recovered (m): 212.93
 Core recovery (%): 102.52
 Total number of cores: 22

Core	Date (Apr 2005)	Local time (h)	Depth (mbsf)		Length (m)		Recovery (%)	Comments
			Top	Bottom	Cored	Recovered		
306-U1314A-								
1H	7	1010	0.0	1.9	1.9	2.0	102.6	
2H	7	1100	1.9	11.4	9.5	9.9	103.8	Mechanical shear
3H	7	1145	11.4	20.9	9.5	9.9	104.3	
4H	7	1235	20.9	30.4	9.5	9.8	102.8	Oriented, nonmagnetic core barrel
5H	7	1320	30.4	39.9	9.5	9.8	103.3	Oriented, nonmagnetic core barrel
6H	7	1400	39.9	49.4	9.5	9.9	104.6	Oriented, nonmagnetic core barrel, mechanical shear
7H	7	1445	49.4	58.9	9.5	10.0	105.4	Oriented, nonmagnetic core barrel
8H	7	1530	58.9	68.4	9.5	10.0	105.5	Oriented, nonmagnetic core barrel
9H	7	1610	68.4	77.9	9.5	9.9	104.6	Oriented, nonmagnetic core barrel
10H	7	1655	77.9	87.4	9.5	9.8	103.6	Oriented, nonmagnetic core barrel, drilled holes in core for gas expansion
11H	7	1740	87.4	96.9	9.5	10.0	104.7	Oriented, nonmagnetic core barrel, mechanical shear, drilled holes in core for gas expansion
12H	7	1830	96.9	106.4	9.5	9.7	101.9	Oriented, nonmagnetic core barrel
13H	7	1910	106.4	115.9	9.5	10.1	105.9	Oriented, nonmagnetic core barrel
14H	7	2000	115.9	125.4	9.5	9.9	104.4	Oriented, nonmagnetic core barrel
15H	7	2040	125.4	134.9	9.5	9.9	104.5	Oriented, nonmagnetic core barrel
16H	7	2125	134.9	144.4	9.5	10.0	105.3	Oriented, nonmagnetic core barrel
17H	7	2210	144.4	153.9	9.5	9.9	103.9	Oriented, nonmagnetic core barrel
18H	7	2250	153.9	163.4	9.5	10.0	104.7	Oriented, nonmagnetic core barrel
19H	7	2330	163.4	172.9	9.5	9.9	104.2	Oriented, nonmagnetic core barrel
20H	8	0015	172.9	182.4	9.5	9.8	103.1	Oriented, nonmagnetic core barrel
21H	8	0105	182.4	191.9	9.5	9.8	103.3	Oriented, nonmagnetic core barrel
22H	8	0145	191.9	201.4	9.5	9.7	101.9	Oriented, nonmagnetic core barrel
23H	8	0235	201.4	210.9	9.5	9.8	103.6	Oriented, nonmagnetic core barrel
24H	8	0325	210.9	220.4	9.5	9.9	103.7	Oriented, nonmagnetic core barrel



Table T1 (continued).

Core	Date (Apr 2005)	Local time (h)	Depth (mbsf)		Length (m)		Recovery (%)	Comments
			Top	Bottom	Cored	Recovered		
25H	8	0405	220.4	229.9	9.5	9.9	104.0	Oriented, nonmagnetic core barrel
26H	8	0450	229.9	239.4	9.5	9.9	103.8	Oriented, nonmagnetic core barrel
27H	8	0540	239.4	248.9	9.5	9.6	101.5	Oriented, nonmagnetic core barrel
28H	8	0725	248.9	258.4	9.5	8.7	91.4	Oriented, nonmagnetic core barrel
			Cored totals:		258.40	267.34	103.46	
306-U1314B-								
1H	8	1235	0.0	4.0	4.0	4.0	100.5	
2H	8	1315	4.0	13.5	9.5	9.4	99.4	
3H	8	1350	13.5	23.0	9.5	8.9	93.6	
4H	8	1430	23.0	32.5	9.5	9.8	102.8	Oriented, nonmagnetic core barrel
5H	8	1515	32.5	42.0	9.5	9.8	103.1	Oriented, nonmagnetic core barrel
6H	8	1630	42.0	51.5	9.5	9.9	104.6	Oriented, nonmagnetic core barrel, sheared pin on GS overshot
7H	8	1720	51.5	61.0	9.5	9.8	103.3	Oriented, nonmagnetic core barrel
8H	8	1800	61.0	70.5	9.5	6.6	69.4	Oriented, nonmagnetic core barrel
9H	8	1845	70.5	80.0	9.5	10.0	104.9	Oriented, nonmagnetic core barrel
10H	8	1925	80.0	89.5	9.5	10.0	104.7	Oriented, nonmagnetic core barrel
11H	8	2010	89.5	99.0	9.5	10.0	105.7	Oriented, nonmagnetic core barrel
12H	8	2050	99.0	108.5	9.5	10.0	104.9	Oriented, nonmagnetic core barrel
13H	8	2135	108.5	118.0	9.5	9.9	104.3	Oriented, nonmagnetic core barrel
14H	8	2215	118.0	127.5	9.5	9.9	104.0	Oriented, nonmagnetic core barrel
15H	8	2255	127.5	137.0	9.5	10.0	105.3	Oriented, nonmagnetic core barrel
16H	8	2320	137.0	146.5	9.5	9.9	104.2	Oriented, nonmagnetic core barrel
17H	9	0020	146.5	156.0	9.5	9.9	104.0	Oriented, nonmagnetic core barrel
18H	9	0105	156.0	165.5	9.5	9.9	104.0	Oriented, nonmagnetic core barrel
19H	9	0150	165.5	175.0	9.5	10.0	104.7	Oriented, nonmagnetic core barrel
20H	9	0235	175.0	184.5	9.5	9.9	103.8	Oriented, nonmagnetic core barrel
21H	9	0325	184.5	194.0	9.5	9.8	103.6	Oriented, nonmagnetic core barrel
22H	9	0405	194.0	203.5	9.5	9.9	103.9	Oriented, nonmagnetic core barrel
23H	9	0450	203.5	213.0	9.5	9.8	103.5	Oriented, nonmagnetic core barrel
24H	9	0540	213.0	222.5	9.5	9.8	102.9	Oriented, nonmagnetic core barrel
25H	9	0620	222.5	232.0	9.5	9.9	104.2	Oriented, nonmagnetic core barrel
26H	9	0705	232.0	241.5	9.5	9.9	104.6	Oriented, nonmagnetic core barrel
27H	9	0750	241.5	251.0	9.5	9.6	100.6	Oriented, nonmagnetic core barrel
28H	9	0835	251.0	260.5	9.5	9.9	103.7	Oriented, nonmagnetic core barrel
29H	9	0925	260.5	270.0	9.5	9.4	99.4	Oriented, nonmagnetic core barrel
30H	9	1040	270.0	279.5	9.5	9.9	104.3	Oriented, nonmagnetic core barrel
			Cored totals:		279.50	285.36	102.10	
306-U1314C-								
1H	9	1340	0.0	8.2	8.2	8.2	100.2	
2H	9	1415	8.2	17.7	9.5	9.7	102.2	
3H	9	1500	17.7	27.2	9.5	9.6	101.5	
4H	9	1540	27.2	36.7	9.5	9.8	103.2	Oriented, nonmagnetic core barrel
5H	9	1620	36.7	46.2	9.5	9.7	102.2	Oriented, nonmagnetic core barrel
6H	9	1715	46.2	55.7	9.5	9.6	100.5	Oriented, nonmagnetic core barrel
7H	9	1755	55.7	65.2	9.5	9.8	103.5	Oriented, nonmagnetic core barrel
8H	9	1845	65.2	74.7	9.5	9.6	100.9	Oriented, nonmagnetic core barrel
9H	9	1930	74.7	84.2	9.5	9.4	98.7	Oriented, nonmagnetic core barrel
10H	9	2020	84.2	93.7	9.5	9.8	103.1	Oriented, nonmagnetic core barrel
11H	9	2100	93.7	103.2	9.5	9.9	104.6	Oriented, nonmagnetic core barrel
12H	9	2145	103.2	112.7	9.5	10.0	104.7	Oriented, nonmagnetic core barrel
13H	9	2230	112.7	122.2	9.5	9.5	99.7	Oriented, nonmagnetic core barrel
14H	9	2310	122.2	131.7	9.5	9.9	104.1	Oriented, nonmagnetic core barrel
15H	9	2355	131.7	141.2	9.5	9.8	103.6	Oriented, nonmagnetic core barrel
16H	10	0030	141.2	150.7	9.5	9.9	104.6	Oriented, nonmagnetic core barrel
17H	10	0200	150.7	160.2	9.5	10.0	104.8	Oriented, nonmagnetic core barrel
18H	10	0245	160.2	169.7	9.5	9.9	104.4	Oriented, nonmagnetic core barrel
19H	10	0340	169.7	179.2	9.5	9.9	104.6	Oriented, nonmagnetic core barrel
20H	10	0505	179.2	188.7	9.5	9.9	104.3	Oriented, nonmagnetic core barrel, sheared pin on GS overshot
21H	10	0600	188.7	198.2	9.5	9.0	94.4	Oriented, nonmagnetic core barrel
22H	10	0755	198.2	207.7	9.5	10.0	105.1	Oriented, nonmagnetic core barrel
			Cored totals:		207.70	212.93	102.52	

Note: GS = pulling tool device attached to the coring line that is used to engage and retrieve inner core barrels and other downhole tools.



Table T2. Isolated gravel data, lithology, diameter, and shape, Holes U1314A, U1314B, and U1314C. (See table note. Continued on next page.)

Core, section, interval (cm)	Depth (mbsf)	Comments
306-U1314A-		
4H-5, 9	26.99	Basalt clast, d = 2 mm, angular, in flow-in
5H-3, 95	34.35	Mud clast, dark gray, d = 20 mm
7H-1, 1	49.41	Unidentified clast, dark gray, d = 10 mm, subrounded, in flow-in
7H-1, 2	49.42	Unidentified clast, dark gray, d = 15 mm, subangular, in flow-in
7H-1, 17	49.57	Siltstone clast, dark gray, d = 35 mm, subangular, in flow-in
7H-5, 143	56.83	Porphyritic clast, felsic (?), d = 10 mm
8H-1, 14	59.04	Unidentified clast, d = 8 mm, subangular, in flow-in
8H-1, 105	59.95	Unidentified clast, d = 7 mm, subrounded
8H-1, 109	59.99	Unidentified clast, d = 5 mm, subrounded
8H-4, 6	475.40	Unidentified clast, d = 8 mm, subangular
8H-5, 117	66.07	Unidentified clast, d = 14 mm
8H-7, 20	8.10	Unidentified clast, d = 3 mm
8H-7, 36	68.26	Unidentified clast, dark gray
8H-CC, 6	68.77	Unidentified clast, d = 4 mm
8H-CC, 7	68.78	Unidentified clast, d = 5 mm
8H-CC, 9	68.80	Unidentified clasts, mafic (x2), d = 15 mm, second in three pieces from same dropstone?
9H-1, 8	68.48	Sandstone clast, fine-grained, d = 20 mm
9H-3, 125	72.65	Unidentified clast, d = 8 mm
9H-4, 56	73.46	Pegmatite clast, d = 40 mm, subrounded
10H-5, 21	83.91	Basalt clast, d = 22 mm, angular
10H-6, 85	86.00	Shale (?) clast, d = 5 mm, angular
11H-1, 2	87.42	Basalt clast, d = 37 mm, subangular, in flow-in
11H-2, 95	89.85	Shale clast, d = 5 mm, angular
11H-3, 96	91.36	Basalt clast, d = 10 mm, angular
12H-1, 73	97.63	Unidentified clast, d = 3 mm, subangular
12H-1, 80	97.70	Unidentified clast, d = 11 mm, subrounded
12H-1, 95	97.85	Unidentified clasts (x2), d = 2 mm, 3 mm, subrounded
12H-1, 100	97.90	Unidentified clast, d = 4 mm, subrounded
13H-1, 112	107.52	Basalt clast, d = 8 mm, subangular, in flow-/fall-in
13H-5, 106	113.46	Sandstone (?) clast, d = 15 mm (long axis), subrounded, elongate
14H-2, 90	118.30	Shale clast, d = 4 mm, angular
14H-5, 35	122.25	Shale (?) clast, d = 3 mm, angular
14H-5, 68	122.58	Basalt clast, d = 7 mm, angular
14H-5, 83	122.73	Sandstone (?) clast, d = 10 mm, angular
14H-5, 115	123.05	Basalt clast, d = 10 mm, angular
15H-1, 58	125.98	Sandstone clast, d = 5 mm, subrounded
15H-5, 147	132.87	Basalt clast, d = 10 mm, angular
18H-5, 85	162.25	Unidentified clast, d = 46 mm, subrounded
18H-6, 19	163.09	Basalt (?) clast, d = 27 mm, subangular
22H-1, 75	192.65	Metamorphic clast, d = 45 mm, subrounded
23H-4, 15	206.05	Shale clast, d = 3 mm, subrounded
23H-4, 17	206.07	Shale clast, d = 2 mm, subrounded
23H-4, 20	206.10	Shale clast, d = 3 mm, subrounded
23H-4, 24	206.14	Basalt clast, d = 2 mm, subangular
24H-3, 148	215.38	Granite clast, d = 3 mm, angular
24H-4, 1	215.41	Unidentified clast, d = 3 mm, subangular
24H-4, 3	215.43	Unidentified clasts (x2), d = 2 mm, 4 mm, subangular
24H-5, 72	217.62	Unidentified clast, d = 7 mm, subangular
24H-6, 36	218.76	Sandstone clast, d = 8 mm, subrounded
25H-6, 43	228.33	Unidentified clast, d = 15 mm, subangular
26H-CC, 11	239.66	Sandstone clast, d = 10 mm, angular
306-U1314B-		
1H-2, 98	2.48	Sandstone clast, d = 15 mm, subangular
2H-5, 85	10.85	Unidentified clast, d = 6 mm, subrounded
2H-5, 132	11.32	Unidentified clast, d = 12 mm, subrounded
3H-6, 103	22.03	Basalt clast, d = 10 mm, subrounded
4H-1, 8	23.08	Basalt clast, d = 40 mm, angular, fall-in
7H-4, 8	57.58	Unidentified clast, d = 8 mm, subrounded
8H-1, 32	61.32	Basalt clast, d = 4 mm, angular
9H-1, 49	70.99	Unidentified clast, 15 × 6 × 2 mm, angular
9H-2, 42	72.42	Basalt clast, d = 5 mm, angular
9H-2, 52	72.52	Basalt clast, d = 10 mm, angular
9H-6, 16	78.16	Volcanic sandstone clast, d = 8 mm, subangular
9H-6, 82	78.82	Quartz clast, d = 8 mm, angular
9H-7, 44	79.94	Unidentified clast, d = 6 mm, angular

Table T2 (continued).

Core, section, interval (cm)	Depth (mbsf)	Comments
10H-1, 58	80.58	Gneiss (?) clast, d = 40 mm
10H-3, 93	83.93	Pyroclastic clast (?), d = 10 mm, angular
10H-6, 142	88.92	Mudstone clasts (x2), d = 7 mm, 8 mm
11H-3, 62	93.12	Volcanic clast, d = 3 mm
11H-3, 79	93.29	Basalt clast, d = 12 mm, subangular
11H-6, 39	97.39	Unidentified clast, d = 5 mm, angular
11H-6, 70	97.70	Quartz clast, d = 5 mm, angular
12H-1, 65	99.65	Unidentified clast, d = 20 mm, subangular
12H-1, 112	100.12	Scoria clast, d = 10 mm, angular
12H-2, 7	100.57	Sandstone clast, d = 4 mm, angular
12H-2, 103	101.53	Carbonate clast, d = 3 mm, angular
12H-5, 141	106.41	Basalt clast (x2), d = 4 mm, angular; Sandstone clast, d = 2.5 mm, subangular
12H-6, 16	106.66	Unidentified clast, d = 7 mm, subrounded
12H-6, 101	107.51	Unidentified clast, d = 2 mm, subrounded
13H-1, 23	108.73	Unidentified clast, d = 3 mm, angular
13H-1, 105	109.55	Quartzite clast, d = 12 mm, angular
13H-4, 67	113.67	Sandstone clast, d = 8 mm, angular
13H-4, 96	113.96	Quartzite clast, d = 14 mm, angular
13H-4, 126	114.26	Scoria clast, d = 10 mm, angular
14H-5, 22	124.22	Unidentified clast, d = 6 mm, sandstone
15H-4, 24	132.24	Sandstone clast, d = 5 mm, subrounded
15H-6, 117	136.17	Carbonate clast, d = 5 mm, subangular
15H-6, 120	136.20	Diorite clast, d = 20 mm, angular
22H-2, 36	195.86	Sandstone clast, d = 3 mm, subangular
22H-2, 48	195.98	Sandstone clast, d = 2 mm, subangular
23H-3, 62	207.12	Sandstone clast, d = 6 mm, angular
23H-5, 94	210.44	Sandstone clast, d = 8 mm, angular
24H-6, 23	220.73	Sandstone clast, d = 2 mm, angular
24H-7, 4	222.04	Sandstone clast, d = 3 mm, angular
25H-2, 104	225.04	Basalt clast, d = 15 mm, subangular
25H-3, 105	226.55	Quartz clast, d = 3 mm, subrounded
<hr/>		
306-U1314C-		
2H-4, 63	13.33	Basalt clast, d = 10 mm, subrounded
2H-4, 132	14.02	Mudstone clasts (x2), d = 8 mm, 10 mm, subangular
2H-5, 97	15.17	Basalt clast, d = 22 mm, subangular,
3H-2, 143	20.63	Quartzite clasts (x2), d = 20 mm, rounded and subangular
5H-4, 133	42.53	Basalt clast, d = 8 mm, subangular
5H-5, 107	43.77	Basalt clast, d = 4 mm, subrounded
5H-6, 68	44.88	Scoria clast, d = 4 mm, subrounded
6H-4, 90	51.60	Mudstone clast, d = 3 mm, subrounded
6H-4, 137	52.07	Basalt clast, d = 6 mm, subrounded
7H-4, 68	60.88	Gneiss clast, d = 50 mm
8H-2, 14	66.84	Gneiss clast, d = 18 mm, rounded
8H-3, 30	68.50	Gneiss clast, d = 18 mm, rounded
8H-3, 48	68.68	Gneiss clast, d = 18 mm, rounded
8H-3, 59	68.79	Sandstone clast, d = 3 mm, subrounded
8H-7, 3	73.73	Basalt clast, d = 8 mm, subrounded
8H-7, 29	73.99	Sandstone clast, d = 10 mm, angular
9H-1, 89	75.59	Sandstone clast, d = 5 mm, subangular
9H-2, 77	76.97	Unidentified clast, d = 3 mm, subrounded
9H-3, 123	78.93	Volcanic sand clast, d = 7 mm, subangular
10H-1, 86	85.06	Sandstone clast, d = 18 mm, subrounded
11H-1, 57	94.27	Carbonate clast, d = 13 mm, angular
12H-3, 95	107.15	Basalt clast, d = 10 mm, subangular
13H-3, 38	116.08	Basalt clasts (x2), d = 20 mm, subangular
14H-6, 10	129.80	Quartzite clast, d = 33 mm, subangular
15H-CC	141.39	Unidentified clast
17H-2, 24	152.44	Volcanic clast, d = 8 mm, angular
17H-5, 48	157.18	Scoria clast, d = 2mm, subrounded
17H-6, 116	159.36	Microgranite clast, d = 18 mm, subangular

Note: Centered on (m).



Table T3. Calcareous nannofossil, planktonic and benthic foraminifer, diatom, and radiolarian bioevents, Holes U1314A, U1314B, and U1314C.

Species event	Age (Ma)	Depth (mbsf)		
		Hole U1314A	Hole U1314B	Hole U1314C
FO <i>Emiliana huxleyi</i>	0.25	25.65	27.75	22.45
LO <i>Rhizosolenia curvirostris</i>	0.30	25.65	18.25	31.95
LO <i>Pseudoemiliania lacunosa</i>	0.41	35.15	37.25	31.95
LO <i>Fragilariopsis reinholdii</i>	0.50		37.25	
FO <i>Helicosphaera inversa</i>	0.51	44.65		50.95
LO <i>Fragilariopsis fassilli</i>	0.70	54.15	56.25	
LO <i>Neodenticula seminae</i>	0.84	63.65	65.75	60.45
LO <i>Reticulofenestra asanoi</i>	0.85	63.65	65.75	69.95
FO <i>Gephyrocapsa parallela</i>	0.95	73.15	75.25	69.95
LO <i>Stilostomella lepidula</i>	1.00	82.65		
FO <i>Reticulofenestra asanoi</i>	1.16	92.15	84.75	88.95
LO large <i>Gephyrocapsa</i> spp.	1.21	92.15	84.75	88.95
FO <i>Neodenticula seminae</i>	1.25	101.65	94.25	88.95
LO <i>Helicosphaera sellii</i>	1.27	101.65	94.25	88.95
FO large <i>Gephyrocapsa</i> spp.	1.45	120.65	113.25	107.95
FO <i>Rhizosolenia curvirostris</i>	1.52	120.65	141.75	107.95
FO <i>Gephyrocapsa oceanica</i>	1.65	130.15	141.75	136.45
FO <i>Gephyrocapsa caribbeanica</i>	1.73	130.15	141.75	145.95
FaO <i>Neogloboquadrina pachyderma</i> (s)	1.78	149.15	141.75	145.95
LO <i>Discoaster brouweri</i>	1.97	158.65	160.75	164.95
FO <i>Globorotalia inflata</i>	2.09	168.15	170.25	174.45
LO <i>Discoaster pentaradiatus</i>	2.38	215.65	217.75	
LO <i>Thalassiosira convexa</i>	2.40	225.15	236.75	
LO <i>Neogloboquadrina atlantica</i> (s)	2.41	206.15	208.25	202.95
LO <i>Globorotalia puncticulata</i>	2.41	206.15	208.25	
LO <i>Discoaster surculus</i>	2.54	234.65	236.75	
LO <i>Spongaster ?tetras</i>	2.60	253.65	246.25	
LO <i>Fragilariopsis jouseae</i>	2.70		246.25	
LO <i>Discoaster tamalis</i>	2.74	253.65	255.75	

Notes: Dark blue = nannofossils, pink = foraminifers, light blue = diatoms, orange = radiolarians. For first occurrences (FO) and first abundant occurrences (FaO), depth is plotted as the midpoint between the depth at which the species was first observed and the depth of the sample below. For last occurrences (LO), depth is plotted as the midpoint between the depth at which the species was last observed and the depth of the sample above.



Table T4. Distribution of calcareous nannofossils, Hole U1314A. (Continued on next page.)

Core, section	Martini (1971) Zone (base)	Age (Ma)	Abundance	Preservation	<i>Cyclolithus tenuis</i>	<i>Cyclolithus granularis</i>	<i>Discoaster brionieri</i>	<i>Discoaster pentadactylus</i>	<i>Discoaster tenuis</i>	<i>Discoaster latidens</i>	<i>Cephalوفорас caribeanus</i>	<i>Cephalوفорас parvula</i>	<i>Cephalوفорас oceanica</i>	<i>Cephalوفорас enigmatica</i>	<i>Helicospira helvetica</i>	<i>Pseudodiscosphaera pseudoluminifera</i>	<i>Reticulofenestra pseudoluminifera</i>	<i>Reticulofenestra pseudoluminifera (5-7 μm)</i>	<i>Sphaerolithus dorsi</i>	<i>Sphaerolithus spp.</i>	<i>Thaumasiosphaera sphaeroides</i>	<i>Umbilicosphaera sphaeroides</i>	
306-U1314A-																							
1H-CC	NN21		V	G	C																		
2H-CC			V	G	C																		
3H-CC	NN20?		V	G	C																		
4H-CC			V	G	C																		
5H-CC			V	G	C																		
6H-CC			V	G	C																		
7H-CC			V	G	C																		
8H-CC			V	G	C																		
9H-CC			V	G	C																		
10H-CC			V	G	C																		
11H-CC	NN19	1.16	V	G-M	A																		
12H-CC		1.21	V	G-M	C																		
13H-CC		1.27	V	G-M	C																		
14H-CC			V	G-M	F																		
15H-CC			A	G-M	C	R																	
16H-CC			A	G-M	C	R	R																
17H-CC			A	G-M	C																		
18H-CC			V	G-M	C	F																	
19H-CC	NN18	A	G	C	C	C																	
20H-CC		A	G	F	F	C																	
21H-CC		A	G-M	F	F	C																	
22H-CC		A	G-M	C	F																		
23H-CC	NN17	V	G-M	F		C	A																
24H-CC		A	G-M	F	R	C	A																
25H-CC		V	G-M	C	F	C	A																
26H-CC	NN16	V	G-M	C	F	C	A																
27H-CC		V	G-M	C	F	R	C																
28H-CC		V	G-M	C	F	F	A																

Notes: Abundance: V = very abundant, A = abundant, C = common, F = few, R = rare, p = present, ? = questionable, * = reworked. Preservation: G = good, M = moderate. See “[Calcareous nannofossils](#)” in the “Site U1312–U1315 methods” chapter. FO = first occurrence, LO = last occurrence.



Table T4 (continued).

Core, section	Martini (1971) Zone (base)	Age (Ma)	Reworked Cretaceous		Reworked Paleogene		Event	
			Abundance	Prevalence	Abundance	Prevalence		
306-U1314A-1H-CC	NN21	V	V	M D D G	W M D D G	Necritostrotius spp.?	FO <i>E. huxleyi</i> ?	
2H-CC	NN20?	V	V	M D D G	W M D D G	Reticulofenestra spp.	LO <i>P. lacunosa</i> ; FO <i>H. inversa</i>	
3H-CC	NN19	V	V	M D D G	W M D D G	Cupulicostatus spp.	LO <i>R. asanoi</i> ; FO <i>G. parallela</i>	
4H-CC		A	V	M D D G	W M D D G	Dictyocoelites bisectus	FO <i>R. asanoi</i>	
5H-CC		A	V	M D D G	W M D D G	Chiasmolithus bilobus	LO large <i>Gephyrocapsa</i> spp. (>5.5 µm)	
6H-CC		A	V	M D D G	W M D D G	Chiasmolithus uncinatus	LO <i>H. sellii</i>	
7H-CC		V	V	M D D G	W M D D G	Chiasmolithus cf. <i>platocysticus</i> ultraforms	FO large <i>Gephyrocapsa</i> spp. (>5.5 µm)	
8H-CC		V	V	M D D G	W M D D G	Chiasmolithus cf. <i>platocysticus</i> ultraforms	FO <i>G. oceanica</i> , <i>G. caribbeanica</i> (>4 µm)	
9H-CC		V	V	M D D G	W M D D G			
10H-CC		V	V	M D D G	W M D D G			
11H-CC	NN18	A	A	M D D G	W M D D G		LO <i>D. brouweri</i>	
12H-CC		A	A	M D D G	W M D D G			
13H-CC		V	V	M D D G	W M D D G			
14H-CC		V	V	M D D G	W M D D G			
15H-CC		A	A	M D D G	W M D D G			
16H-CC		A	A	M D D G	W M D D G			
17H-CC		A	A	M D D G	W M D D G			
18H-CC		V	V	M D D G	W M D D G			
19H-CC		A	A	M D D G	W M D D G			
20H-CC	NN17	A	A	M D D G	W M D D G		LO <i>D. pentaradiatus</i>	
21H-CC		A	A	M D D G	W M D D G			
22H-CC		A	A	M D D G	W M D D G		LO <i>D. surculus</i>	
23H-CC	NN16	V	V	M D D G	W M D D G		LO <i>D. tamalis</i>	
24H-CC		A	A	M D D G	W M D D G			
25H-CC		V	V	M D D G	W M D D G			
26H-CC		V	V	M D D G	W M D D G			
27H-CC		V	V	M D D G	W M D D G			
28H-CC		V	V	M D D G	W M D D G			



Table T5. Distribution of calcareous nannofossils, Hole U1314B. (Continued on next page.)

Core, section	Martini (1971) Zone (base)	Age (Ma)	Abundance	Coccolithus baculumii		Coccolithus crenatus		Coccolithus leptoceras		Coccolithus leptoceras sp.		Sphaerolithus davisii		Sphaerolithus spp.		Thiotricha sp.		Umbilicosphaera spongiae	
				Discoaster tubulus	Discoaster tubulus	Discoaster tubulus	Discoaster tubulus	Discoaster tubulus	Discoaster tubulus	Discoaster tubulus	Discoaster tubulus	Discoaster tubulus	Discoaster tubulus	Discoaster tubulus	Discoaster tubulus	Discoaster tubulus	Discoaster tubulus	Discoaster tubulus	Discoaster tubulus
306-U1314B-																			
1H-CC	NN21		V														R		
2H-CC			V														R	R	F
3H-CC			V														R	R	R
4H-CC	NN20		V														F	F	R
5H-CC			V														A	A	R
6H-CC			V														A	C	R
7H-CC	NN19	0.85	V														A	A	C
8H-CC			V														A	A	C
9H-CC			V														A	A	C
10H-CC			V														A	A	C
11H-CC			V														A	A	C
12H-CC			V														A	A	C
13H-CC			V														A	A	C
14H-CC			V														A	A	C
15H-CC	NN18	0.95	V														A	A	C
16H-CC			V														A	A	C
17H-CC			V														A	A	C
18H-CC			V														A	A	C
19H-CC			V														A	A	C
20H-CC			V														A	A	C
21H-CC			A														A	A	C
22H-CC			A														A	A	C
23H-CC	NN17	1.16	V														A	A	C
24H-CC			V														A	A	C
25H-CC			V														A	A	C
26H-CC			V														A	A	C
27H-CC	NN16	1.21	V														A	A	C
28H-CC			V														A	A	C
29H-CC			V														A	A	C
30H-CC			V														A	A	C

Notes: Abundance: V = very abundant, A = abundant, C = common, F = few, R = rare, ? = questionable, * = reworked. Preservation: G = good, M = moderate. See “Calcareous nannofossils” in the “Site U1312–U1315 methods” chapter. FO = first occurrence, LO = last occurrence.

Table T5 (continued).

Core, section	Martini (1971) Zone (base)	Age (Ma)	Abundance	Reworked Cretaceous		Reworked Paleogene		Event
				Chiloglyptina spp.	Chatostomolithus spp.	Zeegehadolius spp.	Chatostomolithus spp.	
306-U1314B-1H-CC	NN21	0.85	*	*	*	*	*	FO <i>E. huxleyi</i>
2H-CC			*	*	*	*	*	
3H-CC	NN20	0.95	*	*	*	*	*	LO <i>P. lacunosa</i>
4H-CC		1.16	*	*	*	*	*	
5H-CC	NN19	1.21	*	*	*	*	*	LO <i>R. asanoi</i> ; FO <i>G. parallela</i>
6H-CC		1.27	*	*	*	*	*	FO <i>R. asanoi</i>
7H-CC			*	*	*	*	*	LO large <i>Gephyrocapsa</i> spp. (>5.5 µm)
8H-CC			*	*	*	*	*	LO <i>Helicosphaera sellii</i>
9H-CC			*	*	*	*	*	FO large <i>Gephyrocapsa</i> spp. (>5.5 µm)
10H-CC			*	*	*	*	*	
11H-CC			*	*	*	*	*	
12H-CC			*	*	*	*	*	
13H-CC			*	*	*	*	*	
14H-CC			*	*	*	*	*	
15H-CC			*	*	*	*	*	FO <i>G. oceanica</i> , <i>G. caribbeanica</i> (>4 µm)
16H-CC	NN18		*	*	*	*	*	
17H-CC			*	*	*	*	*	LO <i>D. brouweri</i>
18H-CC			*	*	*	*	*	
19H-CC			*	*	*	*	*	
20H-CC			*	*	*	*	*	
21H-CC	NN17		*	*	*	*	*	LO <i>D. pentaradiatus</i>
22H-CC			*	*	*	*	*	
23H-CC			*	*	*	*	*	LO <i>D. surculus</i>
24H-CC	NN16		*	*	*	*	*	LO <i>D. tamalis</i>
25H-CC			*	*	*	*	*	
26H-CC			*	*	*	*	*	
27H-CC			*	*	*	*	*	
28H-CC			*	*	*	*	*	
29H-CC			*	*	*	*	*	
30H-CC			*	*	*	*	*	



Table T6. Distribution of calcareous nannofossils, Hole U1314C. (Continued on next page.)

Notes: V = very abundant; A = abundant, C = common, F = few, R = rare, ? = questionable, * = reworked. See “[Calcareous nannofossils](#)” in the “Site U1312–U1315 methods” chapter. FO = first occurrence, LO = last occurrence.

Table T6 (continued).

Core, section	Martini (1971) Zone (base)	Age (Ma)	Abundance	Reworked Cretaceous				Reworked Paleogene	Event
				Transversopontis puller	Reticulonectes umbilicalia	Dityococcites bestae	Cyclidelloolithus loeblianus		
306-U1314C-1H-CC	NN21	1.16	A	*	*	*	*	*	FO <i>E. huxleyi</i>
2H-CC	NN20	1.27	V	*	*	*	*	*	LO <i>P. lacunosa</i>
3H-CC	NN19		V	*	*	*	*	*	FO <i>H. inversa</i>
4H-CC			V	*	*	*	*	*	FO <i>G. parallela</i>
5H-CC			V	*	*	*	*	*	LO <i>R. asanoi</i>
6H-CC			V	*	*	*	*	*	FO <i>R. asanoi</i>
7H-CC			A	*	*	*	*	*	LO large <i>Gephyrocapsa</i> spp. (>5.5 µm), <i>H. sellii</i>
8H-CC			V	*	*	*	*	*	FO large <i>Gephyrocapsa</i> spp. (>5.5 µm)
9H-CC			V	*	*	*	*	*	
10H-CC			V	*	*	*	*	*	
11H-CC			V	*	*	*	*	*	
12H-CC			V	*	*	*	*	*	
13H-CC			V	*	*	*	*	*	
14H-CC			V	*	*	*	*	*	
15H-CC			A	*	*	*	*	*	
16H-CC			V	*	*	*	*	*	
17H-CC			V	*	*	*	*	*	
18H-CC			V	*	*	*	*	*	
19H-CC			V	*	*	*	*	*	
20H-CC	NN18		A	*	*	*	*	*	FO <i>G. oceanica</i> (>4 µm)
21H-CC			A	*	*	*	*	*	FO <i>G. caribbeanica</i> (>4 µm)
22H-CC			A	*	*	*	*	*	LO <i>D. brouweri</i>



**Table T7.** Compilation of calcareous nannofossil bioevents, Holes U1314A, U1314B, and U1314C.

Core, section	Species event	Core, section	Species event	Core, section	Species event
306-U1314A-		306-U1314B-		306-U1314C-	
1H-CC		1H-CC		1H-CC	
2H-CC		2H-CC		2H-CC	FO <i>Emiliania huxleyi</i> (0.25 Ma)
3H-CC	FO <i>Emiliania huxleyi</i> (0.25 Ma)	3H-CC	FO <i>Emiliania huxleyi</i> (0.25 Ma)	3H-CC	
4H-CC		4H-CC		4H-CC	
5H-CC	LO <i>Pseudoemiliania lacunosa</i> (0.41 Ma) FO <i>Helicosphaera inversa</i> (0.51 Ma)	5H-CC	LO <i>Pseudoemiliania lacunosa</i> (0.41 Ma)	5H-CC	LO <i>Pseudoemiliania lacunosa</i> (0.41 Ma)
6H-CC		6H-CC		6H-CC	
7H-CC		7H-CC		7H-CC	FO <i>Helicosphaera inversa</i> (0.51 Ma) FO <i>Gephyrocapsa parallela</i> (0.95 Ma)
8H-CC	LO <i>Reticulofenestra asanoi</i> (0.85 Ma) FO <i>Gephyrocapsa parallela</i> (0.95 Ma)	8H-CC	LO <i>Reticulofenestra asanoi</i> (0.85 Ma) FO <i>Gephyrocapsa parallela</i> (0.95 Ma)	8H-CC	FO <i>Reticulofenestra asanoi</i> (0.85 Ma)
9H-CC		9H-CC	FO <i>Reticulofenestra asanoi</i> (1.16 Ma)	9H-CC	FO <i>Reticulofenestra asanoi</i> (1.16 Ma)
10H-CC	FO <i>Reticulofenestra asanoi</i> (1.16 Ma)	10H-CC	LO large <i>Gephyrocapsa</i> spp. (1.21 Ma)	10H-CC	LO large <i>Gephyrocapsa</i> spp. (1.21 Ma) LO <i>Helicosphaera sellii</i> (1.27 Ma)
11H-CC	LO large <i>Gephyrocapsa</i> spp. (1.21 Ma)	11H-CC	LO <i>Helicosphaera sellii</i> (1.27 Ma)	11H-CC	FO large <i>Gephyrocapsa</i> spp. (1.45 Ma)
12H-CC	LO <i>Helicosphaera sellii</i> (1.27 Ma)	12H-CC	FO large <i>Gephyrocapsa</i> spp. (1.45 Ma)		
13H-CC	FO large <i>Gephyrocapsa</i> spp. (1.45 Ma)	13H-CC		13H-CC	
14H-CC	FO <i>Gephyrocapsa oceanica</i> (1.65 Ma) FO <i>Gephyrocapsa caribbeanica</i> (1.73 Ma)	14H-CC		14H-CC	FO <i>Gephyrocapsa oceanica</i> (1.65 Ma)
15H-CC		15H-CC	FO <i>Gephyrocapsa oceanica</i> (1.65 Ma) FO <i>Gephyrocapsa caribbeanica</i> (1.73 Ma)	15H-CC	FO <i>Gephyrocapsa caribbeanica</i> (1.73 Ma)
16H-CC		16H-CC		16H-CC	
17H-CC		17H-CC		17H-CC	
18H-CC	LO <i>Discoaster brouweri</i> (1.97 Ma)	18H-CC	LO <i>Discoaster brouweri</i> (1.97 Ma)	18H-CC	LO <i>Discoaster brouweri</i> (1.97 Ma)
19H-CC		19H-CC		19H-CC	
20H-CC		20H-CC		20H-CC	
21H-CC		21H-CC		21H-CC	
22H-CC		22H-CC		22H-CC	
23H-CC		23H-CC			
24H-CC	LO <i>Discoaster pentaradiatus</i> (2.38 Ma)	24H-CC	LO <i>Discoaster pentaradiatus</i> (2.38 Ma)		
25H-CC		25H-CC			
26H-CC	LO <i>Discoaster surculus</i> (2.54 Ma)	26H-CC	LO <i>Discoaster surculus</i> (2.54 Ma)		
27H-CC		27H-CC			
28H-CC	LO <i>Discoaster tamalis</i> (2.74 Ma); TD	28H-CC	LO <i>Discoaster tamalis</i> (2.74 Ma)		
		29H-CC			
		30H-CC	TD		

Notes: FO = first occurrence, LO = last occurrence, TD = total depth.

Table T8. Distribution of planktonic foraminifers, Hole U1314A.

Core, section	Abundance	Preservation	Other species and observations												Stratigraphic event
			Ostracodes	Globotruncanites punctulata (d)	Globotruncanites truncatilobula (s)	Globotruncanites truncatilobula (s)	Globotruncanites transversostriatus	Globotruncanites transversostriatus	Globotruncanites transversostriatus (d)						
306-U1314A-															
1H, top	D	G	—	D	R	F F			R			P			
1H-CC	D	VG	11	R A	R	C A		F	F	R R	R	P			
2H-CC	D	G	21	C		C D		F	F	F R	R				
3H-CC	D	VG	13	A		F C C R		C	R R	C R R		P			
4H-CC	F	G	—	C		C A		C	F	R R					
5H-CC	D	G	20	R A		F C R		C	R	R F					
6H-CC	A	G	30	C		R A D		A		R F R					
7H-CC	D	G	9	R C		R A F R		F		A		R	P		
8H-CC	D	G	11	C		R F D R		R		C					
9H-CC	D	G	8	R A		F A A		C		A F					
10H-CC	D	G	7	R A		F A C F		F		C A R			P		
11H-CC	A	G	17	C		R A R		F		A F					
12H-CC	D	G	7	R C		F A A		F		R R A F					
13H-CC	D	G	11	R F		F F D		R		R A F					
14H-CC	D	G	6	F C F		C A A		F		R C R					
15H-CC	D	G	30	C		A A		A		R R F					
16H-CC	C	M	27	F		F A A		R		R A					FaO <i>N. pachyderma</i> (s) encrusted (1.78 Ma)
17H-CC	A	G	2	F		F D		F		F A					
18H-CC	G	2	F F			F D R		C	F	F F	F				LO <i>G. inflata</i> (2.09 Ma)
19H-CC	G	4	F			F D		C		F F					
20H-CC	G	12	C			F D		F		C C					
21H-CC	G	1	C			F D		C	F F						
22H-CC	G	11	C			F A		A	F F	F					
23H-CC	G	15	A			F C	C	F	F	F F		F			
24H-CC	G	15	A			C A	A	R	F	F F		F			LO <i>G. puncticulata</i> , <i>N. atlantica</i> (s) (2.41 Ma)
25H-CC	G	4	A			A		R		F F		R			
26H-CC	G	6	A			C C A		R	F	F F		F			
27H-CC	M	4	C			D		R	F	F F					IRD, quartz
28H-CC	M	4	F			C		C	F	F F					Fragmentation, very few foraminifers
															Fragmentation, pyrite

Note: Abundance: D = dominant, A = abundant, C = common, F = few, R = rare. Preservation: VG = very good, G = good, M = moderate, P = poor. See “Foraminifers” in the “Site U1312–U1315 methods” chapter. PF = planktonic foraminifers. d = dextral, s = sinistral. P in ostracodes column = presence of valves. IRD = ice-raftered debris, FaO = first abundant occurrence, LO = last occurrence.

Table T9. Distribution of planktonic foraminifers, Hole U1314B.

Core	Abundance	Preservation	Ostracodes												Other species and observations	Stratigraphic event
			Globigerinoides rubens	Globigerinoides sacculinoides	Globigerinoides trilobatus	Globigerinoides inflata	Globigerinoides sinistralis	Globigerinoides rubens	Globigerinoides sacculinoides	Globigerinoides trilobatus	Globigerinoides inflata	Globigerinoides sinistralis	Globigerinoides rubens			
306-U1314B-																
1H, top	F	G	—	P P	P	P A R	P C	R R A	P R R	P R R F	P A R R F	P A R R F	P A R R F	P A R R F	>150 µm; mainly diatoms, only presence (P) of species noted	
1H-CC	D	VG	14	A	F	C C	F C	R R F	F R	F R	F A	F A	F A	F A	IRD including tephra and stained quartz	
2H-CC	D	G	12	D	F	D C	F C	R R F	R R F	R R F	R R F	R R F	R R F	R R F	Few IRD including tephra and stained quartz	
3H-CC	D	G	9	R A	R F D	R F A	R F C	R F A	R F A	R F A	R F A	R F A	R F A	R F A	IRD	
4H-CC	D	G	9	R A	F A	R R	F C	R F A	F F	F F	F F	F F	F F	F F	P	
5H-CC	D	G	12	R A	R F A	R F A	F C	R F A	R F A	R F A	R F A	R F A	R F A	R F A	P	Abundant IRD including tephra and stained quartz
6H-CC	A	G	11	R C	F C D	F C D	F C D	F C D	F C D	F C D	F C D	F C D	F C D	F C D	P	Abundant IRD including tephra and stained quartz
7H-CC	D	G	14	R A	F R A F	F R A F	F R A F	F R A F	F R A F	F R A F	F R A F	F R A F	F R A F	F R A F	P	Few IRD
8H-CC	D	M	8	C	F F A A	F F A A	F F A A	F F A A	F F A A	F F A A	F F A A	F F A A	F F A A	F F A A	P	In-flow! IRD including tephra and stained quartz
9H-CC	D	G	18	R C	R A A	R A A	R A A	R A A	R A A	R A A	R A A	R A A	R A A	R A A	P	Abundant radiolarians
10H-CC	D	G	23	R A	F F A R	F F A R	F F A R	F F A R	F F A R	F F A R	F F A R	F F A R	F F A R	F F A R	P	Few IRD
11H-CC	D	G	16	F A	R A R	R A R	R A R	R A R	R A R	R A R	R A R	R A R	R A R	R A R	P	
12H-CC	D	G	7	A	R A A	R A A	R A A	R A A	R A A	R A A	R A A	R A A	R A A	R A A	P	
13H-CC	A	M	13	D	F R A F	F R A F	F R A F	F R A F	F R A F	F R A F	F R A F	F R A F	F R A F	F R A F	P	Aggregates
14H-CC	D	G	12	R	R C A A	R C A A	R C A A	R C A A	R C A A	R C A A	R C A A	R C A A	R C A A	R C A A	P	
15H-CC	D	G	8	C	F F C A	F F C A	F F C A	F F C A	F F C A	F F C A	F F C A	F F C A	F F C A	F F C A	P	FaO <i>N. pachyderma</i> (s) (1.78 Ma)
16H-CC	D	G	6	R C	F D R	F D R	F D R	F D R	F D R	F D R	F D R	F D R	F D R	F D R	P	
17H-CC	D	G	10	F F	F D	F D	F D	F D	F D	F D	F D	F D	F D	F D	P	
18H-CC	D	G	11	C	C A	C A	C A	C A	C A	C A	C A	C A	C A	C A	P	
19H-CC	D	G	4	F	F D R	F D R	F D R	F D R	F D R	F D R	F D R	F D R	F D R	F D R	P	
20H-CC	D	G	14	C	F D R	F D R	F D R	F D R	F D R	F D R	F D R	F D R	F D R	F D R	P	
21H-CC	D	G	7	F	F D R	F D R	F D R	F D R	F D R	F D R	F D R	F D R	F D R	F D R	P	
22H-CC	D	G	5	C	F D R	F D R	F D R	F D R	F D R	F D R	F D R	F D R	F D R	F D R	P	
23H-CC	D	G	14	C	F A R	F A R	F A R	F A R	F A R	F A R	F A R	F A R	F A R	F A R	P	
24H-CC	D	M	8	A	F C	F C	F C	F C	F C	F C	F C	F C	F C	F C	P	
25H-CC	D	M	10	F	F D	F D	F D	F D	F D	F D	F D	F D	F D	F D	P	Full of aggregates, high fragmentation
26H-CC	D	G	11	A	R F	R F	R F	R F	R F	R F	R F	R F	R F	R F	P	Full of aggregates, high fragmentation
27H-CC	D	M	5	C	D R	D R	D R	D R	D R	D R	D R	D R	D R	D R	P	Full of aggregates, high fragmentation
28H-CC	D	M	9	F	F A	F A	F A	F A	F A	F A	F A	F A	F A	F A	P	Full of aggregates, high fragmentation
29H-CC	D	G	4	C	F A C R	F A C R	F A C R	F A C R	F A C R	F A C R	F A C R	F A C R	F A C R	F A C R	P	Full of aggregates, high fragmentation
30H-CC	D	G	3	R F	C A F C	C A F C	C A F C	C A F C	C A F C	C A F C	C A F C	C A F C	C A F C	C A F C	P	Full of aggregates, high fragmentation

Notes: Abundance: D = dominant, A = abundant, C = common, F = few, R = rare. Preservation: VG = very good, G = good, M = moderate See “[Foraminifers](#)” in the “Site U1312–U1315 methods” chapter. PF = planktonic foraminifers. d = dextral, s = sinistral. P in ostracodes column = presence of valves. IRD = ice-raftered debris, FO = first occurrence, FaO = first abundant occurrence, LO = last occurrence.

Table T10. Distribution of planktonic foraminifers, Hole U1314C.

Core	Abundance	Preservation	Ostracodes												Other species and observations	Stratigraphic event
			<i>Cibotrilla punctulata</i>	<i>Cibotrilla trunctulifera</i> (d)	<i>Cibotrilla transversilobata</i> (s)	<i>Cibotrilla crassidorsata</i>	<i>Cibotrilla inflata</i>	<i>Cibotrilla hirsuta</i>	<i>Cibotrilla scutula</i> (s)	<i>Obulina univisa</i>	<i>Cibotrilla scutula</i> (d)	<i>Cibotrilla sinuosa</i>	<i>Tuberculina rugosa</i>	<i>Globigerinoides rubens</i> white/pink		
306-U1314C-1H, top	A	M	—	D	F	F	D	F	C	R	R	P	Washout and some Holocene sediments, abundant diatoms			
1H-CC	D	VG	4	A	F	A	A	A	F	F	R	R	P	Few IRD		
2H-CC	D	VG	11	R	A	R	A	A	R	F	R	R	P	<i>Beella digitata</i> , few IRD including tephra		
3H-CC	D	VG	3	R	A	R	R	F	R	R	C	A	P	<i>B. digitata</i>		
4H-CC	D	VG	17				R	F	R	R	C	R	P	Abundant IRD (also gravel sized) including tephra		
5H-CC	D	G	7	R	C	R	F	A	F	F	F	C	P	IRD including tephra		
6H-CC	D	G	20	R	C	R	F	C	D	C	R	R	P	Some IRD including tephra and stained quartz		
7H-CC	D	G	18	R	C	R	R	A	A	A	R	R	P	Abundant IRD including stained quartz and abundant tephra		
8H-CC	A	G	22	R	C	R	F	A	A	R	R	F	P	Some IRD		
9H-CC	D	G	30	R	A		F	F	A	F	R	A	P	Abundant sponge spicules		
10H-CC	D	G	9	F	C	R	F	A	R	R	R	A	P	Rare IRD (quartz)		
11H-CC	D	G	30	R	C	R	R	F	A	A	R	R	P	Aggregates, IRD including tephra and stained quartz		
12H-CC	A	M	—	F			F	D	D	F	R	R	P	Abundant IRD		
13H-CC	D	G	3	A			A	R	A	R	R	R	P	Abundant IRD particles, quartz, muscovite, rock fragments	FaO <i>N. pachyderma</i> (s) (1.78 Ma)	
14H-CC	D	G	14	F			F	A	A	R	R	C	P			
15H-CC	F	G	8	F			F	D		R	F	C	P			
16H-CC	D	G	13	F			F	D		F	C	R	P			
17H-CC	D	G	6	C			F	D	F	F	C	C	P			
18H-CC	D	G	10	C			F	A		F	F	C	P		FO <i>G. inflata</i> (2.09 Ma)	
19H-CC	D	G	12	C			F	A		F	R	C	P			
20H-CC	D	G	24	C			F	A		F	R	A	P			
21H-CC	D	G	25	C			F	A		F	R	F	P	Abundant quartz, dominant aggregates	LO <i>N. atlantica</i> (s) (2.41 Ma)	
22H-CC	D	G	14	C			F	F	A	F	F	F	P			

Notes: Abundance: D = dominant, A = abundant, C = common, F = few, R = rare. Preservation: VG = very good, G = good, M = moderate. See “**Foraminifers**” in the “Site U1312–U1315 methods” chapter. PF = planktonic foraminifers. d = dextral, s = sinistral. P in ostracodes column = presence of valves. IRD = ice-raftered debris, FO = first occurrence, FaO = first abundant occurrence, LO = last occurrence.



Table T11. Distribution of benthic foraminifers, Hole U1314A.

Core, section	Agglutinated species	Calcareous species																				Terebellina trachaea	
		<i>Eggerellides laevis</i>	<i>Martinettoella communis</i>	<i>Sigmoilites schumbergi</i>	<i>Bulimina costata</i>	<i>Bulimina exilis</i>	<i>Bulimina minuta</i>	<i>Bursocosta minuta</i>	<i>Chiloglomerina testicostata</i>	<i>Chiloglomerina testilligatum</i>	<i>Astroconchus testicostatus</i>	<i>Ammonia sp.</i>	<i>Spirella testacea</i>	<i>Buliminella setiferum</i>	<i>Buliminella testacea</i>	<i>Cibicides carinata</i>	<i>Cibicides kofoidi</i>	<i>Cibicides lobatulus</i>	<i>Cibicides lobatulus</i>	<i>Cibicides lobatulus</i>	<i>Cibicides lobatulus</i>		
306-U1314A-1H-CC	R	P	P	P	P	P	R	R	P	P	P	P	P	P	P	C	A	R	R	P	R	R	
2H-CC			P	P			P	R	C	F												P	
3H-CC							P	D															R
4H-CC																							
5H-CC	P	P	P																				
6H-CC																							
7H-CC	P	P																					
8H-CC	P																						
9H-CC	R																						
10H-CC	P																						
11H-CC	F	R																					
12H-CC	F																						
13H-CC																							
14H-CC																							
15H-CC	R		P																				
16H-CC																							
17H-CC	P	P																					
18H-CC																							
19H-CC																							
20H-CC																							
21H-CC	P																						
22H-CC																							
23H-CC																							
24H-CC	P																						
25H-CC	R																						
26H-CC																							
27H-CC																							
28H-CC	C	P																					

Notes: D = dominant, A = abundant, C = common, F = few, R = rare, P = present. See “[Foraminifers](#)” in the “Site U1312–U1315 methods” chapter.



Table T12. Distribution of diatoms, Hole U1314A. (Continued on next page.)

Core, section	Abundance	Preservation	Taxa																				Reported elsewhere	Sequences spp.	Taxa listed in this table not elsewhere reported
			T	t	F	R	t	T	F	T	t	t	T	t	T	t	T	t	T	t	T	t			
306-U1314A-																									
1H-CC	A	M (f+d)	1	t																					
2H-CC	VA	M (f+d)	1	T	T																				
3H-CC	A	G-M (f)	1	t																					
4H-CC	C	G-M (f)	1																						
5H-CC	VA	G-M (f)	1																						
6H-CC	R	G-M (f)	1																						
7H-CC	C	G-M (f)	1	T																					
8H-CC	A	G-M (f)	1																						
9H-CC	VA	M (f+d)	1																						
10H-CC	A	G-M (f)	1	t	t																				
11H-CC	R	G-M (f)	1																						
12H-CC	A	G-M (f)	1																						
13H-CC	A	G-M (f)	1	T																					
14H-CC	R	M-P (f+d)	1	t																					
15H-CC	R	M-P (f)	1																						
16H-CC	T	M-P (f)	1																						
17H-CC	A	M (f)	1	R																					
18H-CC	A	M (f)	1	R																					
19H-CC	F	M-P (f+d)	1																						
20H-CC	T	P (d)	1																						
21H-CC	T	P (d)	1																						
22H-CC	C	M (f)	1	F	T																				
23H-CC	C	G-M (f)	1	T																					
24H-CC	A	M (f)	1	T																					
25H-CC	A	G-M (f)	1	T																					
26H-CC	A	G-M (f)	1	F	t																				
27H-CC	C	M (f)	1	T																					
28H-CC	A	P (strong f)	1	T																					

Notes: Abundance: VA = very abundant, A = abundant, C = common, F = few, R = rare, T = trace (2–10), t = single occurrence or fragment. Preservation: G = good, M = moderate, P = poor, d = dissolved, f = fragmented. See “Diatoms” in the “Site U1312–U1315 methods” chapter. FO = first occurrence, LO = last occurrence.

Table T12 (continued).

Core, section	Abundance	Preservation	Comments											
			Silicified trilobites			Unsilicified trilobites			Trilobite sps.			Trilobite sps. chitinozoans		
306-U1314A-														
1H-CC	A	M (f+d)	1		T	T	T	T	C	R	T	T	T	
2H-CC	VA	M (f+d)	1		T	T	T	F	VA	T	R	T	T	
3H-CC	A	G-M (f)	1		t	t	t	T	C	T	T	T	T	
4H-CC	C	G-M (f)	1					T	A	C	T	T	T	
5H-CC	VA	G-M (f)	1	t	t	T	t	R	T	A	T	T	T	
6H-CC	R	G-M (f)	1		T				C	T	T	T	T	
7H-CC	C	G-M (f)	1			T	t	T	A	C	T	T	T	
8H-CC	A	G-M (f)	1			T	t	T	T	T	R	T	T	
9H-CC	VA	M (f+d)	1					R	T	T	T	T	T	
10H-CC	A	G-M (f)	1					T	R	T	T	T	T	
11H-CC	R	G-M (f)	1					T	T	F	C	T	T	
12H-CC	A	G-M (f)	1	t		T		T	C	C	T	T	T	
13H-CC	A	G-M (f)	1					t	F	F	T	T	T	
14H-CC	R	M-P (f+d)	1						T	T	A	R	T	
15H-CC	R	M-P (f)	1						R	T	C	T	T	
16H-CC	T	M-P (f)	1						T	C	C	C	T	
17H-CC	A	MFA)	1		t	T			T	R	F	F	T	
18H-CC	A	MFA)	1			T			T	R	T	T	T	
19H-CC	F	M-P (f+d)	1						T	T	R	T	T	
20H-CC	T	P (d)	1						R	T	C	T	T	
21H-CC	T	P (d)	1						T	C	C	C	T	
22H-CC	C	M (f)	1	T		T			T	T	T	T	T	
23H-CC	C	G-M (f)	1	T		T		t	T	T	T	T	T	
24H-CC	A	M (f)	1		t	p	F	T	T	T	T	T	T	
25H-CC	A	G-M (f)	1			T	T	T	T	T	T	A	T	
26H-CC	A	G-M (f)	1			T	t	T	T	T	F	C	T	
27H-CC	C	M (f)	1	t	t	T	t	T	t	T	T	C	T	
28H-CC	A	P (strong f)	1			T	t	T	T	T	T	A	T	



Table T13. Distribution of diatoms, Hole U1314B. (Continued on next page.)

Notes: Abundance: A = abundant, C = common, F = few, R = rare, T = trace, t = single occurrence or fragment. Preservation: G = good, M = moderate, P = poor. See "[Diatoms](#)" in the "Site U1312–U1315 methods" chapter. FO = first occurrence, LO = last occurrence.

Table T13 (continued).

Core, section	Abundance	Preservation	Transects	Siliciclastic facies												Comments
				Unspeciated fragiment			Tachosiida spp.			Terebellina circumannulata			Thalassinidix longissima			
306-U1314B-																
1H-CC	A	M	1	F			t	T	t	T	A		F			
2H-CC	A	G-M	1	F			t	T	t	T	A	F	F			LO <i>P. curvirostris</i>
3H-CC	A	G-M	1	R				T	T	T	A	F	F	t		LO <i>F. reinholdii</i>
4H-CC	A	M	1	T			t	T	t	T	C	F	R	A		
5H-CC	A	M	1	T				T				t	t	C		
6H-CC	C	M	1									t	F	R	A	
7H-CC	R	G-M	1	T								t	F	R	A	
8H-CC	A	M	1	t	T							t	T	T	C	
9H-CC	A	G-M	1	T	T	t						T	T	T	A	
10H-CC	A	M	1	C								T	T	C	t	
11H-CC	A	G-M	1	F								R	R	A	t	
12H-CC	A	G-M	1	t	T		T					T	T	A		
13H-CC	F	M-P	1									T	T	R		
14H-CC	C	M	1	T			t	R	T	T		T	F	C	t	
15H-CC	A	G-M	1	R			t	T	t	T		F	T	A		
16H-CC	C	M	1					T				T	T	C		
17H-CC	A	M	1	T	T		T	F		R		T	F	R	A	
18H-CC	A	M-P	1	t	t	t		C				t	R	T	F	
19H-CC	C	M-P	1	t	C							t	T	T	F	
20H-CC	F	M-P	1	t				T	t	T		T	T	T	R	
21H-CC	C	M-P	1	T				R	t	T		t	F	T	F	
22H-CC	C	M-P	1					R	t	T		t	F	R		
23H-CC	C	M	1				t	F	T	T		t	T	T	C	
24H-CC	C	M	1	t				F		R		T	t	R	F	
25H-CC	A	M	1	t				C		t		t	t	T	C	
26H-CC	A	M	1					C	p	R		t	t	T	C	LO <i>T. convexa</i>
27H-CC	C	M-P	1	T	T		t	R	F	T		t	T	R	T	LO <i>F. jouseae</i>
28H-CC	C	M-P	1					F	t	t		t	T	T	F	
29H-CC	C	M-P	1	T			t	F	t	T		R	T	R	t	
30H-CC	A	M	1	T			T	R	T	T		T	R	T	C	



Table T14. Distribution of diatoms, Hole U1314C. (Continued on next page.)

Notes: Abundance: A = abundant, C = common, F = few, R = rare, T = trace, t = single occurrence or fragment. Preservation: G = good, M = moderate, P = poor, d = dissolved, rw = reworked. See "[Diatoms](#)" in the "Site U1312–U1315 methods" chapter. FO = first occurrence, LO = last occurrence.

Table T14 (continued).

Core, section	Abundance	Preservation	Siliciclastics												Comments
			Thalassiosira longistriata			Thalassiosira macrocera			Thalassiosira longissima			Thalassiosira longistriata poles			
			T	t	R	T	t	T	C	F	T				
306-U1314C-															
1H-CC	C	G-M	1												LO <i>Proboscia curvirostris</i>
2H-CC	A	G-M	1												Rich in lithics
3H-CC	C	M (rw)	1	t	T	t	T	t	T	A	F	T			LO <i>Neodenticula seminae</i>
4H-CC	A	M	1												Rich in lithics
5H-CC	A	M (d + rw)	1												FO <i>N. seminae</i>
6H-CC	R	M-P	1												FO <i>P. curvirostris</i>
7H-CC	A	G-M	1		R		F	T							Proboscia-Rhizosolenia abundant
8H-CC	F	M-P	1												
9H-CC	C	M	1				t	t	T	F					
10H-CC	A	G-M	1		T	t	R	t	T	A					
11H-CC	C	M	1				T	t	T	R	C	t			
12H-CC	A	M	1				F	t		T	C				
13H-CC	C	M	1							t	F				
14H-CC	A	G-M	1	t	t		T		T	F	A				
15H-CC	R	P	1							C	T	F			Rich in lithics
16H-CC	C	M (rw)	1				t	T		T	F	t			
17H-CC	C	M	1					T		T	F				Rework?
18H-CC	C	M	1					T		R	R				FO <i>F. doliolus</i> ?
19H-CC	R	M (d)	1				t	T		T	R				Rework?
20H-CC	T	P	1							R	T	F			
21H-CC	C	M-P	1		R	t	R	T		T	R	R			
22H-CC	F	M-P	1							T	t	R			



Table T15. Distribution of radiolarians, Hole U1314A. (Continued on next page.)

Core, section	Abundance	Preservation	Geological details	Radiolarian distribution		Hexactinella hololete
				Trace	Common	
306-U1314A-1H-CC	C	G	T	+	+	+
2H-CC	C	M	T	+	+	+
3H-CC	F	M	T	+	+	+
4H-CC	T	M	T	+	+	+
5H-CC	A	G	T	+	+	+
6H-CC	T	P	C	+	+	+
7H-CC	C	G	T	+	+	?
8H-CC	F	M	F	+	+	+
9H-CC	C	M	F	+	+	+
10H-CC	A	G	F	+	+	+
11H-CC	R	M	T	+	+	+
12H-CC	C	G	T	+	+	+
13H-CC	C	M	T	+	+	+
14H-CC	F	M	F	+	+	+
15H-CC	F	M	R	+	+	+
16H-CC	B	M	T	+	+	+
17H-CC	F	M	T	+	+	+
18H-CC	C	M	T	+	+	+
19H-CC	C	M	P	+	+	+
20H-CC	R	P	P	+	+	+
21H-CC	T	P	F	+	+	+
22H-CC	C	G-M	F	+	+	+
23H-CC	A	G-M		+	+	+
24H-CC	A	G		?	+	+
25H-CC	A	G		?	+	+
26H-CC	A	G		?	+	+
27H-CC	F	M		?	?	+
28H-CC	C	G-M		+	+	+

Notes: Abundance: A = abundant, C = common, F = few, R = rare, T = trace, B = barren. Preservation: G = good, M = moderate, P = poor. See “Radiolarians” in the “Site U1312–U1315 methods” chapter. ? = species identification uncertain.





Table T15 (continued).

Core, section	Abundance	Taxa observed in sediments											
		Terrestrial detritus			Terrestrial bacteria			Symbioses			Microbial mats		
306-U1314A-													
1H-CC	C	C	F	T	A	T	C	S	S	S	S	S	S
2H-CC	C	C	F	T	C	F	M	M	M	M	M	M	M
3H-CC	C	C	F	T	C	F	M	M	M	M	M	M	M
4H-CC	C	C	F	T	C	F	M	M	M	M	M	M	M
5H-CC	C	C	F	T	C	F	M	M	M	M	M	M	M
6H-CC	C	C	F	T	C	F	M	M	M	M	M	M	M
7H-CC	C	C	F	T	C	F	M	M	M	M	M	M	M
8H-CC	C	C	F	T	C	F	M	M	M	M	M	M	M
9H-CC	C	C	F	T	C	F	M	M	M	M	M	M	M
10H-CC	C	C	F	T	C	F	M	M	M	M	M	M	M
11H-CC	R	R	C	C	C	C	M	M	M	M	M	M	M
12H-CC	R	R	C	C	C	C	M	M	M	M	M	M	M
13H-CC	C	C	F	F	C	C	M	M	M	M	M	M	M
14H-CC	C	C	F	F	C	C	M	M	M	M	M	M	M
15H-CC	F	F	B	B	F	F	M	M	M	M	M	M	M
16H-CC	F	F	B	B	F	F	M	M	M	M	M	M	M
17H-CC	F	F	C	C	F	F	M	M	M	M	M	M	M
18H-CC	C	C	C	C	C	C	M	M	M	M	M	M	M
19H-CC	C	C	C	C	C	C	M	M	M	M	M	M	M
20H-CC	R	R	T	T	C	C	G-M	G-M	G-M	G-M	G-M	G-M	G-M
21H-CC	T	T	C	C	T	F	P	P	P	P	P	P	P
22H-CC	C	C	T	T	C	F	T	T	T	T	T	T	T
23H-CC	A	A	C	C	A	C	G-M	G-M	G-M	G-M	G-M	G-M	G-M
24H-CC	A	A	F	F	A	F	G	G	G	G	G	G	G
25H-CC	A	A	F	F	C	F	G	G	G	G	G	G	G
26H-CC	A	A	F	F	C	F	G	G	G	G	G	G	G
27H-CC	F	F	C	C	F	F	G	G	G	G	G	G	G
28H-CC	C	C	G	G	C	G	G	G	G	G	G	G	G

Table T16. Distribution of radiolarians, Hole U1314B. (Continued on next page.)

Core, section	Abundance		Ice rafted debris	Tephra grains
	Preservation			
306-U1314B-2H-CC	A	G		<i>Acanthocystis anthemis</i>
3H-CC	A	G		<i>Acrosphaera spinosa</i>
4H-CC	A	G		<i>Actinomma medianum</i>
5H-CC	A	G		<i>Actinomma boreale</i>
6H-CC	F	C		<i>Actinomma haysi</i>
7H-CC	A	G	F	
8H-CC	A	M	T	<i>Actinomma leptoderma</i>
9H-CC	A	M		<i>Actinomma popofskii?</i>
10H-CC	A	M		<i>Actinomma delicatulum</i>
11H-CC	A	G	R	<i>Actinomma sol</i>
12H-CC	A	G		<i>Amphiplecta acrostoma</i>
13H-CC	F	G	T	
14H-CC	A	G		<i>Amphimedusa setosa</i>
15H-CC	A	G		<i>Amphirhopalium ypsilon</i>
16H-CC	T	P		<i>Androcyclas gamphonycha</i>
17H-CC	A	G		<i>Anomalocantha dentata</i>
18H-CC	C	G		<i>Anthocystidium zanguebaricum</i>
19H-CC	R	M-P		<i>Anthocystidium ophiorensense</i>
20H-CC	T	P		<i>Aristotrobus joergenseni</i>
21H-CC	F	M		<i>Aristotrobus annulatus</i>
22H-CC	C	G		<i>Axoptrumnum stauraxonum</i>
23H-CC	F	P		<i>Botryocampe inflatum</i>
24H-CC	A	G		<i>Botryostrobus equiloniaris</i>
25H-CC	F	M-P		<i>Botryostrobus auritus/australis group</i>
26H-CC	C	G		<i>Carpocanarium papillosum</i>
27H-CC	A	G		<i>Carpocanistrum spp.</i>
28H-CC	F	M		<i>Cephalis antarctica?</i>
29H-CC	A	G		<i>Ceratocystis histicus</i>
30H-CC	A	G		<i>Collospheara murryana</i>
				<i>Coracalyptra craspedota</i>
				<i>Comutella profunda</i>
				<i>Cubotholus irregularis</i>
				<i>Cycladophora sakaii?</i>
				<i>Cycladophora davisihana</i>
				<i>Cycladophora davisihana cornutoides</i>
				<i>Dictyocyste profunda/truncatum</i>
				<i>Dictyocyste euclidi</i>
				<i>Dictyophimus crisiae</i>
				<i>Didymocystis tetrathalamus</i>
				<i>Druppatractus group C</i>
				<i>Eucyrtidium acuminatum</i>
				<i>Eucyrtidium calvertense</i>
				<i>Eucyrtidium hexagonatum</i>
				<i>Eucyrtidium teuscheri</i>
				<i>Heliodiscus asteriscus</i>
				<i>Hexacontium hostile</i>

Notes: Abundance: A = abundant, C = common, F = few, R = rare, T = trace. Preservation: G = good, M = moderate, P = poor. See “[Radiolarians](#)” in the “Site U1312–U1315 methods” chapter. ? = species identification uncertain.

Table T16 (continued).

Table T17. Distribution of radiolarians, Hole U1314C. (Continued on next page.)

Notes: Abundance: A = abundant, C = common, F = few, R = rare, T = trace. Preservation: G = good, M = moderate, P = poor. See “[Radiolarians](#)” in the “Site U1312–U1315 methods” chapter. ? = species identification uncertain.

Table T17 (continued).

Core, section	Abundance	Taxa recorded									
		<i>Heterocystis</i>	<i>Leptothrix</i>	<i>Leptothrix</i> nov. sp.	<i>Leptothrix</i> nov. sp. (parasite)						
306-U1314C-1H-CC	A	+	+	+	+	+	+	+	+	+	+
2H-CC	A	+	+	+	+	+	+	+	+	+	+
3H-CC	A	+	+	+	+	+	+	+	+	+	+
4H-CC	C	+	+	+	+	+	+	+	+	+	+
5H-CC	A	+	+	+	+	+	+	+	+	+	+
6H-CC	R	+	+	+	+	+	+	+	+	+	+
7H-CC	A	+	+	+	+	+	+	+	+	+	+
8H-CC	A	+	+	+	+	+	+	+	+	+	+
9H-CC	A	+	+	+	+	+	+	+	+	+	+
10H-CC	A	+	+	+	+	+	+	+	+	+	+
11H-CC	A	+	+	+	+	+	+	+	+	+	+
12H-CC	A	+	+	+	+	+	+	+	+	+	+
13H-CC	T	+	+	+	+	+	+	+	+	+	+
14H-CC	A	+	+	+	+	+	+	+	+	+	+
15H-CC	T	+	+	+	+	+	+	+	+	+	+
16H-CC	A	+	+	+	+	+	+	+	+	+	+
17H-CC	A	+	+	+	+	+	+	+	+	+	+
18H-CC	A	+	+	+	+	+	+	+	+	+	+
19H-CC	A	+	+	+	+	+	+	+	+	+	+
20H-CC	T	+	+	+	+	+	+	+	+	+	+
21H-CC	R	+	+	+	+	+	+	+	+	+	+
22H-CC	F	+	+	+	+	+	+	+	+	+	+



Table T18. Position of paleomagnetic transitions, Holes U1314A, U1314B, and U1314C.

Polarity chron interpretation	Name	Age (Ma)	Hole U1314A		Hole U1314B		Hole U1314C	
			Depth (mbsf)	Relative uncertainty (m)	Depth (mbsf)	Relative uncertainty (m)	Depth (mbsf)	Relative uncertainty (m)
C1n (b)	Brunhes/Matuyama	0.78	57.3	0.1	56.6	0.1	57.7	0.1
C1r.1n (t)	Jaramillo (t)	0.99	74.4	0.2	73.1	0.1	75.0	0.5
C1r.1n (b)	Jaramillo (b)	1.07	79.8	0.2	80.7	0.4	80.7	0.2
C1r.2r-1n (t)	Cobb Mt. (t)	1.19			87.0	0.2	88.2	0.2
C1r.2r-1n (b)	Cobb Mt. (b)	1.215			88.4	0.1	89.7	0.1
C2n (t)	Olduvai (t)	1.77	138.9	0.2	137.5	0.2	139.4	0.2
C2n (b)	Olduvai (b)	1.95	155.3	0.3	155.5	0.2	157.6	0.1
C2r.1n (t)	Reunion (t)	2.115	175.8	0.2	174.9	0.1	176.7	0.1
C2r.1n (b)	Reunion (b)	2.153	178.4	0.1	177.1	0.1	179.3	0.2
C2An.1n (t)	Matuyama/Gauss	2.581	224.7	0.4	222.6	0.2		

Note: t = top, b = bottom.

Table T19. Shipboard composite depths, Holes U1314A, U1314B, and U1314C.

Core	Top depth		Offset (m)	Core	Top depth		Offset (m)				
	(mbsf)	(mcd)			(mbsf)	(mcd)					
306-U1314A-											
1H	0.0	0.00	0.00	13H	108.5	119.15	10.65				
2H	1.9	1.90	0.00	14H	118.0	129.00	11.00				
3H	11.4	11.90	0.50	15H	127.5	139.30	11.80				
4H	20.9	22.65	1.75	16H	137.0	149.60	12.60				
5H	30.4	31.70	1.30	17H	146.5	159.75	13.25				
6H	39.9	42.10	2.20	18H	156.0	170.20	14.20				
7H	49.4	51.20	1.80	19H	165.5	179.95	14.45				
8H	58.9	61.65	2.75	20H	175.0	189.95	14.95				
9H	68.4	72.15	3.75	21H	184.5	199.70	15.20				
10H	77.9	82.90	5.00	22H	194.0	210.20	16.20				
11H	87.4	92.45	5.05	23H	203.5	219.95	16.45				
12H	96.9	103.80	6.90	24H	213.0	230.40	17.40				
13H	106.4	114.20	7.80	25H	222.5	240.75	18.25				
14H	115.9	125.55	9.65	26H	232.0	251.05	19.05				
15H	125.4	136.65	11.25	27H	241.5	262.55	21.05				
16H	134.9	146.15	11.25	28H	251.0	271.45	20.45				
17H	144.4	156.50	12.10	29H	260.5	280.95	20.45				
18H	153.9	167.60	13.70	30H	270.0	290.45	20.45				
19H	163.4	176.95	13.55	306-U1314C-							
20H	172.9	186.50	13.60	1H	0.0	0.00	0.00				
21H	182.4	196.05	13.65	2H	8.2	8.50	0.30				
22H	191.9	206.20	14.30	3H	17.7	17.55	-0.15				
23H	201.4	216.25	14.85	4H	27.2	26.80	-0.4				
24H	210.9	226.45	15.55	5H	36.7	37.05	0.35				
25H	220.4	236.45	16.05	6H	46.2	46.55	0.35				
26H	229.9	246.70	16.80	7H	55.7	57.00	1.30				
27H	239.4	258.95	19.55	8H	65.2	67.40	2.20				
28H	248.9	268.64	19.74	9H	74.7	78.50	3.80				
306-U1314B-											
1H	0.0	0.00	0.00	10H	84.2	89.20	5.00				
2H	4.0	5.25	1.25	11H	93.7	99.90	6.20				
3H	13.5	15.20	1.70	12H	103.2	111.35	8.15				
4H	23.0	24.30	1.30	13H	112.7	122.40	9.70				
5H	32.5	34.95	2.45	14H	122.2	133.30	11.10				
6H	42.0	44.15	2.15	15H	131.7	142.50	10.80				
7H	51.5	54.00	2.50	16H	141.2	152.50	11.30				
8H	61.0	64.65	3.65	17H	150.7	162.00	11.30				
9H	70.5	75.10	4.60	18H	160.2	173.15	12.95				
10H	80.0	86.25	6.25	19H	169.7	182.55	12.85				
11H	89.5	96.50	7.00	20H	179.2	191.30	12.10				
12H	99.0	107.80	8.80	21H	188.7	202.70	14.00				
				22H	198.2	212.35	14.15				

Table T20. Splice tie points, Site U1314.

Core, section, interval (cm)	Depth		Core, section, interval (cm)	Depth	
	(mbsf)	(mcd)		(mbsf)	(mcd)
306-			306-		
1314B-1H-2, 135	2.85	2.85	Tie to	1314C-1H-2, 135	2.85
1314C-1H-5, 130	7.30	7.30	Tie to	1314B-2H-2, 55	6.05
1314B-2H-6, 70	12.20	13.45	Tie to	1314C-2H-4, 45	13.15
1314C-2H-6, 60	16.30	16.60	Tie to	1314B-3H-1, 140	14.90
1314B-3H-4, 55	18.55	20.25	Tie to	1314C-3H-2, 120	20.40
1314C-3H-6, 85	26.05	25.90	Tie to	1314B-4H-2, 10	24.60
1314B-4H-6, 75	31.25	32.55	Tie to	1314C-4H-4, 125	32.95
1314C-4H-7, 5	36.25	35.85	Tie to	1314B-5H-1, 90	33.40
1314B-5H-6, 60	40.60	43.05	Tie to	1314C-5H-4, 150	42.70
1314C-5H-6, 115	45.35	45.70	Tie to	1314B-6H-2, 5	43.55
1314B-6H-6, 5	49.55	51.70	Tie to	1314C-6H-4, 65	51.35
1314C-6H-6, 50	54.20	54.55	Tie to	1314B-7H-1, 55	52.05
1314B-7H-6, 95	59.95	62.45	Tie to	1314C-7H-4, 95	61.15
1314C-7H-6, 130	64.50	65.80	Tie to	1314A-8H-3, 115	63.05
1314A-8H-6, 35	66.75	69.50	Tie to	1314C-8H-2, 60	67.30
1314C-8H-7, 40	74.10	76.30	Tie to	1314B-9H-1, 120	71.70
1314B-9H-6, 95	78.95	83.55	Tie to	1314C-9H-4, 55	79.75
1314C-9H-6, 95	83.15	86.95	Tie to	1314B-10H-1, 70	80.70
1314B-10H-6, 125	88.75	95.00	Tie to	1314C-10H-4, 130	90.00
1314C-10H-7, 35	93.55	98.55	Tie to	1314B-11H-2, 55	91.55
1314B-11H-7, 15	98.65	105.65	Tie to	1314C-11H-4, 125	99.45
1314C-11H-6, 140	102.60	108.80	Tie to	1314B-12H-1, 100	100.00
1314B-12H-7, 35	108.35	117.15	Tie to	1314C-12H-4, 130	109.00
1314C-12H-7, 45	112.65	120.80	Tie to	1314B-13H-2, 15	110.15
1314B-13H-7, 20	117.70	128.35	Tie to	1314C-13H-4, 145	118.65
1314C-13H-7, 40	121.60	131.30	Tie to	1314B-14H-2, 80	120.30
1314B-14H-6, 70	126.20	137.20	Tie to	1314C-14H-3, 90	126.10
1314C-14H-6, 105	130.75	141.85	Tie to	1314B-15H-2, 105	130.05
1314B-15H-7, 15	136.65	148.45	Tie to	1314C-15H-4, 145	137.65
1314C-15H-6, 145	140.65	151.45	Tie to	1314B-16H-2, 35	138.85
1314B-16H-6, 95	145.45	158.05	Tie to	1314C-16H-4, 105	146.75
1314C-16H-7, 20	150.40	161.70	Tie to	1314B-17H-2, 45	148.45
1314B-17H-6, 90	154.90	168.15	Tie to	1314C-17H-5, 15	156.85
1314C-17H-6, 105	159.25	170.55	Tie to	1314B-18H-1, 35	156.35
1314B-18H-6, 135	164.85	179.05	Tie to	1314C-18H-4, 140	166.10
1314C-18H-6, 85	168.55	181.50	Tie to	1314B-19H-2, 5	167.05
1314B-19H-6, 85	173.85	188.30	Tie to	1314A-20H-2, 30	174.70
1314A-20H-6, 135	181.75	195.35	Tie to	1314B-20H-4, 87.5	180.40
1314B-20H-6, 105	183.55	198.50	Tie to	1314A-21H-2, 95	184.85
1314A-21H-6, 95	190.85	204.50	Tie to	1314B-21H-4, 30	189.30
1314B-21H-6, 130	193.30	208.50	Tie to	1314A-22H-2, 80	194.20
1314A-22H-6, 140	200.80	215.10	Tie to	1314B-22H-4, 37.5	198.90
1314B-22H-6, 15	201.65	217.85	Tie to	1314A-23H-2, 10	203.00
1314A-23H-6, 130	210.20	225.05	Tie to	1314B-23H-4, 60	208.60
1314B-23H-6, 90	211.90	228.35	Tie to	1314A-24H-2, 40	212.80
1314A-24H-6, 130	219.70	235.25	Tie to	1314B-24H-4, 35	217.85
1314B-24H-6, 85	221.35	238.75	Tie to	1314A-25H-2, 80	222.70
1314A-25H-6, 100	228.90	244.95	Tie to	1314B-25H-3, 120	226.70
1314B-25H-6, 115	231.15	249.40	Tie to	1314A-26H-2, 120	232.60
1314A-26H-5, 45	236.35	253.15	Tie to	1314B-26H-2, 60	234.10
1314B-26H-6, 145	240.95	260.00	Tie to	1314A-27H-1, 105	240.45
1314A-27H-6, 25	247.15	266.70	Tie to	1314B-27H-3, 112.5	245.65
1314B-27H-6, 35	249.35	270.40	Tie to	1314A-28H-2, 30	250.66
1314A-28H-3, 40	252.26	272.00	Tie to	1314B-28H-1, 55	251.55
1314B-28H-7, 60	260.60	281.05	Append to	1314B-29H-1, 0	260.50
1314B-29H-7, 30	269.80	290.25	Append to	1314B-30H-1, 0	270.00
1314B-30H-7, 65	279.65	300.10	Append to		290.45

Table T21. Disturbed intervals, Holes U1314A, U1314B, and U1314C.

Core, section, interval (cm)	Type of disturbance	Core, section, interval (cm)	Type of disturbance
306-U1314A-		22H-7, 30–150	Disturbed (deformed core liner)
1H-1, 0–10	Mildly disturbed	23H-1, 0–30	Top of core
2H-2, 30–130	Mildly disturbed	26H-1, 0–55	Top of core
2H-2, 130–150	Flow-in	27H-1, 0–30	Top of core
2H-3, 0–150	Flow-in	28H-1, 0–30	Top of core
2H-4, 0–150	Flow-in	306-U1314B-	
2H-5, 0–150	Flow-in	1H-1, 0–5	Mildly disturbed
2H-6, 0–150	Flow-in	2H-1, 0–30	Top of core
3H-1, 0–125	Top of core	3H-1, 0–45	Top of core
4H-3, 0–150	Flow-in	4H-1, 0–10	Top of core
5H-1, 0–5	Top of core	5H-1, 0–20	Top of core
5H-2, 50–150	Disturbed	6H-1, 0–90	Top of core
5H-3, 0–150	Disturbed	7H-1, 0–25	Top of core
5H-4, 0–60	Disturbed	9H-1, 0–35	Top of core
5H-4, 60–150	Mildly disturbed	10H-1, 0–25	Top of core
5H-5, 0–50	Mildly disturbed	11H-1, 0–30	Top of core
5H-5, 50–150	Disturbed	12H-1, 0–30	Top of core
5H-6, 0–150	Disturbed	13H-1, 0–20	Top of core
5H-7, 0–30	Disturbed	15H-1, 0–20	Top of core
6H-1, 0–150	Flow-in	16H-1, 0–30	Top of core
6H-2, 0–150	Flow-in	17H-1, 0–25	Top of core
6H-3, 0–150	Flow-in	20H-1, 0–15	Top of core
6H-4, 0–150	Flow-in	21H-1, 0–20	Top of core
6H-5, 0–150	Flow-in	22H-1, 0–20	Top of core
6H-6, 0–150	Flow-in	24H-1, 0–20	Top of core
6H-7, 0–end	Flow-in	27H-1, 0–20	Top of core
7H-1, 0–55	Top of core	27H-7, 30–150	Top of core
8H-1, 0–25	Top of core	29H-1, 0–15	Top of core
9H-1, 0–10	Top of core	306-U1314C	
10H-1, 0–10	Top of core	1H-1, 0–20	Top of core
11H-1, 0–10	Top of core	2H-1, 0–5	Top of core
11H-1, 90–150	Flow-in	3H-1, 0–30	Top of core
11H-2, 0–150	Flow-in	4H-1, 0–25	Top of core
11H-3, 0–135	Flow-in	5H-1, 0–50	Top of core
12H-1, 120–150	Flow-in	6H-1, 0–50	Top of core
12H-2, 0–150	Flow-in	7H-1, 0–35	Top of core
12H-3, 0–150	Flow-in	8H-1, 0–50	Top of core
12H-4, 0–150	Flow-in	9H-1, 0–55	Top of core
12H-5, 0–150	Flow-in	10H-1, 0–20	Top of core
12H-6, 0–150	Flow-in	11H-1, 0–45	Top of core
12H-7, 0–150	Flow-in	14H-1, 0–10	Top of core
13H-1, 0–60	Top of core	15H-1, 0–60	Top of core
14H-1, 0–65	Top of core	16H-1, 0–5	Top of core
15H-1, 0–10	Top of core	18H-1, 0–10	Top of core
16H-1, 0–15	Top of core	19H-1, 0–35	Top of core
17H-1, 0–15	Top of core	20H-1, 0–150	Flow-in
18H-1, 0–40	Top of core	20H-2, 0–150	Flow-in
19H, all	Double liner	20H-3, 0–80	Flow-in
19H-1, 0–10	Top of core	21H-1, 0–50	Top of core
22H-1, 0–90	Mildly disturbed	22H-1, 0–10	Top of core
22H-1, 74–78	Drop stone		

Notes: The top ~20 cm of all cores should be avoided. When the interval listed is 0–150 cm, the entire section is included even if the true section length is less than 150 cm.



**Table T22.** Interstitial water geochemical data, Hole U1314A.

Core, section, interval (cm)	Depth (mbsf)	Core quality	SO ₄ ²⁻ (mM)	Cl ⁻ (mM)	pH	Alkalinity (mM)	Salinity (g/kg)	Cations (mM)				Trace elements (μM)							
								Na ⁺	K ⁺	Mg ²⁺	Ca ²⁺	NH ₄ ⁺	B	Ba ²⁺	Fe ²⁺	Li ⁺	Mn ²⁺	H ₄ SiO ₄	Sr ²⁺
306-U1314A-																			
2H-4, 145–150	7.9	x	23.2	562.0	7.41	4.34	34	483.8	12.1	55.1	10.3	16.2	455.4	16.6	22.5	17.1	49.1	461.1	69.4
3H-4, 145–150	17.4		20.5	571.9	7.43	5.38	34	482.6	10.9	48.8	8.4	0.0	440.4	17.0	25.5	17.6	46.8	487.6	77.8
4H-4, 145–150	26.9		1.1	539.9	7.41	6.13	34	445.5	11.5	43.2	7.4	4.3	446.4	18.7	31.8	17.5	27.9	529.3	74.4
5H-4, 145–150	36.4		15.7	555.4	7.48	6.48	33	476.9	11.1	45.1	6.5	2.8	465.4	16.9	6.5	17.4	15.9	531.4	79.6
6H-4, 145–150	45.9	x	10.8	540.9	7.41	6.72	32	455.6	12.4	39.0	5.9	8.7	455.6	17.3	11.7	19.0	13.8	571.9	77.3
9H-4, 145–150	74.4		6.8	585.7	7.56	7.46	32	493.7	10.5	37.4	5.2	14.7	457.1	18.3	22.8	20.7	13.1	570.0	93.7
12H-4, 145–150	102.9	x	28.5	551.1	7.57	5.56	31	460.9	9.7	29.8	4.7	23.7	416.4	20.4	21.5	22.1	10.5	633.2	106.4

Notes: x = flow-in. See Table [T21](#).

Table T23. Headspace gases, Hole U1314A.

Core, section, interval (cm)	Depth (mbsf)	C ₁ (ppmv)	C ₂ (ppmv)	C ₂₌ (ppmv)	C _{1/C₂} ratio
306-U1314A-					
2H-5, 0.0–5.0	7.90	1.9	0	0	
3H-5, 0.0–5.0	17.40	3.4	0	0	
4H-5, 0.0–5.0	26.90	3.5	0	0	
5H-5, 0.0–5.0	36.40	4.8	0	0	
6H-5, 0.0–5.0	45.90	4.8	0	0	
7H-5, 0.0–5.0	55.40	1.8	0	0	
8H-5, 0.0–5.0	64.90	1.6	0	0	
9H-5, 0.0–5.0	74.40	1.3	0	0	
10H-5, 0.0–5.0	83.70	1.6	0	0	
11H-5, 0.0–5.0	93.40	1.8	0	0	
12H-5, 0.0–5.0	102.90	2.0	0	0	
13H-5, 0.0–5.0	112.40	1.4	0	0	
14H-5, 0.0–5.0	121.90	1.9	0	0	
15H-5, 0.0–5.0	131.40	1.6	0	0	
16H-5, 0.0–5.0	140.90	1.3	0	0	
17H-5, 0.0–5.0	150.40	1.5	0	0	
18H-5, 0.0–5.0	159.90	1.5	0	0	
19H-5, 0.0–5.0	169.40	2.2	0	0	
20H-5, 0.0–5.0	178.90	3.7	1.9	1.6	1.95
21H-5, 0.0–5.0	188.40	1.8	0	0	
22H-5, 0.0–5.0	197.90	1.6	0	0	
23H-5, 0.0–5.0	207.40	1.6	0	0	
24H-5, 0.0–5.0	216.90	1.3	0	0	
25H-5, 0.0–5.0	226.40	1.3	0	0	
26H-5, 0.0–5.0	235.90	1.8	0	0	
27H-5, 0.0–5.0	245.40	2.7	0	0	
28H-5, 0.0–5.0	254.86	2.8	0	0	

Table T24. Bulk sedimentary C and N, Hole U1314A.

Core, section, interval (cm)	Depth (mbsf)	Carbon (wt%)			Total nitrogen (wt%)
		Inorganic	CaCO ₃	Total	
306-U1314A-					
1H-1, 80–81	0.80	6.99	58.23	7.21	0.22
2H-1, 125–126	3.15	2.64	21.99	2.78	0.14
2H-4, 145–150	7.85	8.28	68.97	8.33	0.05
2H-7, 39–40	11.29	7.37	61.39	7.54	0.17
3H-2, 20–21	13.10	2.82	23.49	3.11	0.29
3H-4, 145–150	17.35	3.46	28.82	3.62	0.16
3H-5, 74–75	18.14	7.42	61.81	7.40	0.00
4H-2, 26–27	22.66	5.35	44.57	5.58	0.23
4H-4, 145–150	26.85	3.11	25.91	3.31	0.20
4H-7, 41–42	30.31	1.53	12.74	1.60	0.07
5H-2, 68–69	32.58	6.64	55.31	6.85	0.21
5H-4, 145–150	36.35	6.58	54.81	6.67	0.09
5H-5, 40–41	36.80	8.46	70.47	8.48	0.02
6H-1, 30–31	40.20	3.81	31.74	4.03	0.22
6H-4, 145–150	45.85	3.94	32.82	4.11	0.17
6H-7, 40–41	49.30	2.47	20.58	2.50	0.03
7H-2, 80–81	51.70	5.65	47.06	5.71	0.06
7H-6, 90–91	57.80	6.62	55.14	6.89	0.27
8H-2, 72–73	61.12	2.84	23.66	3.12	0.28
8H-6, 80–81	67.20	2.82	23.49	3.13	0.31
9H-1, 70–71	69.10	4.57	38.07	4.67	0.10
9H-4, 145–150	74.35	2.99	24.91	3.14	0.15
9H-6, 100–101	76.90	3.69	30.74	3.85	0.16
10H-2, 40–41	79.75	6.94	57.81	7.11	0.17
10H-6, 40–41	85.55	1.57	13.08	1.91	0.34
11H-4, 79–80	92.69	4.34	36.15	4.78	0.44
11H-6, 42–43	95.32	1.39	11.58	1.61	0.22
12H-1, 88–89	97.78	1.14	9.50	1.59	0.45
12H-4, 145–150	102.85	2.75	22.91	3.20	0.45
12H-6, 118–119	105.58	7.00	58.31	7.26	0.26
13H-2, 68–69	108.58	2.33	19.41	2.68	0.35
13H-6, 68–69	114.58	4.68	38.98	4.89	0.21
14H-2, 68–69	118.08	4.86	40.48	5.14	0.28
14H-6, 68–69	124.08	5.41	45.07	5.60	0.19
15H-2, 89–90	127.79	6.03	50.23	6.26	0.23
15H-5, 80–81	132.20	2.60	21.66	2.94	0.34
16H-1, 89–90	135.79	1.02	8.50	1.24	0.22
16H-5, 48–49	141.38	6.34	52.81	6.76	0.42
17H-1, 60–61	145.00	3.52	29.32	3.67	0.15
17H-6, 60–61	152.50	3.89	32.40	4.24	0.35
18H-1, 80–81	154.70	5.60	46.65	5.79	0.19
18H-6, 40–41	161.80	2.20	18.33	2.39	0.19
19H-2, 70–71	165.60	4.94	41.15	5.13	0.19
19H-7, 38–39	172.78	6.31	52.56	6.41	0.10
20H-1, 60–61	173.50	2.50	20.83	2.79	0.29
20H-6, 90–91	181.30	2.49	20.74	2.57	0.08
21H-1, 90–91	183.30	2.73	22.74	2.81	0.08
21H-6, 60–61	190.50	4.46	37.15	4.56	0.10
22H-1, 86–87	192.76	0.44	3.67	0.78	0.34
22H-4, 89–90	197.29	7.21	60.06	7.29	0.08
23H-2, 77–78	203.67	1.85	15.41	2.07	0.22
23H-7, 28–29	210.68	4.91	40.90	5.07	0.16
24H-1, 81–82	211.71	0.96	8.00	1.15	0.19
24H-6, 80–81	219.20	5.71	47.56	5.99	0.28
25H-3, 77–78	224.17	5.35	44.57	5.71	0.36
25H-6, 77–78	228.67	0.90	7.50	1.19	0.29
26H-2, 76–77	232.16	2.56	21.32	2.91	0.35
26H-5, 76–77	236.66	5.43	45.23	5.91	0.48
27H-3, 77–78	243.17	3.19	26.57	3.56	0.37
27H-6, 77–78	247.67	1.30	10.83	1.55	0.25
28H-2, 77–78	251.13	4.96	41.32	5.25	0.29
28H-5, 77–78	255.63	2.13	17.74	2.40	0.27

Note: Italics = values originating from interstitial water squeeze cake samples.



Table T25. Samples used for organic matter investigation and SST calculation in sediments from Hole U1314.

Core, section interval (cm)	Depth		CPI	$U^{k'_{37}}$	SST (°C)
	(mbsf)	(mcd)			
306-U1314A-					
2H-4, 145–150	7.85	7.85	3.7	0.46	12.3
3H-4, 145–150	17.35	17.85	3.9	0.50	13.5
4H-4, 145–150	26.85	28.60	3.7	0.40	10.7
5H-4, 145–150	36.35	37.65	2.7	0.42	11.2
6H-4, 145–150	45.85	48.05	4.2	0.48	12.8
9H-4, 145–150	74.35	78.10	4.2	0.44	11.8
12H-4, 145–150	102.85	109.75	4.0	0.37	9.7
27H-4, 82–84	244.72	264.27	4.2	0.47	12.8

Notes: CPI = carbon preference index (*n*-alkanes), $U^{k'_{37}}$ = C_{37} -alkenone unsaturation index, SST = alkenone-derived sea-surface temperature (°C). For details, see “[Geochemistry](#)” in the “Site U1313” chapter.